

IoRL Deliverable D6.4

Demonstration and Evaluation of Concepts in Buildings

Editor:	Atanas Savov (BRE Group)
Deliverable nature:	Report (R)
Dissemination level: (Confidentiality)	Public (PU)
Contractual delivery date:	November 2020
Actual delivery date:	January 2021
Suggested readers:	Indoor communication experts and providers of indoor communication services. More to be added
Version:	1.0
Total number of pages:	115
Keywords:	IoRL technology, different scenario environments, field tests, Throughput, EVM received power and Reliability, Location Accuracy against a prescribed grid, practical recommendations, on technical and functional performances, performance metrics

Abstract

This deliverable highlights the features provided by IoRL technology on technical and user experience aspects for the different scenario environments. It includes four fields test: 1) VLC Coverage, 2) VLC Location Accuracy against a prescribed grid, 3) mmWave Coverage and 4) EM Exposure. The test results verify the IoRL concept and provide practical indications for improving the design and produce design guidelines for the optimal deployment of the 5G Remote Radio Light Heads (RRLHs) in buildings.

Disclaimer

This document contains material, which is the copyright of certain IoRL consortium parties, and may not be reproduced or copied without permission.

All IoRL consortium parties have agreed to full publication of this document.

The commercial use of any information contained in this document may require a license from the proprietor of that information.

Neither the IoRL consortium as a whole, nor a certain part of the IoRL consortium warrant that the information contained in this document is capable of use, nor that use of the information is free from risk, accepting no liability for loss or damage suffered by any person using this information.

The EC flag in this document is owned by the European Commission and the 5G PPP logo is owned by the 5G PPP initiative. The use of the EC flag and the 5G PPP logo reflects that IoRL receives funding from the European Commission, integrated in its 5G PPP initiative. Apart from this, the European Commission and the 5G PPP initiative have no responsibility for the content of this document.

The research leading to these results has received funding from the European Union Horizon 2020 Programme under grant agreement number 761992 — IoRL — H2020-ICT-2016-2017/H2020-ICT-2016-2.

Impressum

H2020 Internet of Radio Light

IoRL

WP6 Integration, Test and Exhibit

Task 6.4 Demonstration and Evaluation of Concepts in Building Environments

Demonstration and Evaluation of Concepts in Buildings

Editor: Atanas Savov, Building Research Establishment

WP leader: John Cosmas, Brunel University

Copyright: © 2020 Participants in IoRL project

Executive summary

The H2020 Internet of Radio Light (IoRL) project successfully conducted performance tests of a hybrid Visible Light Communications (VLC) and 40GHz mmWave5G compliant system in the Integer House lab at the Building Research Establishment, during the months of August – October 2020. The objective of the trials were to measure the coverage, latency, location accuracy and EM exposure performance of the designed mmWave and VLC system, provide recommendations for improving the design and produce design guidelines for the optimal deployment of the 5G Remote Radio Light Heads (RRLHs) and thereby demonstrate how to solve the problem of broadband wireless access in buildings and promote the 5G global standard.

List of authors

Company	Author	Contribution
Brunel University	John Cosmas	Section 1, 2.1, 3.1, 3.2, 3.3, 4.1, 4.3 and 4.4
Brunel University	Ben Meunier	Section 2.1, 2.2, 3.1, 3.2 and 3.3
Brunel University	Kareem Ali	Section 2.1, 2.2, 3.1, 3.2 and 3.3
Brunel University	Nawar Jawad	Section 2.1
Leicester University	Yue Zhang	Section 2.1, 3.1, 3.2, 3.3 and 4.4
Leicester University	Hequn Zhang	Section 2.1
ISEP	Xun Zhang	Section 3.2, 4.1. 4.2 and 4.4
ISEP	Lina Shi	Section 3.2
FhG	Robert Muller	Section 3.3
Building Research Establishment	Atanas Savov	Section 4 and Annex B
Building Research Establishment	James Gbadamosi	Section 4 and Annex B
Building Research Establishment	Martin Ganley	Section 4 and Annex B
MostlyTek LTD	Moshe Ran	Editorial and Annex A
Ferrovial Agroman	Sara Cuerva	Section 1.3

Table of Contents

1	Introduction	13
1.1	System Architecture	13
1.2	Building Research Establishment (BRE) Deployment.....	15
1.3	Deployment limitations in the train station, museum and supermarket scenarios.....	16
2	Experimental Setup at BRE	17
2.1	VLC Coverage Experiments and mmWave Coverage Experiments.....	17
2.2	VLC Location Experiments	25
3	Results of field tests at BRE.....	27
3.1	VLC Coverage Results	27
3.1.1	No angling of Photodiode Receiver towards Communication LED with Illumination LEDs off	27
3.1.2	Angling of Photodiode Receiver towards Communication LED with Illumination LEDs off.....	27
3.1.3	VLC Coverage Conclusions	28
3.2	VLC Localisation.....	29
3.2.1	Results.....	29
3.2.2	Conclusions	31
3.3	mmWave Downlink Coverage Results	32
3.3.1	mmWave Transmit Antenna Pointing Vertically Down	32
3.3.2	mmWave Transmit Antenna Pointing 30°, 40° from Vertical about antenna y-axis.....	33
3.3.3	mmWave Conclusions.....	34
3.4	Overall Conclusions	35
4	EMF Exposure Analysis – Modelling and Measurements.....	36
4.1	Background.....	37
4.1.1	Quantities, units and interaction mechanisms	37
4.1.2	Human exposure to time-varying electric, magnetic and electromagnetic fields ..	38
4.1.3	Computational Electromagnetics.....	46
4.1.4	Measurements of electromagnetic fields.....	49
4.2	Modelling.....	54
4.2.1	Software selection	54
4.2.2	Simulation Model preparation.....	55
4.2.3	Results.....	66
4.3	Measurements	84

4.3.1	Measurement Instrument selection	84
4.3.2	Measurements - procedures and methodologies	86
4.3.3	Measurement Results	90
4.4	Conclusions.....	91
	References.....	94

List of figures and tables

Figure 1: IoRL Layered Architecture	14
Figure 2: Integer House.....	15
Figure 3: Initial plan for Upper Ground Floor Integer House.....	15
Figure 4: Taking mmWave measurements at ground level with RLHs labelled A, B, C, D and at 0.7 m above ground ...	18
Figure 5: Taking VLC measurements at ground level.....	18
Figure 6: VLC Communications LED and mmWave Tx Antenna.....	19
Figure 7: PCB Horn Antenna.....	19
Figure 8: Transmit antenna 0°, 30°, 40°, 50° angling fixture	20
Figure 9: mmWave and VLC Photodiode receivers on 2-axis gimbal.....	20
Figure 10: Recording measurement result.....	21
Figure 11: Test Receiver Graphical User Interface	22
Figure 12: VLC Floor Plan for RRLH Area 1 (red cross indicates measurement point).....	23
Figure 13: mmWave Floor Plan for RRLH Area 1 (red cross indicates measurement point).....	24
Figure 14: (a) A Flow chart of the demonstration; (b) The realistic scenario; (c) The structure of 5G NR signal.	26
Figure 15: 4 VLC LED TXs EVM Test Rx at ground level pointing vertically up LED A and illumination LEDs off – top Right, B – bottom right, C – bottom left, D – top left.....	27
Figure 16: 4 VLC LED TXs EVM Test Rx at ground level pointing towards communication LED and illumination LEDs off	27
Figure 17: Distribution of test points and estimated points.....	30
Figure 18: CDF of position error (< 10 cm)	30
Figure 19: One mmWave TXs, receiver at 0.7m above ground EVM Test.....	32
Figure 20: One mmWave TXs, receiver at 0 m above ground EVM Test.....	32
Figure 21: One mmWave TXs angled at 30°, receiver at 0m above ground EVM Test (17-09-20)	33
Figure 22: One mmWave TXs angled at 30°, receiver at 0m above ground EVM Test (22-09-20)	33
Figure 23: One mmWave TXs angled at 40°, receiver at 0m above ground EVM Test (22-09-20)	34
Figure 24: One mmWave TXs angled at 30°, receiver at 0.7 m above ground EVM Test (23-09-20).....	34
Figure 25: Field Regions of an antenna.....	39
Figure 26: Field regions around an EM source (the antenna maximum dimension D is supposed to be large compared with the wavelength λ) [4].....	40
Figure 27: Alternative routes to evaluate in-situ RF exposure [1].....	51
Figure 28: Detailed model of house used in home scenario.....	56
Figure 29: Simplified model of house used in home scenario with layers representing used building materials	57
Figure 30: WinProp Supported object categories	58
Figure 31: Electrical material properties within WallMan environment.....	60
Figure 32: Building materials - propagation properties.....	61
Figure 33: LTE-XPOL-002-V2 directional LTE MIMO antenna pattern	62
Figure 34: IoRL mmWave antenna pattern in FEKO (dBV).....	63
Figure 35: IoRL mmWave antenna pattern in FEKO (Gain).....	63
Figure 36: IoRL mmWave antenna pattern in AMan	64
Figure 37: CADFEKO model development	65
Figure 38: CADFEKO model setup	66
Figure 39: Single mmWave E-Field strength for all vertical prediction planes (most left: 1.29 m; middle: 1.5 m; most right: 3.10 m). V/m linear scale	67
Figure 40: Single mmWave E-Field strength for the first vertical prediction plane. V/m linear scale.....	67
Figure 41 – Indoors 3D view of four mmWave transmitters at height of 1.8 m	68
Figure 42 - Four mmWave transmitters power level at height of 1.8 m. Log scale	69
Figure 43 - Simulation of E-Field strength for 4 mmWave Tx and 40 additional Tx at height of 0.70m.....	70
Figure 44 - Simulation of E-Field strength for 4 mmWave Tx and 40 additional Tx at height of 1.20m.....	71

Figure 45 - Simulation of E-Field strength for 4 mmWave Tx and 40 additional Tx at height of 1.80m	72
Figure 46 – Horizontal prediction plane at height of 0.70 m, excluding mmWave and including 38 transmitters of lower band communication frequencies (868 MHz to 5 GHz) only. V/m linear scale	73
Figure 47 – Horizontal prediction plane at height of 1.20 m, excluding mmWave and including 38 transmitters of lower band communication frequencies (868 MHz to 5 GHz) only. V/m linear scale	74
Figure 48 – Horizontal prediction plane at height of 1.80 m, excluding mmWave and including 38 transmitters of lower band communication frequencies (868 MHz to 5 GHz) only. V/m linear scale	75
Figure 49 – 3D Horizontal prediction plane at height of 1.80 m, including single mmWave antenna and 38 transmitters of lower band communication frequencies (868 MHz to 5 GHz). V/m linear scale	76
Figure 50 – 2D Horizontal prediction plane at height of 1.80 m, including single mmWave antenna and 38 transmitters of lower band communication frequencies (868 MHz to 5 GHz). V/m linear scale	77
Figure 51: Simulation of E-Field strength for 4 mmWave transmitters at 1.80m height.....	78
Figure 52: Simulation of E-Field strength for 4 mmWave transmitters and 38 additional Tx (WiFi router not included) at 1.80m height.....	79
Figure 53 - Individual transmitter power for all devices at vertical prediction plane 1.29 m. Logarithmic scale dBm	80
Figure 54 - Dominant E-Field strength for all devices, in a vertical line, directly below mmWave antenna, at vertical prediction plane 1.29 m. Linear scale V/m	81
Figure 55 – Summed broadband electric field strength at a point for all heights, in a vertical line, directly below mmWave antenna (summation of electric field strengths, assuming in-phase constructive interference)	82
Figure 56 - POSTFEKO Average SAR solution and dielectric data	83
Figure 57 – E-Field probe EF4091.....	85
Figure 58 – E-Field probe EF4091.....	86
Figure 59: New Location of RRLH Controller and RRLHs for EM Radiation Measurements.....	87
Figure 60: New Location of mmWave Antenna	88
Figure 61: IoRL Head-end and End User systems.....	88
Figure 62: EM Radiation Level Measurement device.....	89
Figure 63 – Diagram of measurement grid.....	89
Figure 64 - Comparisons between measured and simulated results (summation of electric field strengths, assuming in-phase constructive interference)	92
Figure 65 - Comparisons between measured and simulated results (Dominant electric field).....	92
Figure 66 - NARDA NBM-520 Calibration certificate	114
Figure 67 – EF4091 Probe certificate	115
Table 1: VLC Location Error.....	29
Table 2 - Physical quantities [1]	37
Table 3 - Constants [1].....	37
Table 4 – Main properties of electromagnetic field in different field regions [4]	40
Table 5 - Approximate comparison between groups and locations selected in the standards.....	41
Table 6 - Comparison of basic biological restrictions (SAR limits) and reference levels (current parameters)	42
Table 7 - Comparison of derived levels; E field (RMS values V/m) *	43
Table 8 - Comparison of derived levels; H field (RMS values A/m) ^{(1), (2)}	44
Table 9 - Comparison of derived levels; power density (W/m ²) ⁽³⁾	45
Table 10 - Selection of numerical techniques [4]	47
Table 11 - Conductivity of tissue types [7]	48
Table 12 – Guidance on selecting between broadband and frequency-selective measurement.....	53
Table 13 – Dry skin electrical properties [9].....	66
Table 14 – Summation of Exposure Ratio contributors (in-phase constructive interference at a point – at the antenna)	82
Table 15 – Measured electric field strength (V/m), spaced averaged, with mmWave transmitter turned on	90
Table 16 - Measured electric field strength (V/m), spaced averaged, with mmWave transmitter turned off	91
Table 17: Key Performance Metric Requirements for IoRL	96

<i>Table 18 – Electrical properties wood and concrete</i>	<i>104</i>
<i>Table 19 - Electrical properties plasterboard and glass.....</i>	<i>105</i>
<i>Table 20 - Electrical properties chipboard and ceiling board.....</i>	<i>106</i>
<i>Table 21 - Electrical properties floorboard</i>	<i>107</i>
<i>Table 22 – Transmitters list and parameters</i>	<i>108</i>

Abbreviations

5G	Fifth Generation (mobile/cellular networks)
5G PPP	5G Infrastructure Public Private Partnership
A/D	Analog to Digital
AFB	Airforce Base
AI	Artificial Intelligence
CDF	Complementary Distribution Function
CEM	computational electromagnetics
CPRI	Common Public Radio Interface
CRC	Cyclic Redundancy Check
D/A	Digital to Analog
DC	Direct Current
DRAN	Dynamic Radio Access Network
EIRP	Effective Isotropic Radiated Power
EM	Electromagnetic
EMF	Electromagnetic Field
EPC	Evolved Packet Core
EPROM	Electronically Programmable Read Only Memory
EVM	Error Vector Magnitude
FDTD	finite-difference time-domain
FOV	Field of View
GUI	Graphical User Interface
GPS	Global Positioning System
GTD	geometrical theory of diffraction
HDTV	High Definition Television
HPC	High Performance Computing

ICNIRP	International Commission on Non-Ionizing Radiation Protection
IHPEG	Intelligent Home IP Gateway
IFC	Industry Foundation Classes
IFFT	inverse Fast Fourier Transform
IoRL	Internet of Radio Light (project)
IoT	Internet of Things
IP	Internet Protocol
IRT	Intelligent Ray Tracing
LED	Light Emitting Diode
LDPC	Low-density parity-check
LTE	Long Term Evolution
MIMO	Multiple Input Multip Output
MISO	Multiple Input Single Output
MNO	Mobile Network Operator
MoM	Method of Moments
MR/FDTD	multiple-region finite-difference time-domain
NIR	Non-Ionizing Radiation
NFC	Near Field Communications
NR	New Radio
OFDM	Orthogonal Frequency Division Multiplexing
PCB	Printed Circuit Board
PD	Photodiode
PDSCH	Physical Downlink Shared Channel (
PHY	Physical
QAM	Quadrature Amplitude Modulation
QoS	Quality of Service

QPSK	Quadrature Phase Shift Keying
r.m.s	root mean squared
RCS	radar cross section
RLH	Radio Light Head
RRLH	Remote Radio Light Head
RSS	Received Signal Strength
Rx	Receiver
SAR	Specific absorption rate
SCS	Sub Carrier Spacing
SDN	Software Defined Networks
TDoA	Time Difference of Arrival
Tx	Transmitter
UE	User Equipment
USRP	Universal Software Radio Peripheral
UTD	uniform theory of diffraction
VLC	Visible Light Communications
WHO	World Health Organisation

1 Introduction

The Internet of Radio Light has successfully conducted performance tests of a hybrid Visible Light Communications (VLC) and 40GHz mmWave 5G compliant system in the Integer House lab at the Building Research Establishment, during the months of August – December 2020.

The objective of the trial is to measure the coverage, latency, location accuracy and EM exposure performance of the designed mmWave and VLC system, provide recommendations for improving the design and produce design guidelines for the optimal deployment of the Remote Radio Light Heads (RRLHs) in buildings.

It thereby demonstrates how to solve the problem of broadband wireless access in buildings and promote 5G global standard.

In line with its commitment to open research data the project is in the process to release the measurement datasets through Zenodo. The actual licensing terms are still being determined.

1.1 System Architecture

The IoRL architecture is a layered architecture consisting of four layers namely: Service, Network Function Virtualisation (NFV), Software Defined Network (SDN) and Access, as shown in Figure 1.

The Service layer is required to run server-side applications to stream audio-video, receive, store results on databases and monitor security etc. from a multi-core Cloud Home Data Centre Server (CHDCS) and is required to run mobile apps from User Equipment (UE) i.e. Smart Phones, Tablet PCs, Virtual Reality Headsets and HDTVs.

At the SDN Layer resides the SDN Forwarding Device (FD) to route IP packets to/from their 5G Layer 2/3 Protocol Processors and the SDN Controller. The Network Function Virtualization Orchestrator (NFVO) invokes various virtual functions required for an Intelligent Home IP Gateway such as Access & Mobility Management, Deep Packet Inspection and Network Security Functions.

The Access Layer consists of up to 32 RRLH Controllers. Each RRLH Controller drives up to four/eight VLC and mmW RRLH pairs with the same Transmission Block Sub-Frame, thereby providing a Multiple Input Single Output (MISO) transmission on downlink paths and Single Input Multiple Output (MISO) on uplink paths for its coverage area, which is typically a room or floor areas of a building.

Each room or floor areas in a building can be provisioned by a single RRLH Controller with its group of RRLHs and intra-building handover performed between these areas with the aid of VLC and mmW location sensing application that continuously records the positions of UE in the building.

A UE can either obtain direct access to the Internet, by only using 5G protocols on the Access Layer interface to the UE, to deliver IP packets to the Network Layer and thence to the Server Applications in the Service Layer or obtain access to the Mobile Network Operator's (MNO) Evolved Packet Core (EPC), by using 5G protocols on the Access Layer interfaces to both the UE and EPC, to deliver IP packets to the Network Layer and thence to the applications supported by the MNO. This latter approach allows applications, such as Facebook, on a Smart phone to be accessed on both the outside Mobile Network as well as the Intelligent Home Network with handover between them. The Virtual Network Functions on the NFV Layer identify the destination of IP packets and the SDN Controller directs these IP packets to their appropriate destination.

Therefore, our proposed solution enables the building owner to have connectivity to different operators to facilitate the use of different devices registered with different operators, as well as exploiting the license-free spectrum for accessing the home network.

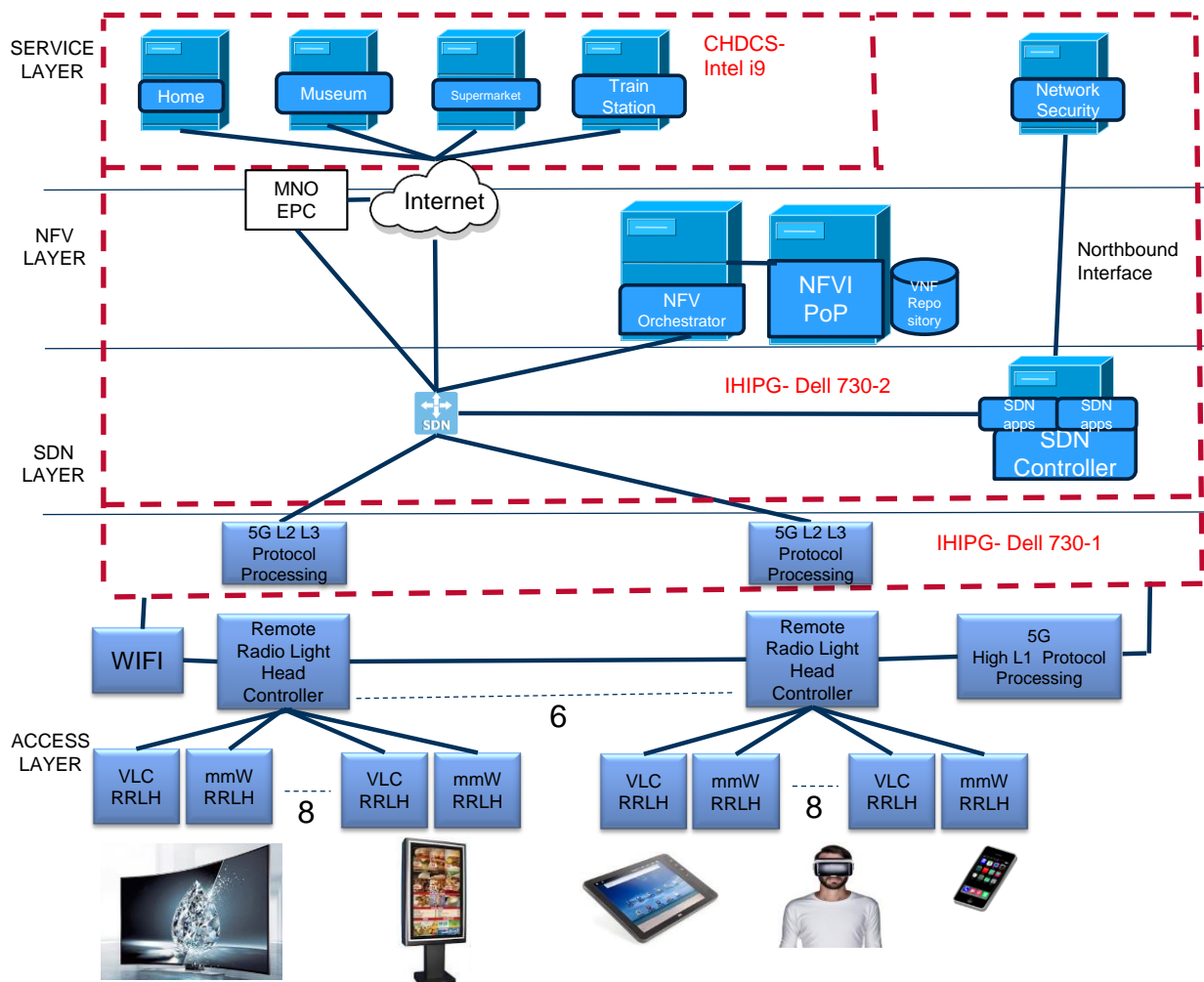


Figure 1: IoRL Layered Architecture

The Access Layer architecture uses a 10G Common Public Radio Interface (eCPRI) ring Ethernet, to interconnect a Distributed Radio Access Network (DRAN) processor with up to 32 Remote Radio Light Head (RRLH) Controllers each hosting two Lower Layer 1 processors, the first that generates an IF signal to drive up to 4 VLC MISO modules using a 1 to 4 RF splitter and a second that generates an IF signal to drive or be driven by up to 4 mmWave RF Duplex modules using a 1 to 4 RF splitter. The functional split between the RRLH Remote Unit and the DRAN in the Physical Layer is planned to be in-line with option 7 of the e-CPRI architecture. The Upper PHY layer unit includes the interface with the MAC and upper RAN layers and mainly includes the FEC encoders (LDPC and Polar) and decoders and drive over the 10 Gbps Ethernet ring the data units along with their related control descriptors destined to the RRLH Controller units. The 10 Gbps Ethernet ring can be looped from room to room in a building from one RRLH to another in a similar way to the electric light circuit in a home. A 10 MHz GPS reference is sent to IHIPG, High L1 Protocol Processor and RRLH Controller for use in 5G synchronization algorithms at these layers.

The aim of the project trial was to measure the coverage, latency, location accuracy and EM exposure performance of the designed mmWave and VLC system.

42 Mbps was obtained on the VLC system with 10 MHz bandwidth, 4-QAM and SCS=30kHz on the Viavi testbed. 310 Mbps was obtained on the mmWave system with 100 MHz bandwidth, 64-QAM and SCS = 30 kHz on the Viavi testbed. 70 Mbps using 100 MHz bandwidth with 4-QAM and SCS = 30 kHz at mmWave in the laboratory using the RunEL testbed. Less 0.5 ms latency has been measured at 10 MHz bandwidth at the physical layer between the UE and the DRAN.

1.2 Building Research Establishment (BRE) Deployment

The performance tests of a hybrid Visible Light Communications (VLC) and 40 GHz mmWave 5G compliant system is being conducted in 4 m x 6 m RRLH Area 1 (see Figure 3) on the upper ground floor of the Integer House lab (see Figure 2) at the Building Research Establishment.



Figure 2: Integer House

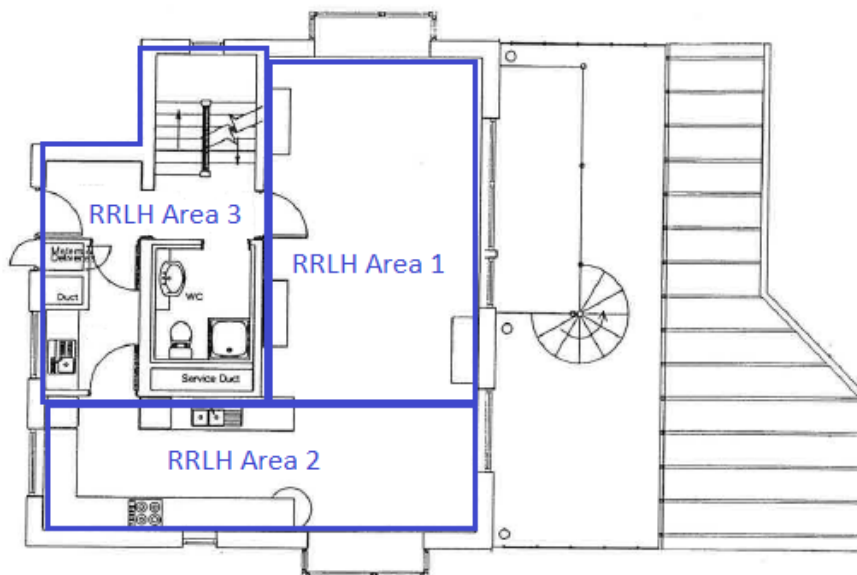


Figure 3: Initial plan for Upper Ground Floor Integer House

1.3 Deployment limitations in the train station, museum and supermarket scenarios

This deliverable presents the results of the field tests carried out in BRE, in the home scenario. Unfortunately, because of the situation with COVID-19 and the restrictions all around the world, it has not been possible to demonstrate and highlight the features provided by IoRL technology from technical and user experience aspects in the other three scenario environments planned at the beginning of the project, although they were already prepared and waiting for the demonstration to take place. For an in-situ demonstration of the IoRL system, it would have been necessary not only to ship the equipment to the three remaining scenario locations (a train station scenario in Spain, a museum scenario in France, a supermarket scenario in China), but also to accompany by key experts from the UK partners to support the on-site set-up of the system in each locations. Deliverable 6.3 of IoRL project details all aspects, requirements and constraints for each of the scenarios, including a description of each of the scenarios, the on-site preparation steps, the real living environment settings describing the specific requirements and characteristics in order to install IoRL technology, a planning for all the demonstration phases (equipment arrival, purchase of needed additional material, commissioning, demonstration period, events timetable, dismantling...) and a materials breakdown and manpower needed for the installation.

By the end of 2019 and beginning of 2020, the planned timeline to demonstrate the system in the four scenarios was the following:

Scenario	May 2020	Jun. 2020	Jul. 2020	Aug. 2020	Sept. 2020	Oct. 2020	Nov. 2020
Train station in Spain							
Museum in France							
Home in UK							
Supermarket in China							

In March 2020, in the light the COVID-19 situation, and foreseeing the possible national lockdowns, it was decided to postpone all the scenarios:

Scenario	May 2020	Jun. 2020	Jul. 2020	Aug. 2020	Sept. 2020	Oct. 2020	Nov. 2020
Train station in Spain							
Museum in France							
Home in UK							
Supermarket in China							

Besides, Viavi laboratories became inaccessible to the project due to COVID-19 restriction measures and still some IoRL system integration was needed. The last stages of the system

integration were moved to the Building Research Establishment (BRE) in UK, as well as system performance verification and all demonstration work, since August 2020. Back then, the new optimistic timeline was set as follows:

Scenario	May 2020	Jun. 2020	Jul. 2020	Aug. 2020	Sept. 2020	Oct. 2020	Nov. 2020
Train station in Spain							
Museum in France							
Home in UK							
Supermarket in China							

In September 2020, in the light of the new and even tighter restrictions in Paris and in Madrid because of the pandemic situation the project was forced to complete all the performance verification tests and the demonstration work at the Building Research Establishment.

The different scenarios were chosen, because each of them would challenge IoRL technology differently. For example, in the train station scenario it was key to improve communications under conditions in which there is no signal, such as below ground sites or tunnels, which is crucial because of safety reasons and to provide internet access to potential thousands of travellers. The museum scenario was chosen because it is also a public space where wireless access in its basement area is impossible as it is encased in a large metallic drum to avoid water seepage from an underground stream and to provide appealing location-based applications such as visitor guidance applications to guide guests through the museum.

In the light with the results presented in this deliverable and demonstrated at the home scenario in the Building Research Establishment, it is foreseen that the IoRL system could be successfully installed in the other scenarios in which special attention should be taken because of the fact of being public spaces and the difficulties related to below ground scenarios or encased spaces.

2 Experimental Setup at BRE

2.1 VLC Coverage Experiments and mmWave Coverage Experiments

This experiment provides us with important dimensioning information of the expected coverage from 5G compliant VLC and mmWave access points to determine the number required per room in property and also location accuracy information that can be obtained for RSS VLC localisation and TDoA mmWave localisation systems. It allowed us to measure coverage, latency, location accuracy and EM exposure performance.

Figure 4 shows a Brunel student taking mmWave measurements at ground level and 0.7 m above ground on a Viavi test receiver from transmissions of a RRLH.



Figure 4: Taking mmWave measurements at ground level with RLHs labelled A, B, C, D and at 0.7 m above ground



Figure 5: Taking VLC measurements at ground level

The VLC communications LED and mmWave Tx antenna systems are shown in Figure 6. The transmit antenna is constructed with PCB waveguides, which are horned in its x axis and non-horned in its y axis, as shown in Figure 7. The transmit antenna is mounted on a fixture that allows

it to be rotated by 0° , 30° , 40° , 50° from the vertical axis, as shown in Figure 8. Since the transmit mmWave antenna is singularly polarized either in the vertical or horizontal directions, the receive mmWave antenna must be oriented in the same direction for the transmitted signal to be successfully received.

The mmWave and VLC Photodiode receivers are shown in Figure 9 on a 2-axis gimbal, which allows the Receive antenna to be pointed towards the transmit antenna and the receive antenna angle to be measured.

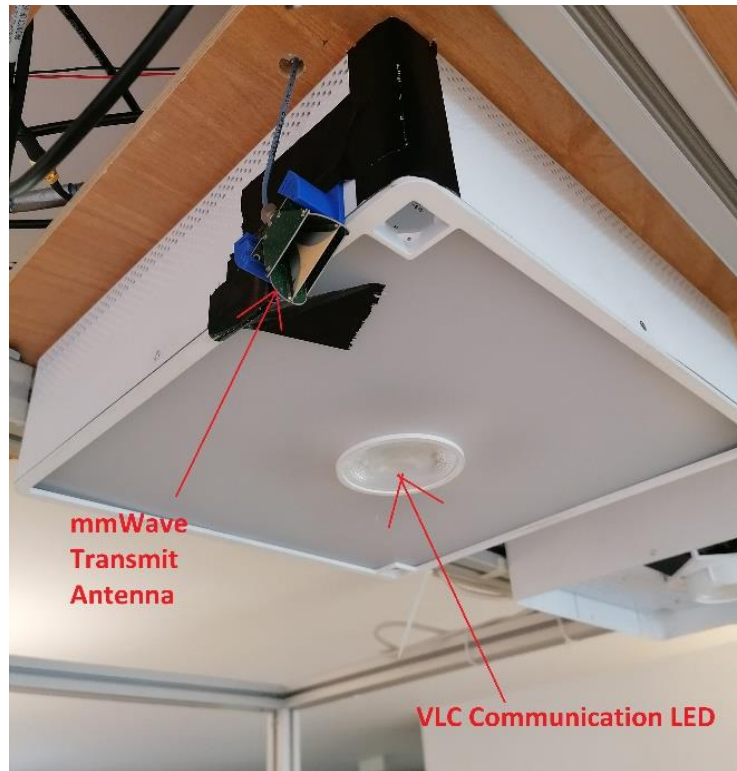
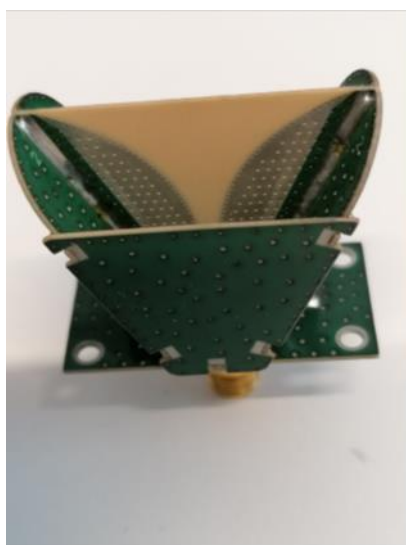


Figure 6: VLC Communications LED and mmWave Tx Antenna



(a) Horned Guides



(b) Non-Horned guides

Figure 7: PCB Horn Antenna

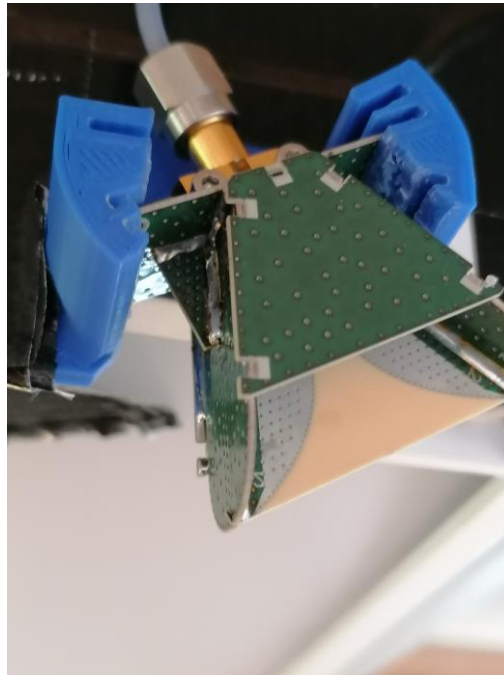
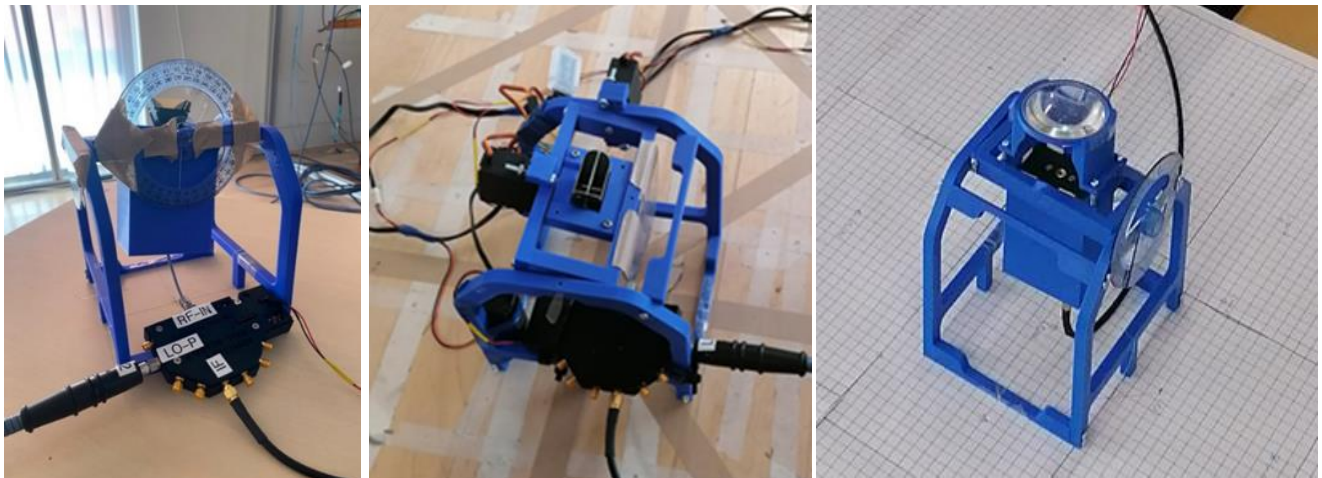


Figure 8: Transmit antenna 0°, 30°, 40°, 50° angling fixture



(a) mmWave Antenna

(b) remote controlled mmWave Antenna

(c) VLC Photodiode Receiver and Lens

Figure 9: mmWave and VLC Photodiode receivers on 2-axis gimbal

We have performed coverage, latency, location accuracy and EM exposure performance measurements in the setup. Figure 10 shows a student recording measurement results.

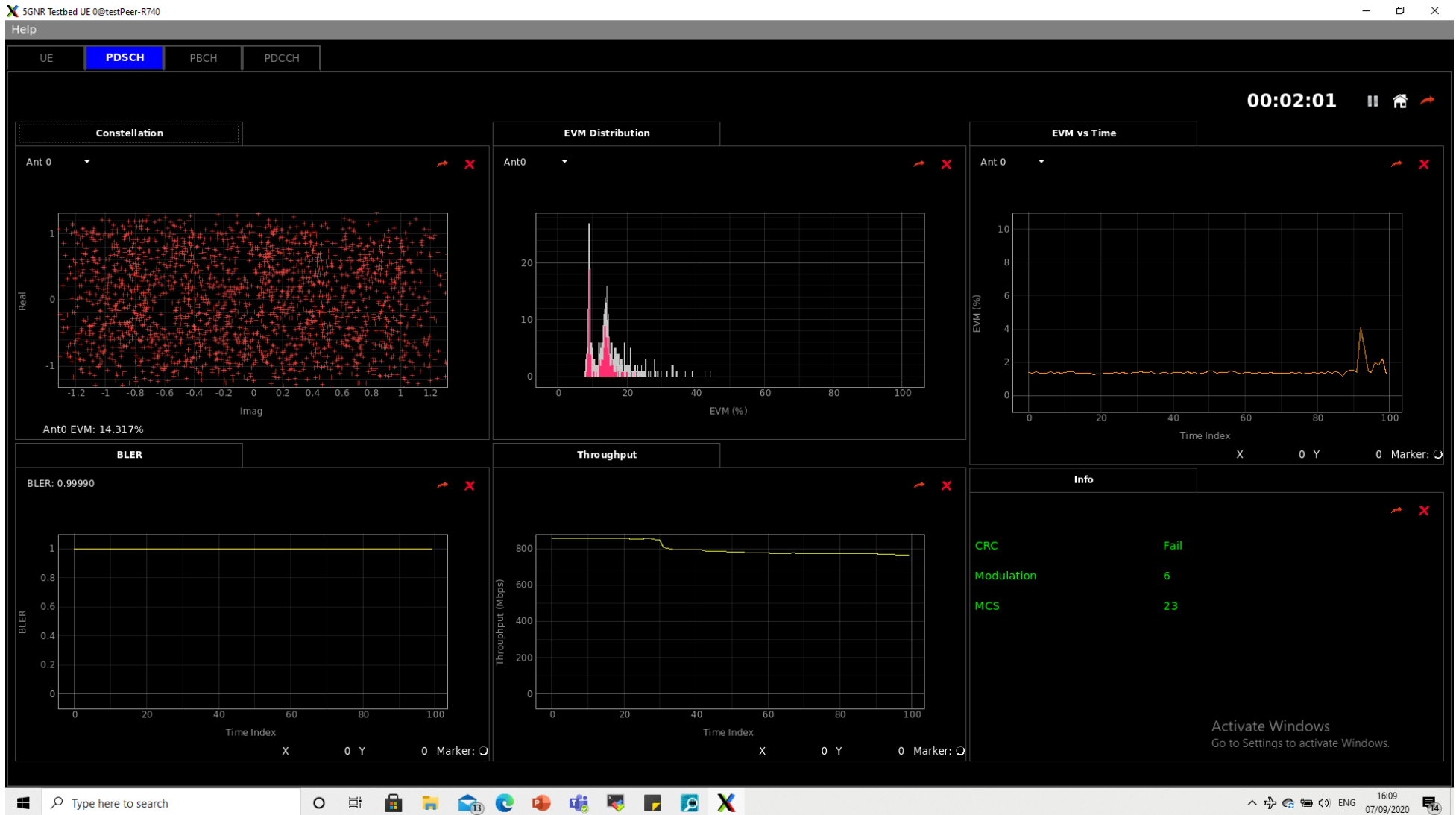


Figure 11: Test Receiver Graphical User Interface

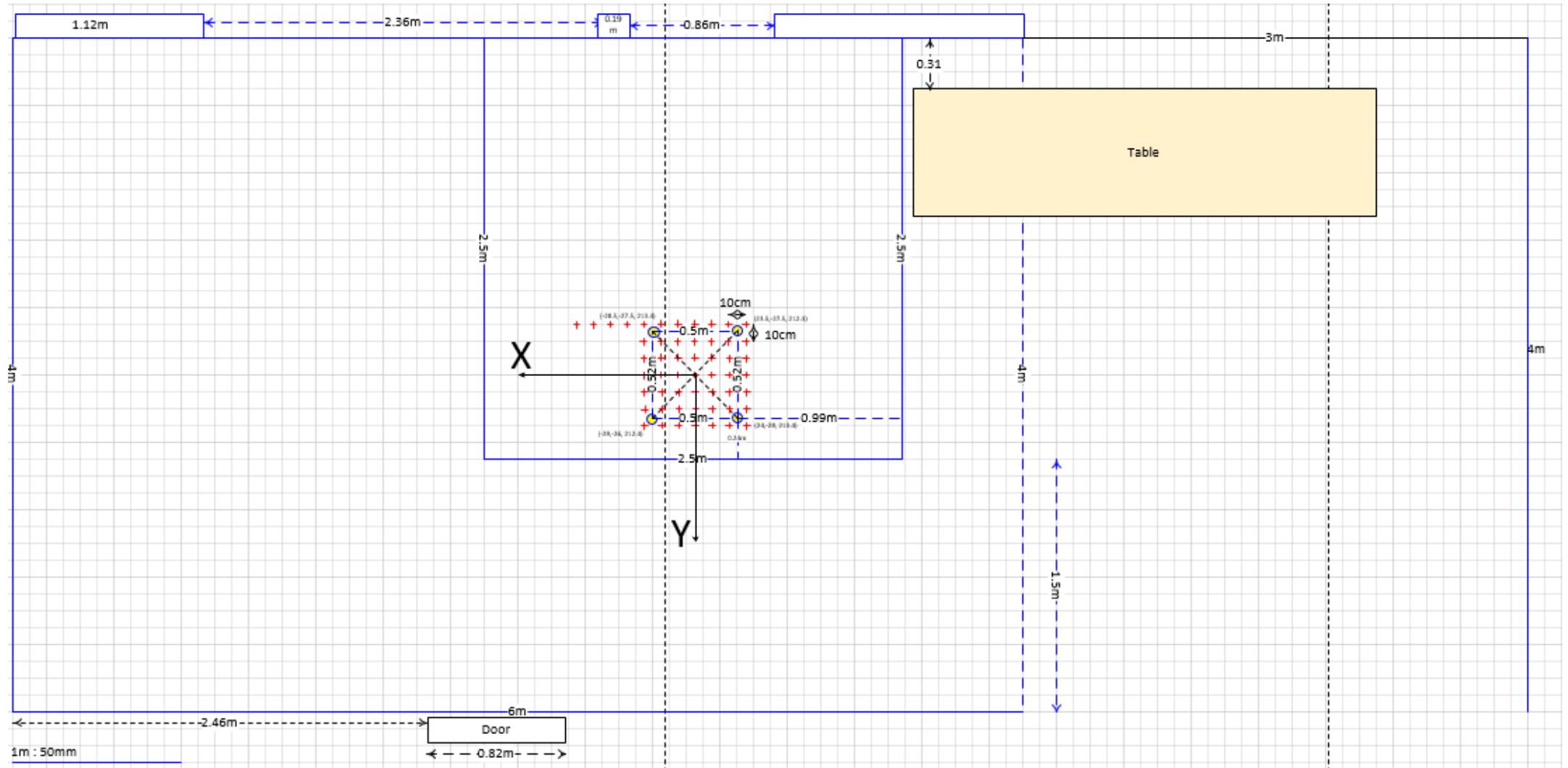


Figure 12: VLC Floor Plan for RRLH Area 1 (red cross indicates measurement point)

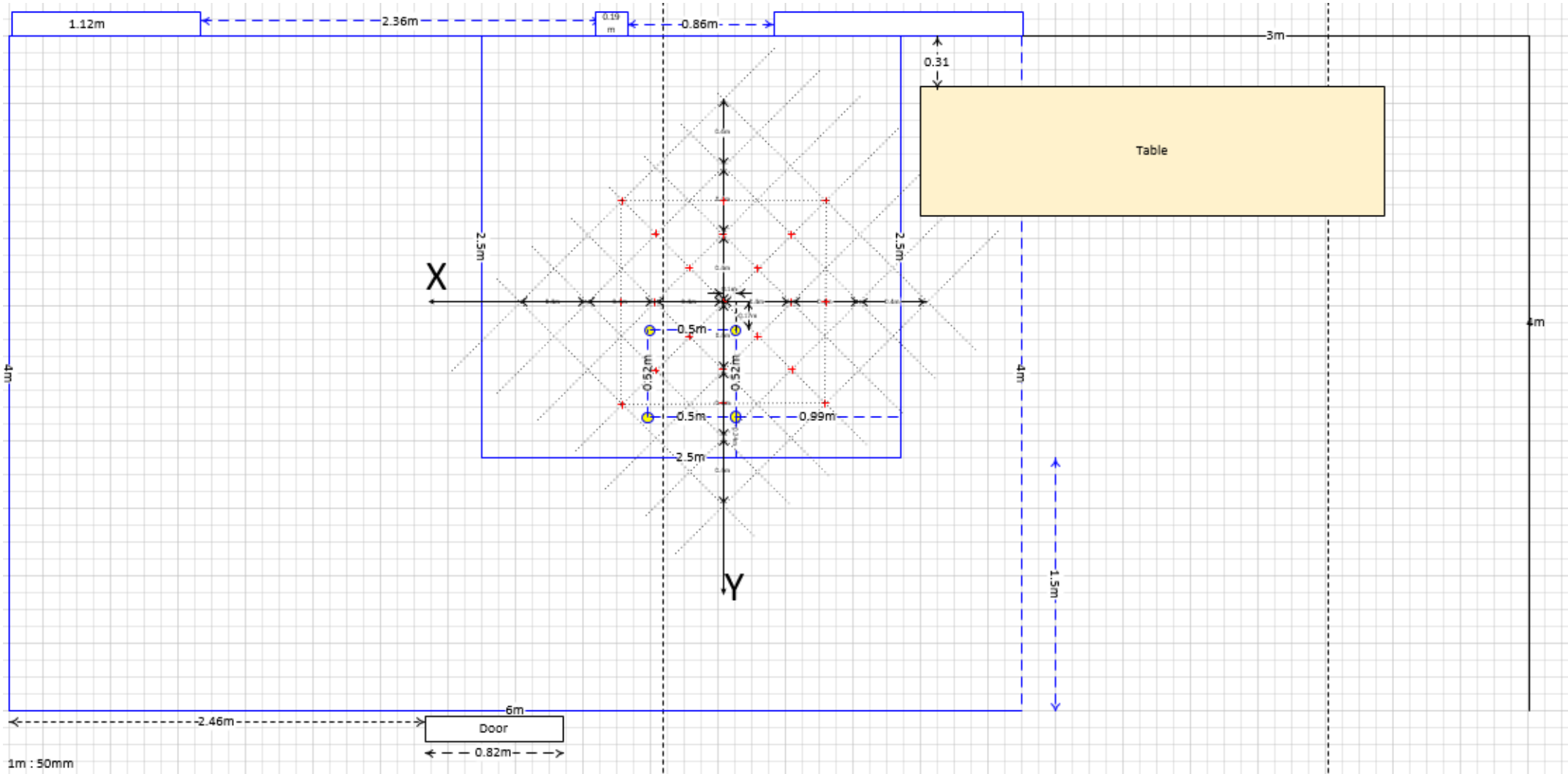


Figure 13: mmWave Floor Plan for RRLH Area 1 (red cross indicates measurement point)

2.2 VLC Location Experiments

A flow chart of the demonstration and its realistic scenario are shown in Figure 14 (a) and (b). A server (Dell R740) acts as the 5G NR transmitter generated 5G baseband signal. It modulates the user data with different modulation schemes which include QPSK, 16-QAM, 64-QAM and 256-QAM. As the modulated symbols were assigned to the 5G NR frame shown in Figure 14 (c), inverse Fast Fourier Transform (IFFT) processing and IQ modulation were applied to convert the OFDM frame to the time-domain and guarantee the signal well matched with IM/DD VLC system. Subsequently, a digital-analog (D/A) converter (USRP 2944R) and a DC bias transformed this digital signal to analog signal with an appropriate DC component. This signal is sent to four LEDs (LUXEN 5050). Through an optical wireless channel, the signal from each LED is captured by a commercial receiver (HAM C5331-11) in sequence and digitized by analog-digital (A/D) converter (USRP 2944R). Finally, the received signal is transferred back to server to extract fingerprints.

A 3D coordinate system was established to demonstrate the feasibility and accuracy of the proposed method for various distances and environments. According to the Figure 14 (b), four LEDs were fixed on the ceiling in a known location. The receiver kept 1.042 m height and moved on a plane parallel to the ground. The distribution of the EVM (Error Vector Magnitude) of each LED in the whole area was tested to describe the optical wireless channel. Subsequently, signal samples from each LED were collected 10 times by the receiver at 24 different points. By using the proposed method, 960 LED fingerprints were extracted from all the samples and were randomly divided into training set and testing set in a ratio of 6:4. Several types of classifier were employed to verify the accuracy of the extracted LED fingerprints.

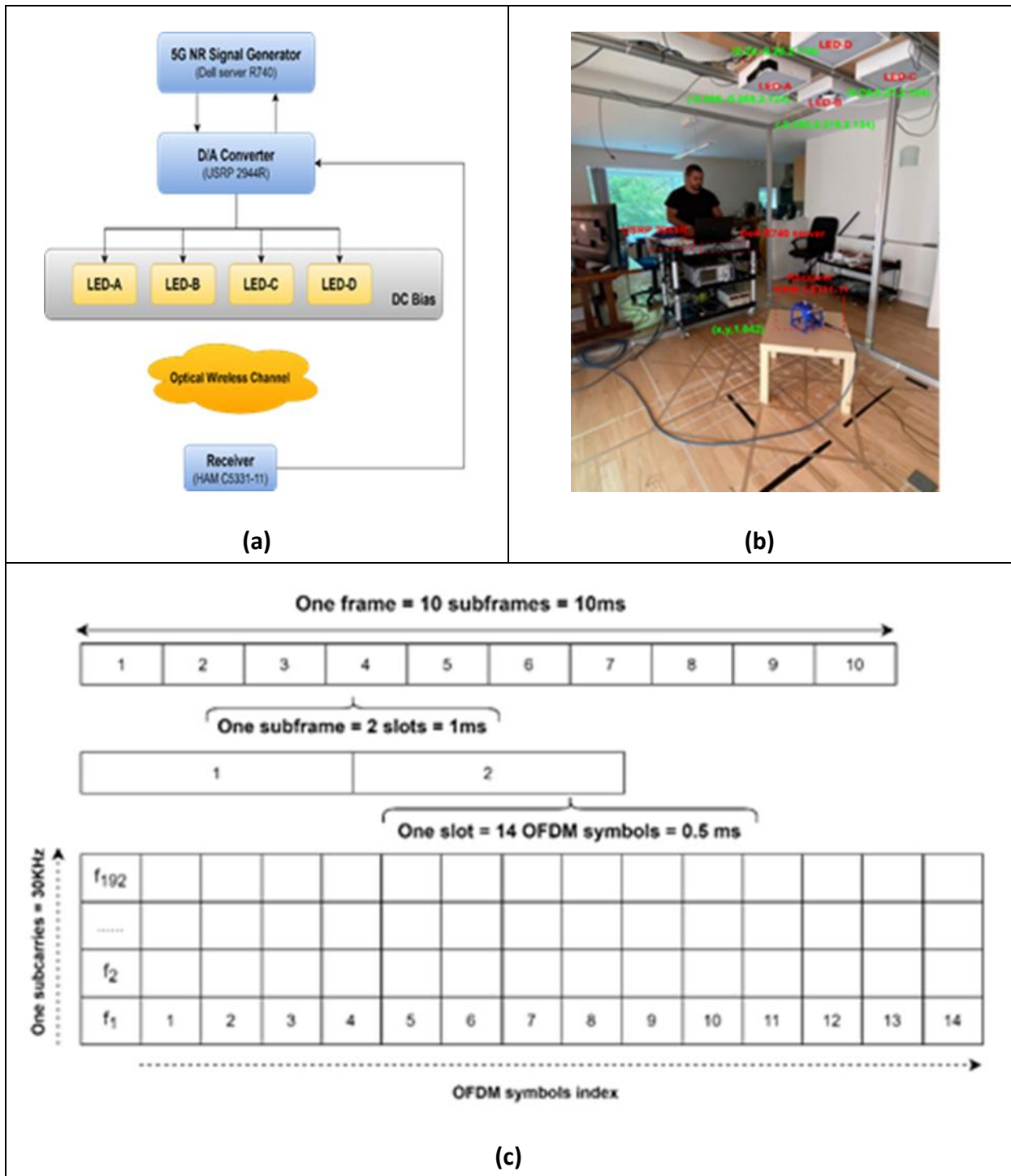


Figure 14: (a) A Flow chart of the demonstration; (b) The realistic scenario; (c) The structure of 5G NR signal.

3 Results of field tests at BRE

3.1 VLC Coverage Results

3.1.1 No angling of Photodiode Receiver towards Communication LED with Illumination LEDs off

Figure 15 shows sample results of coverage for 4 VLC LED TXs EVM Test at 2 m distance with illumination LEDs off and Rx PD angle vertically up. The best performing RLH is A which provide a coverage area of radius 0.3 m.

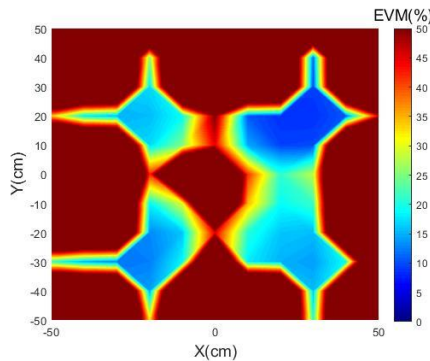


Figure 15: 4 VLC LED TXs EVM Test Rx at ground level pointing vertically up LED A and illumination LEDs off – top Right, B – bottom right, C – bottom left, D – top left

3.1.2 Angling of Photodiode Receiver towards Communication LED with Illumination LEDs off

Figure 16 shows sample results of coverage for 4 VLC LED TXs EVM Test at 2 m distance with illumination LEDs off and Rx PD angled towards the communication LED. The best performing RLH is A which provides a coverage area of radius 0.5m.

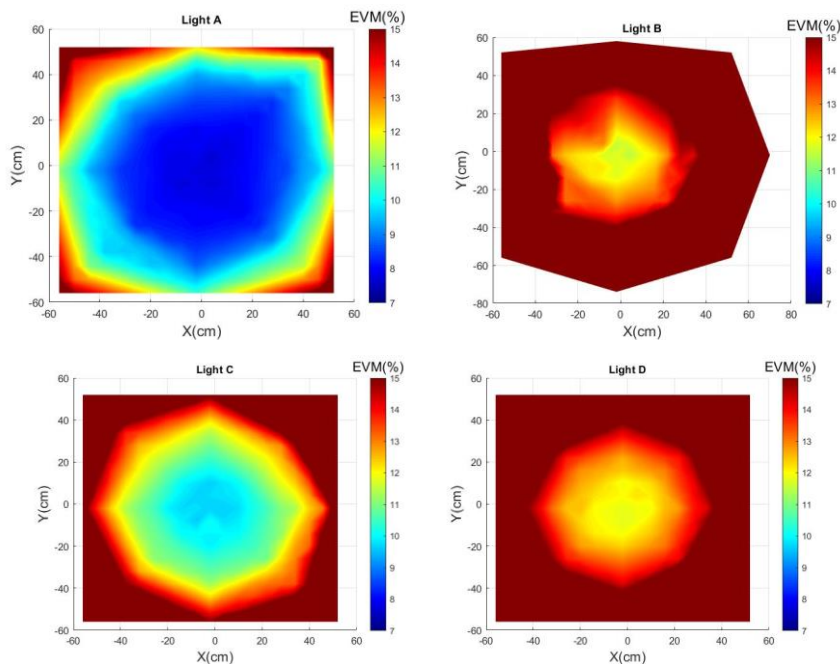


Figure 16: 4 VLC LED TXs EVM Test Rx at ground level pointing towards communication LED and illumination LEDs off

3.1.3 VLC Coverage Conclusions

Results from VLC measurements shows that the coverage has a diameter of about 0.6 m and maximum propagation distance of 2m, as shown in Figure 14. This limited coverage was attributed to the physical construction of the PD sensor housing. The variation in performance between communication LEDs A, B, C and D was attributed to the variability in transmitted light intensities between them.

When angling the PD receiver towards the transmit LED, this improves the quality of the received signal so that the coverage has a diameter of about 1m and maximum propagation distance of 2 m, as shown in figure 15. Again, the variation in performance between communication LEDs A, B, C and D was attributed to the variability in transmitted light intensities between them.

3.2 VLC Localisation

3.2.1 Results

Figure 16 illustrates 4 LEDs' distribution of the EVM in the whole area. According to the results, LED-A and LED-C had the largest and the second largest coverage of the high-quality communication environment. On the contrary, channel of the LED-B and LED-D had limited quality. The phenomenon that the same type of four LEDs has different communication performance was caused by the non-linearity of the optical wireless channel. The effective coverage is limited because of minimum EVM should be guaranteed for a high quality VLC communication link.

Based on this environment, only 27 reference points are available for VLC positioning testing. According to 27 testing areas in an illumination area which is 30 cm², using VLC and adjusting the receiver PD and lens to face the communications LED obtained the location error where the lowest was 0.55 cm and the highest is 11.94 cm with an average of 5.28 cm, this is shown in Table 1 below. A location estimation algorithm [2], which uses Artificial Intelligence (AI) was used to figure out the optimum position of four Remote Light Heads reduce the location error of measurements taken in a grid of points within the coverage area in order to get the average location error of these points as 5.28 cm, minimum error of 0.55 cm, and a maximum error of 11.94 cm where 80% of the errors are less than 10 cm.

Table 1 – VLC Location Error

pe_min(cm)	pe_max(cm)	pe_avg(cm)
0.55	11.94	5.28

Distribution of test points and estimated points is shown in Figure 17.

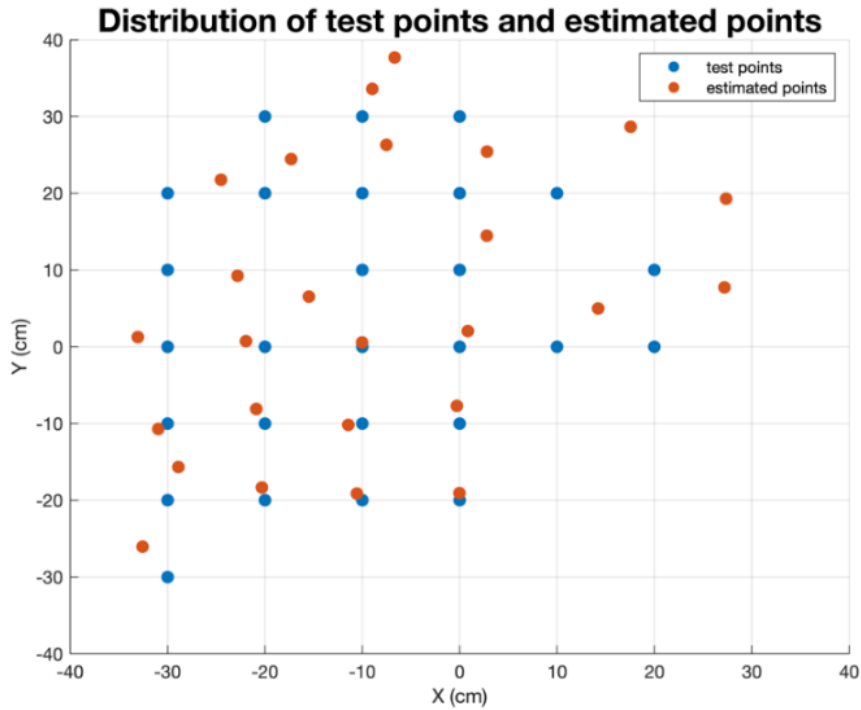


Figure 17: Distribution of test points and estimated points

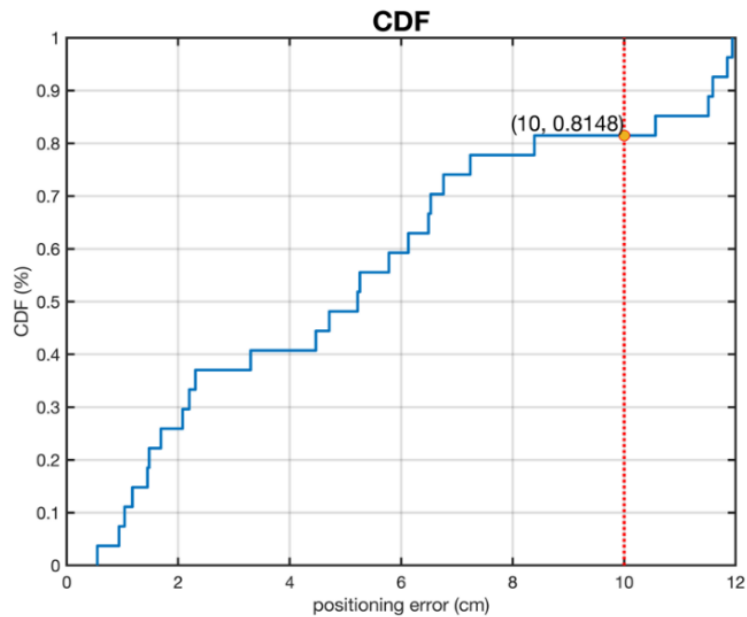


Figure 18: CDF of position error (< 10 cm)

Cumulative distribution function (CDF) plot of position error (<10 cm) is seen in Figure 18 where 81.48% estimated position error is less than 10 cm.

Inside an effective coverage area, we can get a high positioning accuracy. In order to evaluate the positioning performance and further analysis our positioning algorithm.

Based on the same algorithm, we compare the result with another real Visible light positioning proof concept platform which was built in ISEP. Table 2 summarises the average positioning errors of the two testbeds.

Table 2 – Average positioning errors comparison between the testbeds

	Positioning Performance		
	Pe_min (cm)	Pe_max (cm)	Pe_avg (cm)
BRE IoRL platform testbed with PSO	0.55	11.94	5.28
ISEP Visible light positioning testbed with fingerprint	0.45	13.94	6.19
ISEP Visible light positioning testbed without fingerprint	1.0	38	18

The positioning performances are very similar. Both testbeds could achieve a high positioning accuracy. However, ISEP testbed has a large positioning coverage (a positioning area (L*W): 2 m x 1 m). In conclusion, IoRL platform positioning area is limited by EVM effective caused by the non-linearity of the LED optical wireless channel. It could be improved by 5G NR signal power and adaptation of new LED device with a large FOV and better non-linearity characteristic. Once the 5G baseband signal power could be improved by 5G NR transmitter, the effective coverage could be improved, and meanwhile the positioning area can be enhanced.

3.2.2 Conclusions

IoRL VLC positioning system has a small coverage. This effective coverage is limited because of minimum EVM should be guaranteed for an effective VLC communication link. This limitation leads to a small positioning area. In comparing with classic RSS algorithm and enhanced RSS algorithm we used in IoRL project on ISEP positioning testbed. The positioning performances are very similar [16]. It proves that IoRL VLC positioning system can achieve a high positioning accuracy. However, ISEP testbed has a larger positioning coverage (a positioning area (L*W): 2 m x 1 m). The main reason is that IoRL platform positioning area is limited by EVM effective caused by the non-linearity of LED the optical wireless channel. In the future, it could be improved by 5G NR signal power and adaptation of new LED device with a large FOV and better Non-linearity characteristic. Once the 5G baseband signal power could be improved by 5G NR transmitter, the effective coverage could be improved, and meanwhile the positioning area can be enhanced.

3.3 mmWave Downlink Coverage Results

3.3.1 mmWave Transmit Antenna Pointing Vertically Down

Figure 19 shows sample results of coverage for one mmWave TXs EVM Test at height above ground 0.7 m (1.3 m from Tx antenna) without/with Rx Antenna angled towards Tx antenna, and Tx antenna pointing vertically down. In most areas of the coverage region the EVM $\leq 8\%$ making it suited for 64-QAM transmission (for 4-QAM this is 12% and for 16-QAM this is 10%). The propagation in the x direction (1.2m) is greater than in the y direction (0.8m) due to the physical construction of the PCB Horn Antenna where the horn slant is only applied in x direction and not in the y direction. Note that the antenna is polarised in one direction so that the transmit and receive antennas have to be oriented in the same direction so their polarisations are aligned with each other, otherwise reception is poor.

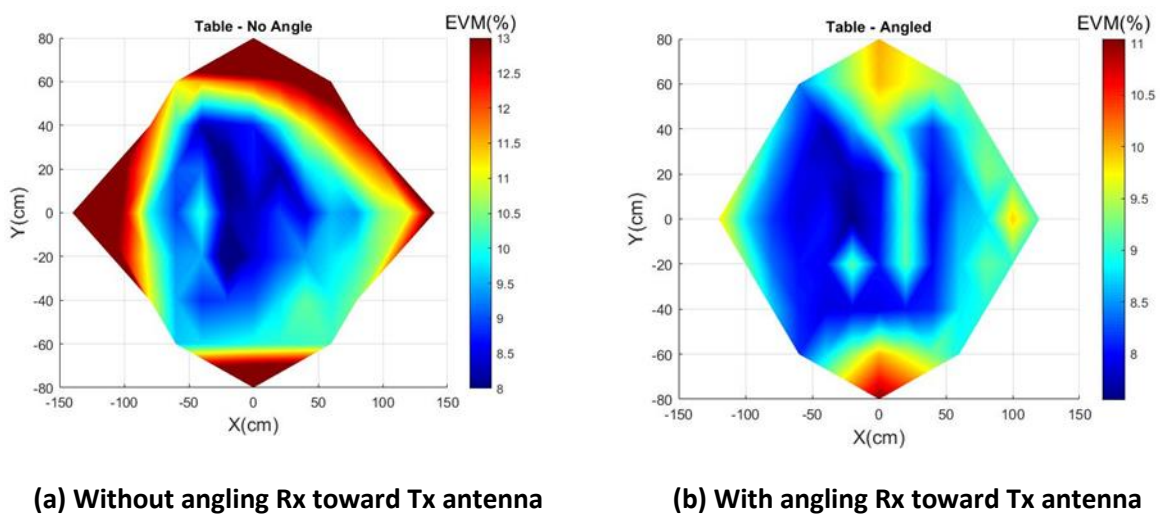


Figure 19: One mmWave TXs, receiver at 0.7m above ground EVM Test

Figure 20 shows sample results of coverage for one mmWave TXs EVM Test at height above ground 0 m (2.1 m from Tx antenna) without/with Rx Antenna angled towards Tx antenna, and Tx antenna pointing vertically down. In a lot of areas of the coverage region the EVM $\leq 8\%$ making it suited for 64-QAM transmission.

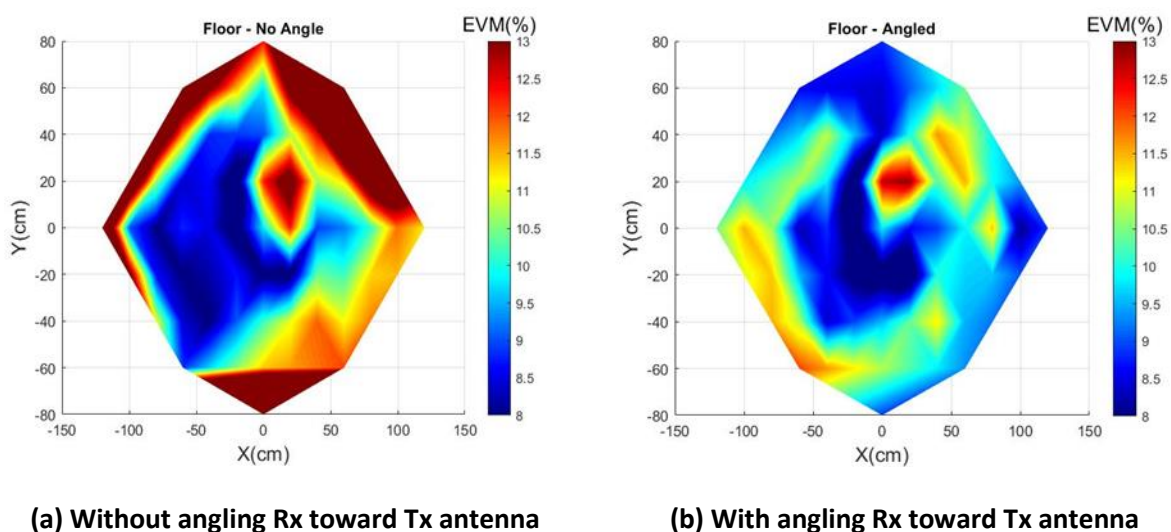
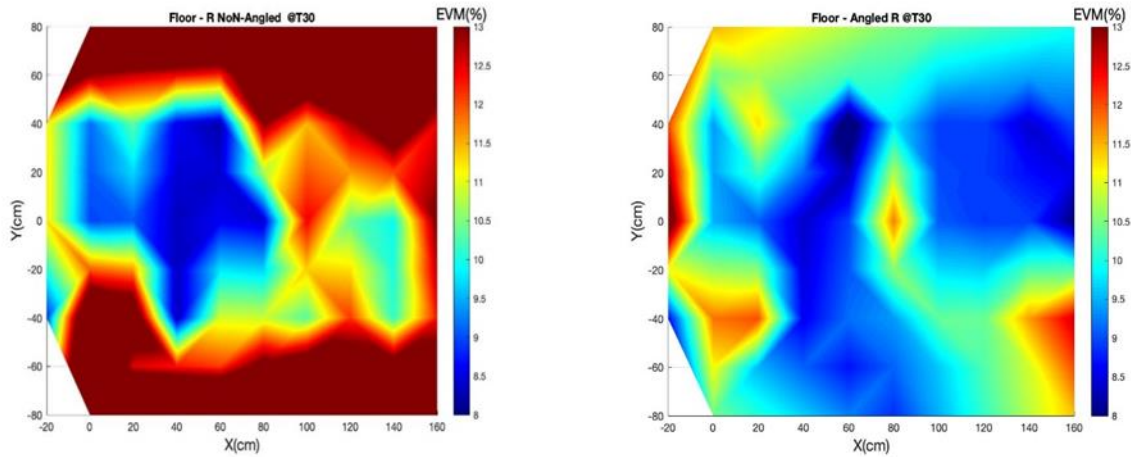


Figure 20: One mmWave TXs, receiver at 0 m above ground EVM Test

3.3.2 mmWave Transmit Antenna Pointing 30°, 40° from Vertical about antenna y-axis

Angling the transmit antenna along the room in x direction by 30 degrees and the receive antenna towards the transmit antenna produced a coverage area of at least $x = 1.6$ m by $y = 1.6$ m, as shown in Figure 21 (b), whereas without directing the receiver this is restricted to $x = 0.8$ m by $y = 1.2$ m, as shown in Figure 21 (a). These were measurements taken on 17th September 2020.

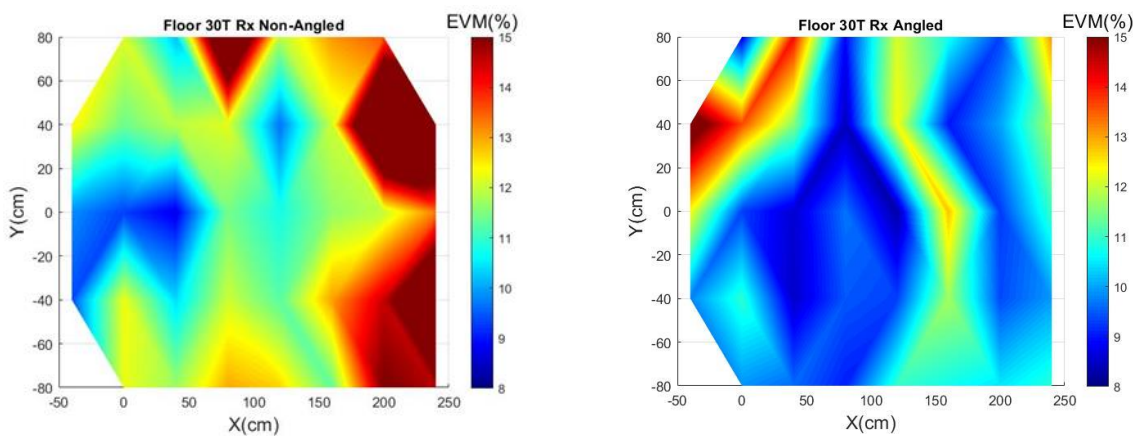


(a) Without angling Rx toward Tx antenna

(b) With angling Rx toward Tx antenna

Figure 21: One mmWave TXs angled at 30°, receiver at 0m above ground EVM Test (17-09-20)

Whereas similar measurements at 0m above ground taken on 22nd September 2020 is shown in Figure 22. This shows that the performance of the mmWave system is dependent on external factors which could not be identified.

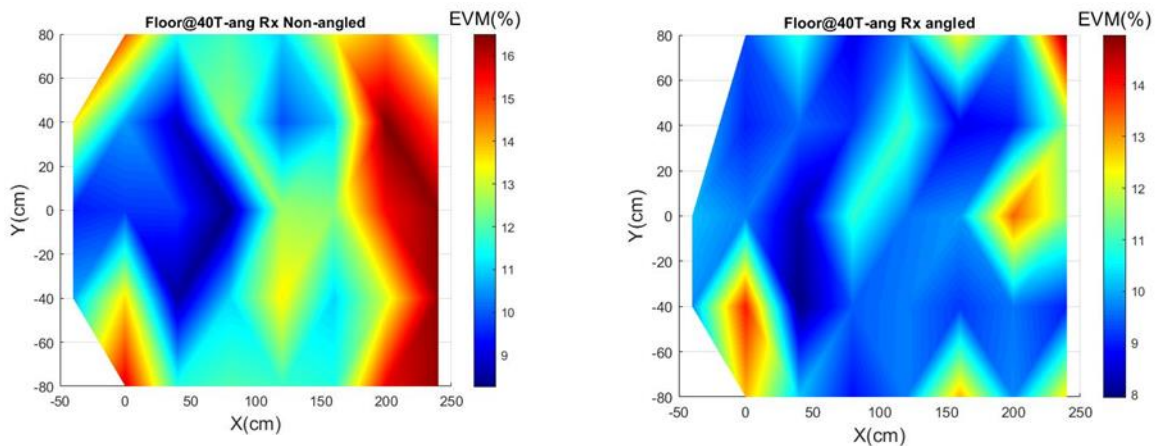


(a) Without angling Rx toward Tx antenna

(b) With angling Rx toward Tx antenna

Figure 22: One mmWave TXs angled at 30°, receiver at 0m above ground EVM Test (22-09-20)

Measurements at 0m above ground with angling of the transmit antenna along the room in x direction by 40 degrees taken on 22nd September 2020 is shown in Figure 23. This shows that the performance of the mmWave system does improve with Tx angling at 40 degrees.

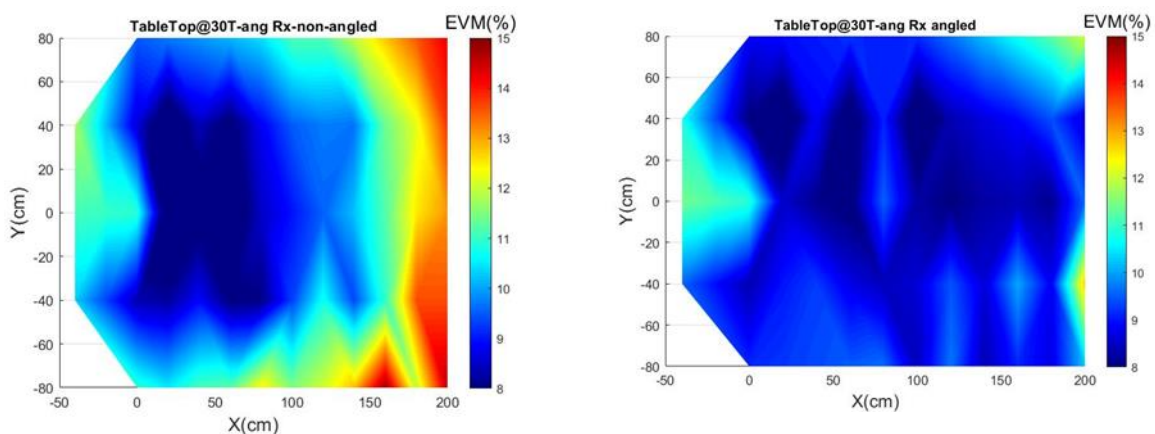


(a) Without angling Rx toward Tx antenna

(b) With angling Rx toward Tx antenna

Figure 23: One mmWave TXs angled at 40°, receiver at 0m above ground EVM Test (22-09-20)

Measurements at 0.7 m above ground taken on 23rd September 2020 is shown in Figure 24. This shows that the performance of the mmWave system does improve with Rx angling towards the Tx antenna and at location nearer to the Tx antenna.



(a) Without angling Rx toward Tx antenna

(b) With angling Rx toward Tx antenna

Figure 24: One mmWave TXs angled at 30°, receiver at 0.7 m above ground EVM Test (23-09-20)

3.3.3 mmWave Conclusions

Results from mmWave 64 QAM transmissions have shown that for a single polarization transmit antenna pointing vertically down, there was a reasonably consistent coverage area of about two meters diameter at 0.7 m above ground (1.3 m from transmit antenna) with and without angling the receive antenna towards the transmit antenna, as shown in Figure 19. There was a slight improvement of results when angling the receive antenna towards the transmit antenna. The asymmetry of the coverage performance was attributed to a glass door on one side of the coverage area, which produced mmWave reflections that impaired the performance of the receiver. An improved design of the mmWave, which more effectively processes multipath propagations, would provide more symmetric coverage performance results.

Results from mmWave 64 QAM transmissions have shown that for a single polarization transmit antenna pointing vertically down, there was a patchy coverage area of about two meters diameter at 0.0m above ground (2.0 m from transmit antenna) with and without angling the receive antenna towards the transmit antenna, as shown in Figure 20. There was no noticeable improvement of results when angling the receive antenna towards the transmit antenna. Again, the asymmetry of the coverage performance was attributed to a glass door on one side of the coverage area, which produced mmWave reflections that impaired the performance of the receiver.

When the transmit antenna was rotated towards the receive antenna at 30 degrees from the vertical, a patchy coverage area was measured, which has a width of 2.0 m and length of at least 1.6 m at 0.0 m above ground level when the receive antenna is rotated towards the transmit antenna, as shown in Figure 21 (b). When the receive antenna was not angled towards the transmit antenna, the coverage area has been reduced to a width and length of about 1m, as shown in Figure 21 (a). When the same experiment was repeated five days later on 22nd September, similar performance coverage area results were obtained but with different patchy patterns, as shown in Figure 22 (a) and Figure 22 (b), the difference of which were not able to be explained.

When the transmit antenna was rotated towards the receive antenna at 40 degrees from the vertical, a patchy coverage area was measured, which has a width of 2.0 m and length of 2.0 m at 0.0 m above ground level when the receive antenna is rotated towards the transmit antenna, as shown in Figure 23 (b). When the receive antenna was not angled towards the transmit antenna, the coverage area has a reduced width of 1.6 m and reduced length of about 1m, as shown in Figure 23 (a).

When the transmit antenna was rotated towards the receive antenna at 30 degrees from the vertical, a uniform coverage area was measured, which has a width of 2.0 m and length of more than 2.0 m (6 m as measured in laboratory) at 0.7 m above ground level when the receive antenna is rotated towards the transmit antenna, as shown in Figure 24 (b). When the receive antenna was not angled towards the transmit antenna, the coverage area has the same width but a reduced length of about 1m, as shown in Figure 24 (a).

3.4 Overall Conclusions

The level of performance that was measured for the 5G VLC communications system is more suited to very short range Near Field Communication (NFC) applications such as that required for transmission to passengers on seating within aircraft and trains or for controlling home devices such as washing machines and TVs from smart phones. Performance of the VLC communications system would have to increase propagation distance by a factor of 3 to 6m and increase the coverage area by a factor of six to 6 meters for it to be a general-purpose communications competitor to the mmWave communication system in indoor environments. Furthermore, enhancements to the PD receiver would also be required so that it has the multidirectional photo sensing properties of a fly's eye, which could possibly be achieved using a Fresnel lens at the receiver.

The level of performance that was measured for the 5G mmWave communications system has shown the viability of a 5G networked home since just four mmwave radio heads would be required to provide sufficient coverage for a family sized sitting room, whilst also providing sufficient numbers of mmWave radio access point to be able to measure location. The best position of these radio heads are at the four corners of the room pointing at 30

degrees from the vertical towards the centre of the room. The transmit antenna would be required to be enhanced so that it is circular or polarized or at the least provide both vertical and horizontal polarized antennas transmitters. Further experiments need to be performed from four transmit antennas to show that this man made multipath environment does away with the requirement of angling the receive antenna towards any one transmit antenna to obtain improved performance, which would be physically impossible to achieve when simultaneously transmitting the same radio signal from four different transmit antennas at the same time.

4 EMF Exposure Analysis – Modelling and Measurements

This section addresses electromagnetic field (EMF) radiation levels of the mmWave system and compare them with associated human exposure limits. For the purpose of this assessment, combined field from all sources at a given location (ambient fields) will also be determined. All fixed permanently installed RF sources operating between 27 MHz and 6 GHz will be identified and reasonable endeavours shall be applied to recognise all RF emissions between 6 GHz and 40 GHz.

This work gives an indication of the estimated levels of risk associated with the scenarios modelled. However, this work should not be taken as any kind of approval for such products to be placed for sale on the market. Any manufacturers placing such products on the market should go through the necessary product approval processes to meet the necessary regulations and standards, including any national standards and guidance, and perform their own assessments of their specific system specifications. International Committee on Non-Ionizing Radiation Protection (ICNIRP) guidelines are used worldwide, either directly or as the basis for national regulations. These ICNIRP levels have been used in this report as a reference level. It is recognised that there are some variations in some national regulations, and these should be taken into account for any product manufacturers looking to take products to market.

The emissions from other wireless devices in addition to IoRL were included in the calculations to give estimates of other background field strength levels. However, this report is only assessing the potential impact of the IoRL devices with respect to human exposure limits, not any other wireless devices.

Some calculations use a number of worst-case assumptions, such as the contributions from all devices being in-phase and all with 100% activity. These results should not be taken as a representation of actual field strengths that would be experienced in practice. Measurements were made of actual devices which took into account how the devices operate in practice.

Due to practicality, the EMF evaluation was carried out for the Home Scenario only. It comprised the simulation model for the Home, which employed Computational Electromagnetics principles to predict estimated radiated electric field strength. In addition, in-situ, measurements were performed using a broadband field meter, capable of detecting the same parameter. The electric field strengths were captured with flat frequency response probes, allowing the measurement values to be assessed against an environmental or occupational safety guidelines and recommendations.

4.1 Background

The following background information is referenced from IEC 62232.

4.1.1 Quantities, units and interaction mechanisms

4.1.1.1 Physical quantities

Table 3 - Physical quantities [1]

Symbol	Quantity	Unit	Dimension
a	Attenuation coefficient	reciprocal metre	m^{-1}
B	Magnetic flux density	tesla	$\text{T}, \text{V s m}^{-2}$
c_h	Specific heat capacity	joule per kg per K	$\text{J kg}^{-1} \text{K}^{-1}$
E	Electric field strength	volt per metre	V m^{-1}
f	Frequency	hertz	s^{-1}
H	Magnetic field strength	ampere per metre	A m^{-1}
J	Current density	ampere per square metre	A m^{-2}
T	Temperature	Kelvin	$\text{K}, ^\circ\text{C}$
ϵ	Permittivity	farad per metre	F m^{-1}
λ	Wavelength	metre	m
μ	Permeability	henry per metre	H m^{-1}
S	Power density	watts per square metre	W m^{-2}
Ω	Resistance	Ohm	V A^{-1}
ρ	Mass density	kilogram per cubic metre	kg m^{-3}
σ	Electric conductivity	siemens per metre	S m^{-1}

4.1.1.2 Constants

Table 4 - Constants [1]

Symbol	Physical Constant	Magnitude
c	Speed of light in vacuum	$2,997\,9 \times 10^8 \text{ m s}^{-1}$
$\eta_0 (Z_0)$	Impedance of free space	$376,730\,3 \, \Omega$ (approx. $120\pi \, \Omega$)
ϵ_0	Permittivity of free space	$8,854\,188 \times 10^{-12} \text{ F m}^{-1}$
μ_0	Permeability of free space	$4\pi \times 10^{-7} \text{ H m}^{-1}$

4.1.1.3 Specific absorption rate (SAR)

Time derivative of the incremental electromagnetic energy (dW) absorbed by (dissipated in) an incremental mass (dm) contained in a volume element (dV) of given mass density (ρ) [1].

4.1.1.4 Exposure ratio ER (Wt)

Ratio of the exposure metric and the relevant exposure limit, both expressed in terms of power (at a given location and for each operating frequency of the considered RF sources).

$$\text{EXAMPLE ER} = S/S_{\text{lim}}, \text{ ER} = \max[(E/E_{\text{lim}})^2, (H/H_{\text{lim}})^2]$$

Note: The exposure ratio can also be expressed as a percentage, i.e. ER % = ER (dimensionless) × 100 %.

4.1.2 Human exposure to time-varying electric, magnetic and electromagnetic fields

The International Commission on Non-Ionizing Radiation Protection (ICNIRP) provides scientific advice and guidance on the health and environmental effects of non-ionizing radiation (NIR) to protect people and the environment from detrimental NIR exposure. Non-ionizing radiation refers to electromagnetic radiation such as ultraviolet, light, infrared, and radio waves. ICNIRP guidelines are mentioned in nearly every electro-magnetic radiation (EMR) standard or paper internationally.

High Frequency (HF) is the term used to describe that part of the electromagnetic spectrum comprising the frequency range from 100 kHz to 300 GHz. At high frequency, the electric and the magnetic fields, which together make up the electromagnetic field (EMF), are interrelated and considered jointly for measurements.

To link the problem with this project, we would clarify that mmWaves, correspond to the range of frequencies located between 30 and 300 GHz (wavelengths from 10 mm to 1 mm). Many applications exist and are emerging in this band, including wireless telecommunications, imaging and monitoring systems. As more and more systems come online and are used in everyday applications, the possibility of inadvertent exposure of personnel to mmWaves increases.

The critical effect of HF exposure relevant to human health and safety is heating of exposed tissue. All RF fields can penetrate into the body (the higher the frequency, the lower the penetration depth) and cause vibration of charged or polar molecules inside. This results in friction and thus heat [2].

4.1.2.1 Field Regions

In the far-field region, an electromagnetic field is predominantly plane wave in character. This means that the electric and magnetic fields are in phase, and that their amplitudes have a constant ratio. Furthermore, the electric fields and magnetic fields are situated at right angles to one another, laying in a plane, which is perpendicular to the direction of propagation. It is often taken that far-field conditions apply at distances greater than $2D^2/\lambda$ where D is the maximum linear dimension of the antenna (see Figure 25 below) [3].

However, care must be exercised when applying this condition to broadcast antennas for the following reasons:

- it is derived from considerations relating to planar antennas;
- it is assumed that D is large compared with λ .

Where the above conditions are not met, a distance greater than 10λ should be used for far field.

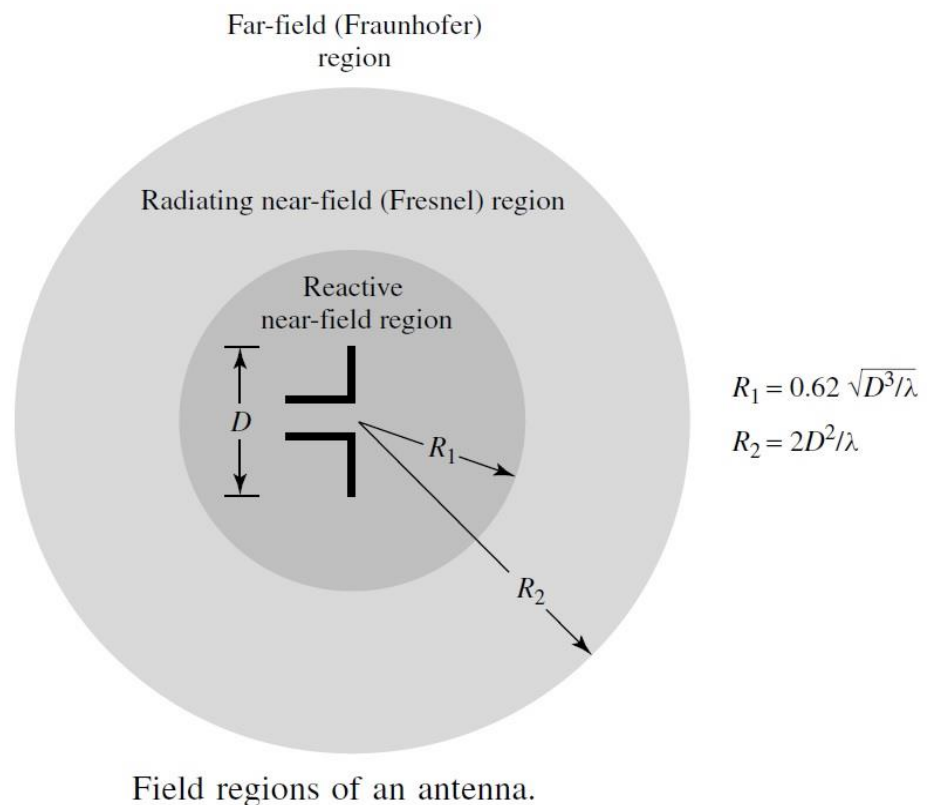


Figure 25: Field Regions of an antenna

Following from the above, taking the maximum linear dimension of the antenna and exploring that the fact that, for frequency of 40 GHz, the wavelength $\lambda = 7.495$ mm, we have calculated the Far Field conditions apply at distance greater than 54 cm.

These were necessary calculations in order to distinguish, if the simulation area was part of the Near Field region of the electric field around the antenna. The near-field region is complicated, because the maxima and minima of E (Electric) and H (Magnetic) fields do not occur at the same points along the direction of propagation as they do in the far field.

Using analytical formulas, an estimation of the field strength in the near field is only feasible for simple ideal radiators such as the elementary dipole. In the case of more complex antenna systems, other mathematical techniques must be used to estimate field strength levels in the near-field region. These other techniques allow relatively precise estimations of the field strength, the power density and other relevant characteristics of the field, even in the complex near-field region.

The above regions are shown in **Figure 25** (where D is supposed to be large compared with the wavelength λ) and the main properties of an electromagnetic field in different field regions are shown in **Table 5**.

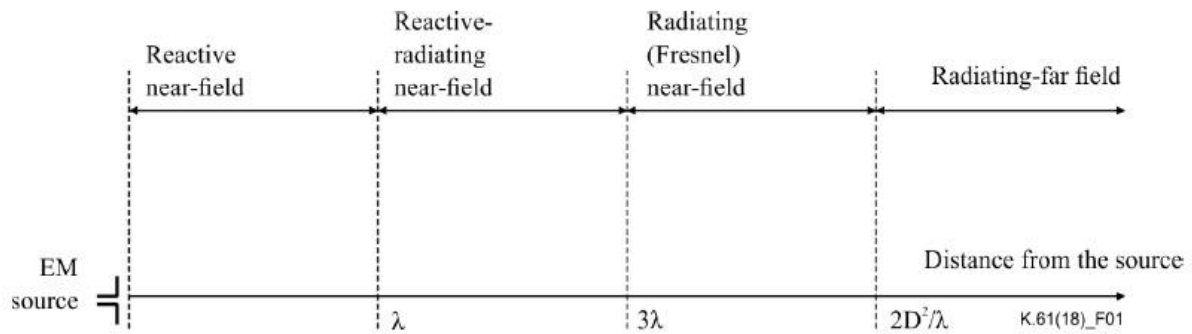


Figure 26: Field regions around an EM source (the antenna maximum dimension D is supposed to be large compared with the wavelength λ) [4]

Table 5 – Main properties of electromagnetic field in different field regions [4]

	Reactive near-field	Reactive-radiating near-field	Radiating near-field	Radiating far-field
Inner boundary	0	λ	3λ	Max (3λ ; $2D^2/\lambda$)
Outer boundary	λ	3λ	Max (3λ ; $2D^2/\lambda$)	∞
Power density S [W/m ²]	$S \leq E H $	$S \leq E H $	$S \leq E H $ $= \frac{ E ^2}{Z_0} = Z_0 H ^2$	$S = E H $ $= \frac{ E ^2}{Z_0} = Z_0 H ^2$
$E \perp H$	No	No	Locally	Yes
$Z = E/H$	$\neq Z_0$	$\neq Z_0$	$\approx Z_0$	$= Z_0$

4.1.2.2 Basic restrictions and limits

Exposure standards usually refer to electric and magnetic component of the field, or power density limits. They are individually measured only when it is required by the field properties related to the field regions. Power density, S , i.e., the power per unit area normal to the direction of propagation, is related to the electric and magnetic fields, by the impedance of free space.

There is no international consensus on the EMF exposure limits, but WHO (World Health Organization) recommends the adoption of limits based on the ICNIRP and IEEE C.95.1 guidelines. Nevertheless, national regulations have priority. Exposure limits in various countries can be found on the WHO website: <http://www.who.int/gho/phe/emf/legislation/en/>.

In most cases, the EMF exposure limits are based on ICNIRP or IEEE C95.1 standard, that are based on the scientific research and currently available knowledge.

Exposure limits are defined for the general public (uncontrolled environment) and for occupational exposure (controlled environment) (see Table 6). It is understandable that exposure limits for the general public are more conservative (restrictive) than those for occupational exposure.

Table 6 - Approximate comparison between groups and locations selected in the standards

	IEEE/ANSI	ICNIRP
Groups	No	General Public Occupationally exposed people
Locations	Controlled (Awareness of exposed people) Uncontrolled (No awareness)	No

Two kinds of guidance exist: 1) basic restrictions based directly on established adverse health effects; 2) reference levels provided for practical exposure assessment purposes, to determine whether basic restrictions are likely to be exceeded.

The reference levels as exposure limits are used in all the countries that regulate exposure limits. In contrast, basic restrictions may be defined differently. For example, instead of SAR the energy loading value as the quantity for basic restriction is used, time and space averaging procedures are different, or instead of the average a maximum value over certain space and/or time is used, etc.

As mentioned above the ICNIRP guidelines are used worldwide, either directly or as the basis for national regulations. These ICNIRP levels have been used in this report as a reference level. It is recognised that there are some variations in some national regulations, and these should be taken into account for any product manufacturers looking to take products to market. In those countries where the regulations concerning human protection against non-ionizing radiation do not exist, the guidelines give the opportunity to take some protective measures. As previously mentioned, national regulations have priority and could possibly feature limits that are lower than limits used in this report. Thus, the ICNIRP guidelines constitute a reliable and established reference basis for applications, discussion and further development of the domain. A similar role can be played by the IEEE guidelines [IEEE C.95.1]. For this reason, both ICNIRP and IEEE/ICES limits are given for information in this section [5].

Most documents provide safety limits in terms of basic restrictions and reference (or derived) levels. The basic restrictions address the fundamental quantities that determine the physiological response of the human body to EMFs. Basic restrictions apply to a situation with the body present in the field. The basic restrictions for human exposure are expressed as the specific absorption rate (SAR), specific absorption (SA) and current density.

As the basic restrictions are difficult to measure directly, most documents provide derived reference levels for electric field, magnetic field and power density. The reference levels apply to a situation where the assessment of electromagnetic field is not influenced by the presence of a body. If we are well into the near field zone, then the presence of a person’s head might well influence the electromagnetic field.

Reference levels may be exceeded if the exposure condition can be shown to produce SAR, SA and induced current density below the basic limits.

In establishing exposure limits, the International Commission on Non-Ionizing Radiation Protection recognizes the need to reconcile a number of differing expert opinions. The validity of scientific reports has to be considered, and extrapolations from animal experiments to effects on humans have to be made. The restrictions in these guidelines

were based on scientific data alone; currently available knowledge, however, indicates that these restrictions provide an adequate level of protection from exposure to time-varying EMF [6].

Standards and guidelines give “basic limits” for contact current, current density and SAR and are reported in Table 7, together with measuring conditions [3].

Table 7 - Comparison of basic biological restrictions (SAR limits) and reference levels (current parameters)

Parameter	IEEE/ANSI		ICNIRP	
	Controlled	Uncontrolled	Occupational	General public
RMS induced or contact current (mA)	$1\,000 f$ (13a)	$450 f$ (13a)	100 (2)	45 (2)
	100 (1), (13b)	45 (1), (13b)	40 (3)	20 (3)
Current density RMS (A/m^2) Averaging area (cm^2) Averaging times	$350 f$ 1 1 (4)	$15.7 f$ 1 1 (4)	$10 f$ 1 (4)	$2 f$ 1 (4)
Whole-body-average (W/kg) SAR	0.4 (5a)	0.08 (5b)	0.4 (5a)	0.08 (5a)
Local SAR (W/kg) Averaging mass (kg)	8 (13c) 0.001 (6)	1.6 (13c) 0.001 (6)	10 (13d) 0.001 (5a), (7)	2 (13d) 0.01 (5a), (7)
Local SAR ⁽⁷⁾ (W/kg) Averaging mass (kg)	20 (13c) 0.010 ⁽⁸⁾	4 (13c) 0.010 ⁽⁸⁾	20 (13d) 0.01 ^{(5a), (9)}	4 (13d) 0.01 ^{(5a), (9)}
Power density (W/m^2) Averaging time (min)			50 $68/f^{1.05}$ (12), (13)	10 $68/f^{1.05}$ (12), (13)

f : frequency in MHz (unless otherwise stated).

- (1) Current through each foot. f : frequency (MHz).
- (2) Current induced in any limb (10-110 MHz).
- (3) Contact current from conductive objects (100 kHz-110 MHz).
- (4) Current density over any $1\,cm^2$ area of tissue.
- (5) a) The SAR limits relate to an averaging time of 6 min.
b) The SAR limits relate to an averaging time as given in Table 8.
c) The SAR limits relate to an averaging time of 15 min.
- (6) Localized SAR except for the hands, wrists, feet and ankles (100 kHz-6 GHz).
- (7) Localized SAR for head and trunk (100 kHz-10 GHz).
- (8) Localized SAR for the hands, wrists, feet and ankles (100 kHz-6 GHz).
- (9) Localized SAR for limbs (100 kHz-10 GHz).
- (10) Localized SAR for head, neck, trunk and foetus (10 MHz-10 GHz).
- (11) 10 g for the head and foetus; 100 g for the neck and trunk.
- (12) For frequencies between 10 and 300 GHz. f : frequency (GHz).

- (13) Averaged over any 20 cm² of exposed area:
- a) 3 kHz < *f* < 100 kHz
 - b) 100 kHz < *f* < 100 MHz
 - c) 100 kHz < *f* < 6 GHz
 - d) 100 kHz < *f* < 10 GHz.

The direct measurement of the current density and specific absorption rate can be made using “Phantom heads” in specialised laboratories. Therefore, derived levels are given in addition to the basic limits, in the standards and guidelines considered here (see **Table 8**, **Table 9** and **Table 10**). Values show the maximum level respectively of E, H and power density in various bands in the frequency range 1 kHz 300 GHz. The limits are calculated under the conservative assumption of optimum electromagnetic coupling between the EMF and the body [3].

Table 8 - Comparison of derived levels; E field (RMS values V/m) *

Frequency range	IEEE/ANSI		ICNIRP	
	Controlled	Uncontrolled	Occupational	General public
0.6-3 kHz				
3-30 kHz	614		610 (1)	87
30-38 kHz				
38-65 kHz				
65-100 kHz				
100-410 kHz				
410-600 kHz				
600-610 kHz				
610-680 kHz				
680-920 kHz				
0.92-1 MHz				
1-1.34 MHz				
1.34-3 MHz	614	823.8/ <i>f</i>	610/ <i>f</i>	87/ <i>f</i> ^{0.5}
3-10 MHz	1 842/ <i>f</i>	823.8/ <i>f</i>		
10-12 MHz				
12-30 MHz				
30-60 MHz	61.4	27.5	61	28
60-100 MHz				
100-137 MHz				
137-200 MHz				
200-300 MHz				
300-400 MHz				
400-800 MHz				
0.8-1.1 GHz				
1.1-1.55 GHz			3 <i>f</i> ^{0.5}	1.375 <i>f</i> ^{0.5}
1.55-2 GHz				
2-3 GHz				

Frequency range	IEEE/ANSI		ICNIRP	
	Controlled	Uncontrolled	Occupational	General public
3-15 GHz			137	61
15-300 GHz				

f: frequency (MHz, unless otherwise stated).

* Values should be averaged over 6 min, except as shown below:

a) $f^2/0.3$

b) 30 min

⁽¹⁾ This value is in the range 0.82 kHz to 1 MHz.

⁽²⁾ Plane wave equivalent value of the E field.

Table 9 - Comparison of derived levels; H field (RMS values A/m) ^{(1), (2)}

Frequency range	IEEE/ANSI		ICNIRP	
	Controlled	Uncontrolled	Occupational	General public
1-3 kHz				
3-30 kHz	163			5 ⁽³⁾
30-38 kHz				
38-65 kHz				
65-100 kHz				
100-140 kHz	16.3/ <i>f</i>		1.6/ <i>f</i>	0.73/ <i>f</i>
140-150 kHz				
150-535 kHz				
535-610 kHz				
610-680 kHz				
0.68-1 MHz				
1-1.34 MHz				
1.34-3 MHz				
3-10 MHz				
10-12 MHz				
12-30 MHz	16.3/ <i>f</i>	158.3/ <i>f</i> ^{1.668} (1a))	0.16	0.073
30-60 MHz				
60-100 MHz	0.163	0.0729 (1b))		
100-137 MHz				
137-200 MHz				
200-300 MHz			0.008 <i>f</i> ^{0.5}	0.0037 <i>f</i> ^{0.5}
300-400 MHz				
400-800 MHz				
0.8-1.1 GHz				
1.1-1.55 GHz				
1.55-2 GHz				

2-3 GHz				
3-15 GHz			0.36	0.16
15-300 GHz				

f: frequency (MHz, unless otherwise stated).

⁽¹⁾ Values should be averaged over 6 min, except as shown below:

- a) $0.0636 f^{1.337}$ min
- b) 30 min.

⁽²⁾ Plane wave equivalent value of the H field based on power density values given for adults.

NOTE – These values are not given explicitly in the same way as the E field and power density values are specified.

⁽³⁾ This value is valid in the range 0.8 kHz to 150 kHz

Table 10 - Comparison of derived levels; power density (W/m²)⁽³⁾

Frequency range	IEEE/ANSI ⁽¹⁾				ICNIRP	
	Controlled		Uncontrolled		Occupational	General public
	E field	H field	E field	H field		
<100 Hz						
0.1-1 kHz						
1-3 kHz						
3-30 kHz						
30-100 kHz	1 000	10×10^6	1 000	10×10^6		
100-410 kHz						
0.41-1 MHz	1 000	$10^5 f^2$	1 000	$10^5 f^2$		
1-1.34 MHz						
1.34-3 MHz	1 000	$10^5 f^2$	$1 800/f^2$ (2), (3a))	$10^5 f^2$ (2)		
3-10 MHz						
10-12 MHz	$9 000/f^2$	$10^5 f^2$	$1 800/f^2$ (2), (3b))	$10^5 f^2$ (2)	10	2
12-30 MHz						
30-60 MHz			2 (2), (3b))	$(9.4 \times 10^6)/f^{8.336}$ (2), (3c))		
60-100 MHz	10	$10^5 f^2$				
100-137 MHz						
137-200 MHz	10		2 (3b))			
200-300 MHz						
300-400 MHz						
400-800 MHz						
0.8-1.1 GHz	$f/30$		$f/150$		$f/40$	$f/200$
1.1-1.55 GHz			(3b))			
1.55-2 GHz						
2-3 GHz						
3-15 GHz	100		$f/150$ (3d))		50	10
15-300 GHz	$100^{(3e)}$					

f: frequency (MHz, unless otherwise stated).

⁽¹⁾Below 100 MHz, plane-wave equivalent values are given for the E and H fields.

⁽²⁾As given by some commercially available meters.

⁽³⁾Values should be averaged over 6 min, except as shown below:

- a) $f^2/0.3$ min
- b) 30 min
- c) $0.0336 f^{1.337}$ min
- d) $90\,000/f$ min
- e) $616\,000/f^{1.2}$ min.

UK NRPB sections are removed from the above tables, since this project is international and such standards are more appropriate in this case.

4.1.3 Computational Electromagnetics

There are many methods of calculation with varying degrees of accuracy and complexity. It is advised to use the simplest appropriate method for the exposure assessment. The choice is highly dependent on the field region in which points of investigation are located in relation to the radiating source [5].

4.1.3.1 Required data

Exposure assessment by calculation in all cases requires information concerning radiating sources. In general, the more detailed the information, the more accurate are the results of calculations. These data are required for each operating (or planned) frequency. The required data put in order of growing level of accuracy of the exposure assessment by calculation are presented below.

The minimum data required for calculation, which leads to the most conservative approach, are:

- operating frequency;
- distance to the transmitting antenna;
- maximum equivalent isotropic radiated power (EIRP).

The next step in improving accuracy is obtaining:

- radiation patterns of the transmitting antenna.

Additional details can be found in [IEC 62232], [ITU-R BS.1698], [ITU-R BS.1195], [ITU-T K.70] and [b-EN 50413] [5].

4.1.3.2 Calculation methods

There are several methods useful for determining compliance with exposure limits:

- 1) finite-difference time-domain (FDTD);
- 2) multiple-region finite-difference time-domain (MR/FDTD);
- 3) ray tracing model;
- 4) hybrid ray tracing/FDTD methods; and
- 5) near-field antenna models such as method of moments (MOM) and the numeric electromagnetic code (NEC) [4].

The selection of the appropriate numerical method depends on the following factors:

- 1) the field zone where the exposure evaluation is required;

- 2) the quantities being evaluated (SAR or reference fields); and
- 3) the topology of the environment where the exposure occurs.

The selection criteria are summarized in Table 11:

Table 11 - Selection of numerical techniques [4]

Field Zone	Topology	Evaluated quantity	Suitable numerical technique
Near-field	Open	Field	FDTD, MOM
Near-field	Open	SAR	FTDT
Near-field	Closed, multiple scatterers	Field	FDTD, MOM
Near-field	Closed, multiple scatterers	SAR	FDTD, MR/FDTD
Far-field	Open	Field	Ray tracing, MOM
Far-field	Multiple scatterers (complex urban environment)	Field	Ray tracing

MoM is used to numerically solve integral equation formulations of Maxwell's equations. In principle, the radiated electromagnetic fields are obtained by following a two-step procedure.

a) First, structures which are represented with a mesh are replaced by equivalent currents. A matrix is derived which represents the effect of each element/segment on each other segment/element and the surface currents are solved.

b) Secondly, these currents are integrated to obtain the electric and magnetic fields at the points of interest.

More detailed information on numerical techniques can be found in [IEC 62232].

4.1.3.3 Electrical properties of tissue

There have been several investigations into the electrical characteristics of various tissue types [c.4 [7]]. In most cases, these were published for specific frequencies or ranges of frequencies. It has been shown that these properties vary with frequency and values have been interpolated between frequencies and tissue types when modelling. It is also possible that further interpolation and/or averaging of property values is required to match the exact tissue characterisation of particular anatomical models.

Gabriel, et al., made an extensive evaluation of this in published papers and reports during 1995/1996. The work included new measurements, a comparison of existing literature and an algorithm to calculate the properties across a wide range of frequencies [7]. This is generally accepted to be the most comprehensive work on the subject, at the date of issue of this standard. A significant proportion of current modelling work uses these values as a basis, supplementing them with information from previous work where appropriate. The

uncertainties grow larger at the ends of the frequency range and this has to be taken into consideration. Further information can be found in the referenced document.

Work continues in this field, however, and this may produce new results in the future.

It must be noted that some tissue types are anisotropic (i.e., have different properties in different directions). It is not always possible to model this effect, however, and so an average (or similar) value is used in the model.

The table of values provided here (Table 12) [c.4 [7]] was obtained from calculations made by the Electromagnetic Wave Research Institute of the Italian National Research Council, based on the algorithms provided in the Gabriel report to the Brooks AFB. These tables are example values, which may be used or interpolated for numerical modelling purposes. More precise values, at specific frequencies, may also be obtained from the quoted references or work of a similar nature.

Table 12 - Conductivity of tissue types [7]

Conductivity (S/m)										
Frequency	10 Hz	100 Hz	1 kHz	10 kHz	100 kHz	1 MHz	10 MHz	100 MHz	1 GHz	10 GHz
Tissue type										
Air	0,00	0,00	0,00	0,00	0,00	0,00	0,00	0,00	0,00	0,00
Aorta	0,25	0,28	0,31	0,31	0,32	0,33	0,34	0,46	0,73	9,13
Bladder	0,20	0,21	0,21	0,21	0,22	0,24	0,27	0,29	0,40	3,78
Blood	0,70	0,70	0,70	0,70	0,70	0,82	1,10	1,23	1,58	13,13
Bone (cancellous)	0,08	0,08	0,08	0,08	0,08	0,09	0,12	0,17	0,36	3,86
Bone (cortical)	0,02	0,02	0,02	0,02	0,02	0,02	0,04	0,06	0,16	2,14
Bone (marrow)	0,00	0,00	0,00	0,00	0,00	0,00	0,01	0,02	0,04	0,58
Brain (grey matter)	0,03	0,09	0,10	0,11	0,13	0,16	0,29	0,56	0,99	10,31
Brain (white matter)	0,03	0,06	0,06	0,07	0,08	0,10	0,16	0,32	0,62	7,30
Breast fat	0,02	0,02	0,02	0,02	0,03	0,03	0,03	0,03	0,05	0,74
Cartilage	0,16	0,17	0,17	0,18	0,18	0,23	0,37	0,47	0,83	9,02
Cerebellum	0,05	0,11	0,12	0,13	0,15	0,19	0,38	0,79	1,31	9,77
Cerebro spinal fluid	2,00	2,00	2,00	2,00	2,00	2,00	2,00	2,11	2,46	15,38
Cervix	0,30	0,41	0,52	0,54	0,55	0,56	0,63	0,74	0,99	10,05
Colon	0,01	0,12	0,23	0,24	0,25	0,31	0,49	0,68	1,13	11,49
Cornea	0,41	0,42	0,42	0,44	0,50	0,66	0,87	1,04	1,44	11,33
Duodenum	0,51	0,52	0,52	0,53	0,54	0,58	0,78	0,90	1,23	13,31
Dura	0,50	0,50	0,50	0,50	0,50	0,50	0,54	0,74	0,99	8,58
Eye sclera	0,50	0,50	0,50	0,51	0,52	0,62	0,80	0,90	1,21	11,31
Fat	0,01	0,02	0,02	0,02	0,02	0,03	0,03	0,04	0,05	0,59
Gall bladder	0,90	0,90	0,90	0,90	0,90	0,90	0,90	1,01	1,29	12,53
Gall bladder bile	1,40	1,40	1,40	1,40	1,40	1,40	1,40	1,54	1,88	15,36
Heart	0,05	0,09	0,11	0,15	0,22	0,33	0,50	0,73	1,28	11,84
Kidney	0,05	0,10	0,11	0,14	0,17	0,28	0,51	0,81	1,45	11,57
Lens	0,26	0,26	0,26	0,27	0,28	0,30	0,43	0,56	0,83	8,53

Liver	0,03	0,04	0,04	0,05	0,08	0,19	0,32	0,49	0,90	9,39
Lung (deflated)	0,20	0,21	0,22	0,24	0,27	0,33	0,44	0,56	0,90	10,12
Lung (inflated)	0,04	0,07	0,08	0,09	0,11	0,14	0,23	0,31	0,47	4,21
Mucous membrane	0,00	0,00	0,00	0,00	0,07	0,22	0,37	0,52	0,88	8,95
Muscle	0,20	0,27	0,32	0,34	0,36	0,50	0,62	0,71	0,98	10,63
Nerve	0,02	0,03	0,03	0,04	0,08	0,13	0,22	0,34	0,60	6,03
Oesophagus	0,51	0,52	0,52	0,53	0,54	0,58	0,78	0,90	1,23	13,31
Ovary	0,31	0,32	0,32	0,33	0,34	0,36	0,46	0,75	1,34	9,82
Pancreas	0,05	0,10	0,11	0,14	0,17	0,28	0,51	0,81	1,45	11,57
Prostate	0,41	0,42	0,42	0,43	0,44	0,56	0,78	0,91	1,25	12,38
Skin (dry)	0,00	0,00	0,00	0,00	0,00	0,01	0,20	0,49	0,90	8,01
Skin (wet)	0,00	0,00	0,00	0,00	0,07	0,22	0,37	0,52	0,88	8,95
Small intestine	0,51	0,52	0,53	0,56	0,59	0,86	1,34	1,66	2,22	12,69
Spinal cord	0,02	0,03	0,03	0,04	0,08	0,13	0,22	0,34	0,60	6,03
Spleen	0,04	0,10	0,10	0,11	0,12	0,18	0,51	0,80	1,32	11,38
Stomach	0,51	0,52	0,52	0,53	0,54	0,58	0,78	0,90	1,23	13,31
Tendon	0,25	0,30	0,38	0,39	0,39	0,39	0,41	0,49	0,76	10,34
Testis	0,41	0,42	0,42	0,43	0,44	0,56	0,78	0,91	1,25	12,38
Thymus	0,51	0,52	0,52	0,53	0,54	0,60	0,72	0,79	1,08	12,13
Thyroid	0,51	0,52	0,52	0,53	0,54	0,60	0,72	0,79	1,08	12,13
Tongue	0,26	0,27	0,27	0,28	0,29	0,39	0,57	0,67	0,98	11,08
Trachea	0,30	0,30	0,30	0,31	0,34	0,37	0,46	0,55	0,80	8,54
Uterus	0,20	0,29	0,49	0,51	0,53	0,56	0,75	0,94	1,31	12,49
Vacuum	0,00	0,00	0,00	0,00	0,00	0,00	0,00	0,00	0,00	0,00
Vitreous humor	1,50	1,50	1,50	1,50	1,50	1,50	1,50	1,50	1,67	15,13

4.1.4 Measurements of electromagnetic fields

4.1.4.1 Required data

In general, measurements can be done without complete knowledge of the radiating sources if proper equipment that covers the full range of frequencies is available, knowing at least the range of frequencies to be measured. If measurements are made with wideband equipment (without frequency selection or shaped response), the results of such measurement will be conservative, because it requires the use of the limit value, which is more restrictive. In all cases of measurements, the information concerning the radiating sources is very helpful and makes the measurements more accurate and reliable.

The following data are very helpful during measurements (for each radiating source):

- operating frequency – this allows use of a probe that has a band covering all operating frequencies;
- distance to the transmitting antenna – this allows one to determine the field region (for each operating frequency) and to choose a proper measurement procedure;

- maximum equivalent radiated power (ERP) – this allows estimation of the required dynamic range of the measurement equipment and the expected levels of the measured values;
- whether the antennas are operating at the maximum transmitter power at the time of the measurements;
- modulation characteristics – especially pulsed, intermittent or continuous operation.

Usually this information can be obtained from the documentation of the transmitting systems. Some data can be obtained during the site inspection (e.g., distances to the transmitting antennas, operating frequencies based on the types and sizes of the transmitting antennas) [5].

4.1.4.2 Evaluation process

The measurement of external fields regarding human exposure assessment depends upon the objective. In the first instance it may be that the measurements are simply to assess compliance with external field strength reference level values contained in exposure guidelines. For some guidelines additional information may be required to enable calculation of the spatial averaging of inhomogeneous field distributions. In other cases, detailed field distribution data may be needed to provide input to other analytical or computational techniques for assessing compliance with the basic quantities underpinning guidelines. The approaches used, and the spatial resolution of instrumentation used to carry out these tasks may differ substantively.

The appropriate evaluation process for this project is for in-situ RF exposure assessment (See Clause 6 of [1]).

The in-situ RF exposure evaluation or assessment shall be performed at one location or area, known as the measurement area.

The process shall start by identifying all relevant fixed and permanently emitting RF source installations in the surrounding area. The measurement system(s) and the post processing shall cover the RF emissions from the product and all relevant ambient sources between at least 100 kHz and 300 GHz as determined by the site analysis.

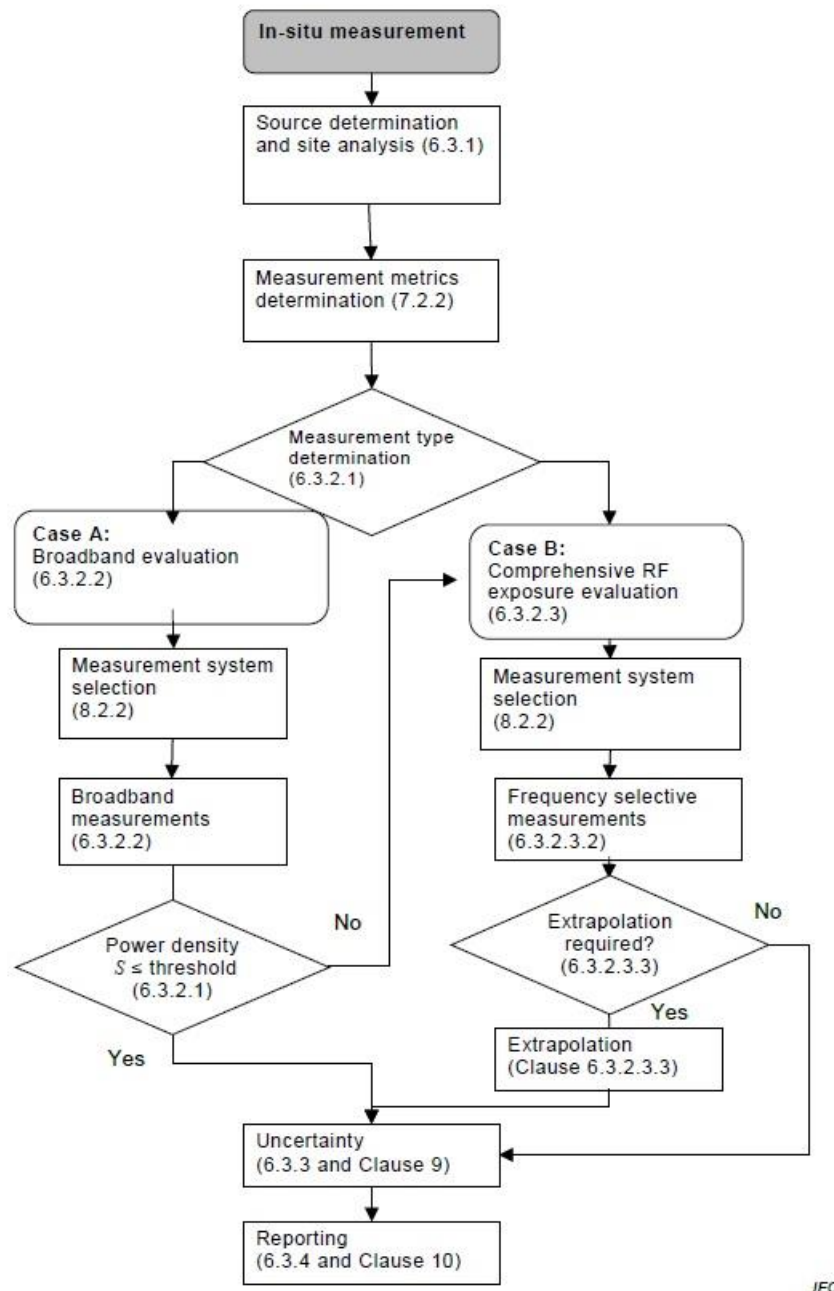


Figure 27: Alternative routes to evaluate in-situ RF exposure [1]

Next step is to choose between two evaluation approaches, known as Case A and Case B as indicated in Figure 27. Case A provides a set of results covering all sources and frequencies at one measurement area. Case B provides separate sets of field values for each source, frequency or frequency sub-band present in the measurement area.

The choice of the measurement type depends on the objective of the in-situ evaluation.

- If the objective is to provide a global evaluation of RF exposure level from all sources together “as observed” (i.e. no extrapolation, no signal spectrum differentiation) then the evaluation shall start with Case A evaluation. However, if the power density assessment based on Case A is above applicable RF exposure limits (i.e. the threshold defined under Case A in Figure 27 is the applicable exposure limits) or if it is

necessary or desired to investigate the contribution from each RF source, the Case A evaluation shall be complemented by a Case B evaluation.







- If the objective is to provide a detailed evaluation of RF exposure levels (i.e. combining the contributions of all RF sources, spectrum differentiation above a certain threshold), the evaluation shall start using Case A. If the power density level is above 10 mW/m^2 (i.e. threshold defined under Case A in Figure 27), the Case A evaluation shall be complemented by a Case B evaluation. However, if there are pre-existing national requirements, a different threshold between 5 mW/m^2 and 100 mW/m^2 may be used. Further, some national requirements may specify one method or another.
- If the objective is to provide a comprehensive evaluation of RF exposure, i.e. investigating every contribution from RF sources using a frequency selective analysis, then a Case B evaluation shall be conducted. It is recommended that a Case B evaluation is preceded by a Case A evaluation [1].

It is recommended to use first the simplest method (i.e., broadband RF EMF measurement). If the measured exposure level is not in compliance with the reference level, then the frequency selective RF EMF measurement should be used to get more accurate results. If there is still no compliance with the exposure limit, then the most sophisticated method based on the SAR measurement against basic restrictions may be used.

Additional details can be found in [IEC 62232], [ITU-T K.61] and [ITU-R BS.1698] [5].

Table 13 presents tabular view of guidance on selecting between broadband and frequency selective measurements [Annex A [1]].

Table 13 – Guidance on selecting between broadband and frequency-selective measurement

Broadband (see B.3.1.2.3)		Frequency-selective (see B.3.1.2.4)
<p><u>Indication of total field:</u> A broadband measurement can provide a simple means to indicate the total field and may require care in certain circumstances to ensure that the results are correctly interpreted and presented:</p> <ul style="list-style-type: none"> • no frequency discrimination required; • precise knowledge/control of evaluation parameters; • as indicative evaluation – for example, an initial scan to find the peak field using a broadband probe can be followed by a more detailed measurement using a frequency-selective instrument. 		<p><u>Indication of total field:</u> Frequency-selective measurement is required when frequency discrimination is required, for example:</p> <ul style="list-style-type: none"> • to evaluate constant part of transmitted signal for extrapolation (see F.4); • to evaluate frequency weighting for exposure ratio.
<p><u>Comparison with a limit:</u></p> <p>Where the field strengths are significantly below the relevant limit.</p> <p>Where the RBS is the single dominant source and either as an “as observed” evaluation without extrapolation is required; or, the output power of the RBS is controlled during the measurement.</p>		<p><u>Comparison with a limit:</u> Identifying and evaluating single and multi-frequency signals for comparison with a limit.</p> <p>Where extrapolation is required from a constant level part of the signal in the presence of other signals.</p>
		<p><u>Limit exceedance:</u> In case of any doubt, or when the purpose is to confirm that a limit has been exceeded, the frequency-selective method is recommended.</p>
		<p><u>Signal discrimination:</u> A frequency-selective method is essential for evaluating individual frequency bands or signal types. This includes identifying ambient fields for either inclusion or exclusion from final processing and reporting of results.</p>
		<p><u>Low level fields:</u> Identifying and measuring signals in low RF field strength environments (e.g. public areas).</p>
<p>NOTE 1 The term “frequency-selective” is used rather than “narrow band” to imply the ability to discriminate between frequencies. The term “broadband” is used when a wide spectrum range is measured simultaneously without frequency discrimination. An instrument which can indicate the RF field strength from a logical channel (e.g. using a channel decoder) is also deemed to be “frequency-selective”.</p>		

4.1.4.3 Broadband measurement

Broadband measurements give the sum of all signals over the frequency range of the probe without distinguishing the contribution of different frequencies (whether from the EUT or from ambient sources). These may give an instantaneous or time-averaged field strength value.

The method gives an informative environmental field strength reading as observed at the time of measurement and is adequate for monitoring the RF field.

A broadband measurement is suitable for determining overall levels in the environment and may be helpful in determining if a more comprehensive measurement using the frequency selective method is required.

Extrapolation of broadband measurement results is not recommended. Such extrapolation can result in a vast overestimation depending on the characteristics of the probe and the characteristics of the EUT/ambient signals. Therefore frequency-selective measurements are recommended where accurate extrapolation is required [Annex B [1]].

Broadband measurement of the RF EMF in the far field region is the simplest measurement method for compliance assessment. In this method, the sum of the RF EMF contributions (electric or magnetic field depending on probe type) from all the radio sources within a wide frequency range is measured. Problems may occur if the radio sources operating outside frequency range of the probe are present. On the market there are electric field probes available that cover these frequency bands, for example, from 100 kHz to 6 GHz or 3 MHz to 18 GHz.

For broadband measurement, the exposure ratio corresponding to the most restrictive reference level at the considered frequency range has to be taken, unless the measurement device incorporates a weighting function consistent with the exposure limits. This means that the broadband measurement usually gives conservative results.

The broadband measurements are simpler and less time consuming than the frequency selective ones but tend to be less sensitive for measurement of low-level exposures. Even though they are less accurate, however, they can be applied in many cases. If the exposure level is not compliant with the limit, then the frequency selective measurements are required.

Additional information can be found in [IEC 62232] [5].

If several frequencies (and varying modulations) are present in the frequency range to be observed, either the peak value or the r.m.s. values (irrespective of signal shape) can be measured directly with appropriate broadband measuring equipment.

4.2 Modelling

As part of the evaluation process that was planned, software modelling took place. This section explains the choice of software, preparing of the simulation model and yielded results.

4.2.1 Software selection

Two electromagnetic simulation software packages were considered, FEKO and WinProp from Altair. Link: <https://www.altair.com/feko-applications/>.

FEKO is a comprehensive computational electromagnetics (CEM) software used widely in the telecommunications, automobile, aerospace and defence industries. FEKO offers several frequency and time domain EM solvers, including MoM and FDTD. Hybridization of these methods enables the efficient analysis of a broad spectrum of EM problems, including antennas, microstrip circuits, RF components and biomedical systems, the placement of antennas on electrically large structures, the calculation of scattering as well as the investigation of electromagnetic compatibility (EMC).

FEKO and WinProp are used globally across multiple industries including aerospace, defence, automotive, communications, and consumer electronics to reduce the time-to-market. FEKO addresses the broadest set of high-frequency electromagnetics applications, allowing teams

to optimize wireless connectivity, including 5G, ensure electromagnetic compatibility (EMC), and perform radar cross section (RCS) and scattering analysis.

Due to the complex nature of near field, a software simulation is preferred over measurements. In the near field, the electromagnetic field structure may be highly inhomogeneous, and there may be substantial variations from the plane-wave impedance of 377 ohms; that is, there may be almost pure electric (E) fields in some regions and almost pure magnetic (H) fields in others. Exposures in the near field are more difficult to specify, because both fields must be measured and because their field patterns are more complex.

Full wave analysis techniques (e.g. methods requiring Maxwell's equations to be solved anywhere) are essentially used when high accuracy is desired for the evaluation of RF fields, for example for RF field strength, power density or SAR evaluation in source region I (the reactive near-field of the antenna(s)) where ray tracing methods cannot be employed with sufficient accuracy. An accurate and realistic numerical model of the antenna shall be created for a full wave field analysis.

Method of Moments (MoM) or finite-difference time-domain (FDTD) method is used to numerically solve integral equation formulations of Maxwell's equations. In principle, the radiated electromagnetic fields are obtained by following a two-step procedure.

a) First, structures which are represented with a mesh are replaced by equivalent currents. A matrix is derived which represents the effect of each element/segment on each other segment/element and the surface currents are solved.

b) Secondly, these currents are integrated to obtain the electric and magnetic fields at the points of interest.

4.2.2 Simulation Model preparation

Two models were prepared for each of the two components of the chosen Altair's software product: WinProp and FEKO. A model the size of a house, would be very computationally expensive for FEKO, if the solver of choice was method of moments. That is not the case for WinProp, which uses ray tracing as a method of solving. Therefore, the idea was to use a suitable approach to compute complex near field – method of moments, and ray tracing method for the far field region.

4.2.2.1 Initial house model

A detailed model of the house was created in the form of IFC (industry foundation class) file – see **Figure 28**.

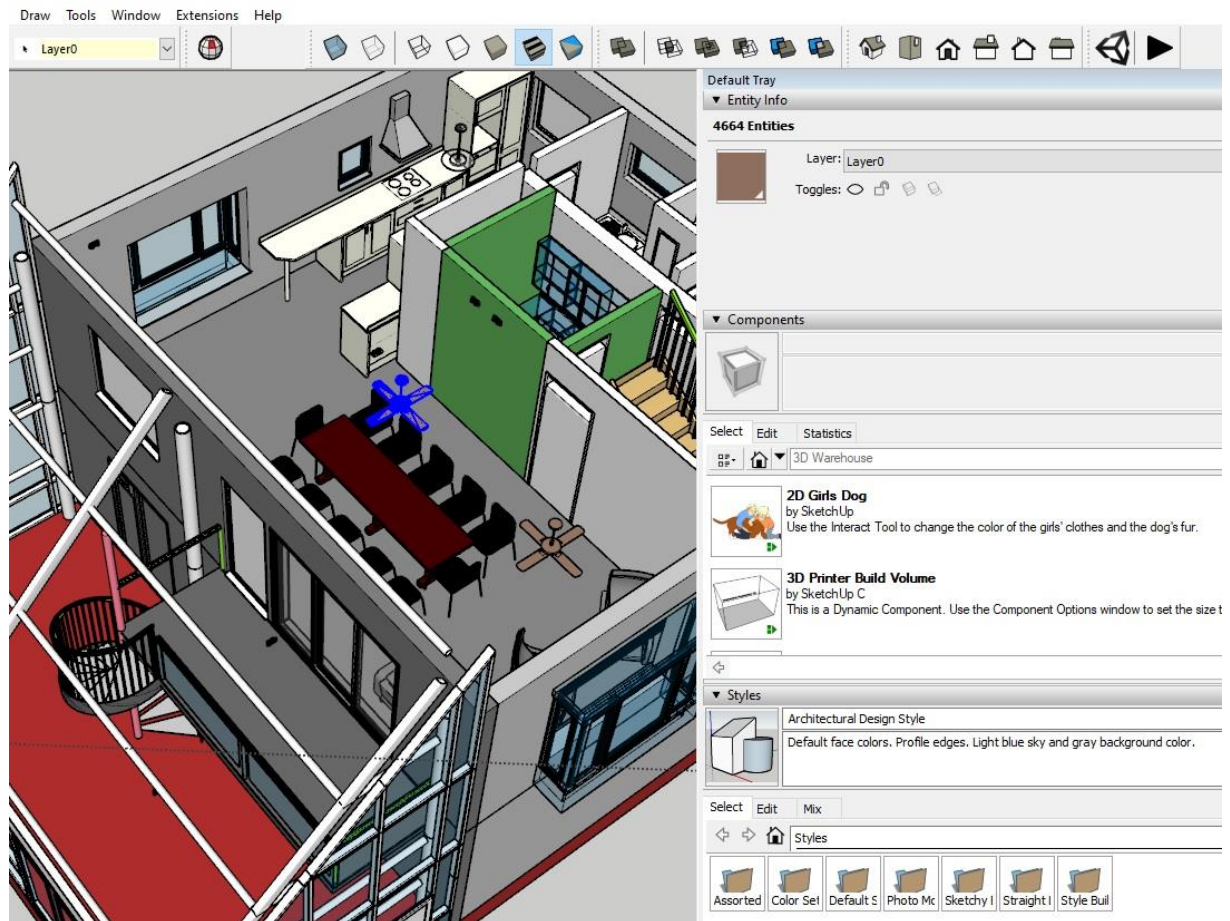


Figure 28: Detailed model of house used in home scenario

This model was not suited for the purpose of computation electromagnetics simulation for the following reasons:

- **Level of detail.** Generally, a low-polygon representation of any structure is essential for sensible computation time and resource. As seen from the illustration, the exploded light element alone equals to 4664 entities. Many objects had to be omitted or redesigned to a simpler shape.
- **Accuracy of presented building materials.** On the contrary, a great level of detail was required for representing the exact structure of walls, slabs, windows, furniture, etc. For instance, the walls in this house are made of multiple layers of insulation materials, plasterboard, wood and air (cavity), which are not reflected in this model.
- **Dimensional accuracy of model.** The house was measured with a calibrated laser range finder to detect any discrepancies in dimensions, specifically on the upper-ground floor, where the system was planned to be installed. According to what was found at this stage and the requirements of the previous point, necessary adjustments were made.
- **Material partitioning.** Finally, all objects were grouped and prepared to be assigned with their respective building material – concrete, metal, plasterboard, wood, glass, Si (silicon for the solar PV on roof), etc. Each solid in the model was attached to a corresponding layer, which layer would later be utilised (see Figure 29).

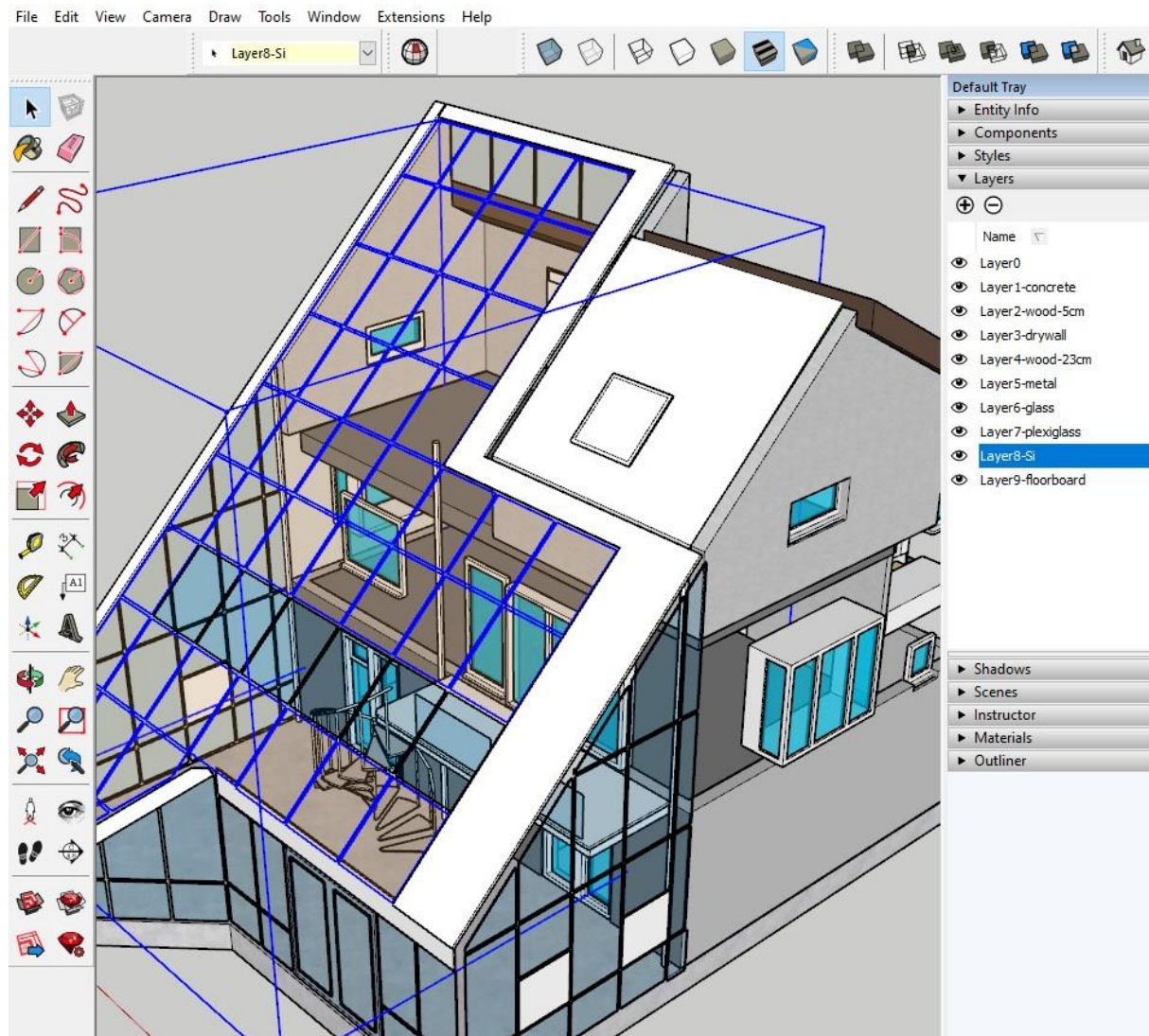


Figure 29: Simplified model of house used in home scenario with layers representing used building materials

- File export.** There was extensive research on what format we should use, and which one is best used for this situation. IFC file is not compatible and cannot be imported directly into WinProp. AutoCAD® drawing databases in the *.dwg and *.dxf format can be converted to WinProp building databases. Following extensive testing, the targeted export format was chosen to be *.dxf. Major advantage was the retaining of material layers, which was not present with *.dwg. However, not all object categories available in AutoCAD®, are supported by the converter. The following list shows the AutoCAD® object categories supported by the converter module (see Figure 30).

AutoCAD® object categories	Indoor mode	Urban mode	Overlay mode
Proxy Objects ²⁾	✓	✓ ¹⁾	✓
2D Polyline	-	✓ ^{1),3)}	✓
2D Solid	✓	✓	✓
3D Box	-	-	-
3D Face	✓	-	✓
3D Mesh	-	-	-
3D Polyline	✓	✓ ¹⁾	✓
3D Solid	-	-	-
3D Sphere	-	-	-
3D Surface	-	-	-
Arc	✓	-	✓
Arc aligned text	-	-	-
Circle	✓	✓	✓
Donut	-	-	-
Ellipse	✓	✓	✓
Hatch	✓	-	✓
Line	✓	-	✓
MLine	-	-	-
MText	-	-	-
MInsertBlock	-	-	-
PolyFaceMesh	✓	-	✓
Polygone	✓	✓ ¹⁾	✓
PolygonMesh	-	-	-
Polyline	✓	✓ ¹⁾	✓
Text	-	-	✓

Figure 30: WinProp Supported object categories

Notes:

- 1) The AutoCAD® objects must have a closed form, in order to be converted to urban buildings.
- 2) The current version supports polyline and polygon proxy objects.
- 3) The AutoCAD® objects must have a height value assigned for a correct conversion.
 - **File import.** The REVIT-made IFC file had to be translated to *dxf file format, ready for WinProp import, with all the amendments described above in place. Extra care was taken during file conversions, as potential data loss was possible. SKETCHUP PRO was used as intermediate platform to link the model between REVIT and WinProp. The polished final *dxf file was AutoCAD® Version 2013.

4.2.2.2 WinProp

Wave propagation and radio network planning software WinProp consists of a number of packages, of which three were used for this prediction simulation: WallMan (wall manager), Aman (antenna manager) and ProMan (propagation manager).

4.2.2.2.1 WallMan

The model from Figure 29 was imported into WallMan and converted to an Indoor database. The following preparation steps were performed prior to pre-processing the model:

- **Simplify Database.** Further Simplification of Objects in the Indoor may be required. It is recommended to use the Simplify function to make indoor databases, which consist of very many polygons, simpler. Adjacent polygons are combined, if they are located in the same plane. This means, all of their corners must be in the same plane and the normal vectors must point in the same direction.
- **Define Material Properties for Objects in the Database.** In WallMan, every object has its own properties. The consideration of the different material properties of the buildings/walls has a significant influence on the results of the wave propagation models. Therefore, for each object (i.e. building in urban databases and wall/subdivision in indoor databases) the corresponding material properties should be assigned. The handling of the different materials in a so-called material catalogue is explained in the following. The consideration of different materials is even more important for the indoor scenarios (as there is a large spectrum of wall properties concerning thickness and material). Because the electrical properties of the materials depend on the frequency, individual electrical properties for different frequency bands were defined (see Figure 31). A full list of electrical properties of used materials for each frequency can be found in Annex B - Table 19, Table 20, Table 21 and Table 22 [8].

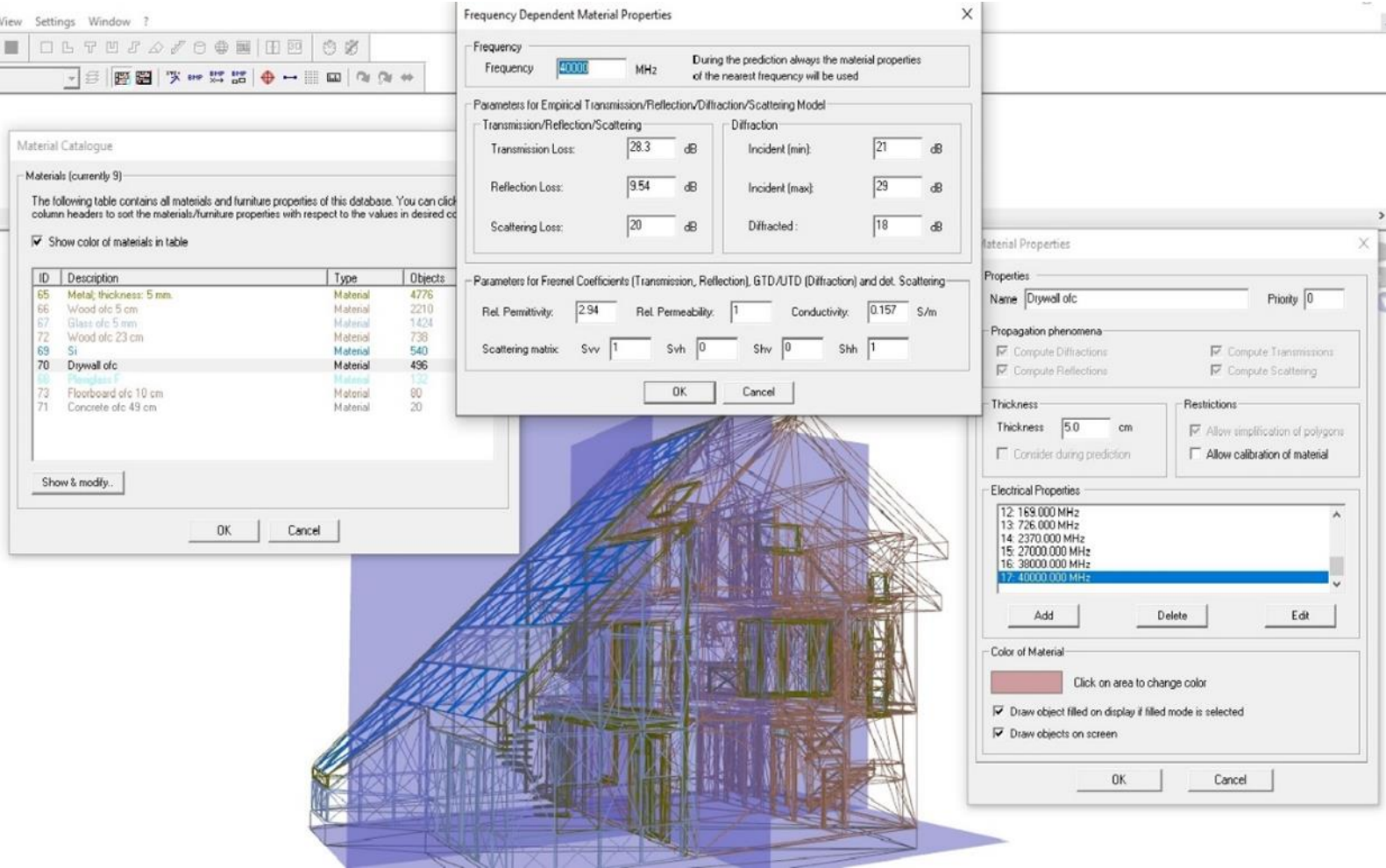


Figure 31: Electrical material properties within WallMan environment

Additionally, multiple data sources were explored, to get as accurate as possible electric material propagation properties. Example is illustrated in the Figure 32 below.

Material	Description	Source	ϵ_r Measured at Frequency [MHz]	Losses Computed for Frequency [MHz]	ϵ_r'	ϵ_r''	μ_r	Conductivity [S/m]	Thickness of Wall or Object [m]
<i>Losses computed for Frequency f:</i>				40000 MHz					
Concrete									
Concrete	Dry without Steel	Lah94b	1800	40000	5	0.4	1.0	0.8889	0.2
Concrete	40 Years Old	Zol93	1500	40000	4.5	0.3	1.0	0.6667	0.2
Foam Concrete	Siporex	Zol93	1500	40000	2.3	0.15	1.0	0.3333	0.2
Concrete		VAD98	200	40000	6	0.8	1.0	1.7778	0.2
Roam Concrete	Siporex	VAD98	200	40000	2.5	0.15	1.0	0.3333	0.2
Concrete	Medium	EPMCC99	1000	40000	6	0.7	1.0	1.5556	0.2
Concrete	Heavy	EPMCC99	1000	40000	9	0.9	1.0	2.0000	0.31
Concrete	Light	EPMCC99	1000	40000	2	0.5	1.0	1.1111	0.1
Cement		Megla62	1000	40000	3.35	0.01	1.0	0.0222	0.1

Figure 32: Building materials - propagation properties

- Set Prediction Planes.** The simulation of this model was performed over three prediction planes: 0.7 m, 1.2 m, and 1.8 m above Upper Ground floor level. The prediction plane essentially is an infinitely thin horizontal slice across the model, for which the strength of electric field is simulated (predicted). In addition to this, three vertical predictions planes were added: 1.29 m (to coincide with mmWave antenna placed in the home), 1.5 m and 3.10, from nearest window inwards. This was to account for vertical distribution of energy from the source of mmWave transmitter, which was mounted 20 cm from the ceiling and directed downwards.
- Indoor database pre-processing.** Nearly all wave propagation predictions require a few computations that are different for each database but exactly the same for all transmitters. For example, the visibility relations between objects never change. No matter what kind of antenna pattern or how much output power the transmitter uses. To decrease computation times WallMan performs such computations just once for each database so that ProMan can use this computation for the actual predictions later.

The pre-processing for the empirical prediction models consists of a check of the different objects within the building database. Both the definition of each single object itself and the interaction between different objects are verified. In the urban mode the pre-processing for the vertical plane models (COST 231 Walfisch-Ikegami, knife edge diffraction model) determines also the pixels which are located inside the buildings.

The pre-processing for the Standard Ray Tracing performs the same building check as for the empirical models. Additionally, for the urban mode the visibility relations between walls can be computed and stored, which increases the computation time of the pre-processing slightly but reduces the time of the prediction. The pre-processing for the Intelligent Ray Tracing (IRT) requires a longer computation time, because detailed visibility relations are computed and stored in a file. This procedure reduces the computation time of the prediction significantly and was chosen as most preferable and suitable from all other available options.

Resolution of grid/matrix for the model was selected to be very high (0.06 meters), so that the result display is extra refined and more accurate. This value defines the basic resolution (in meters) the prediction will be computed with. The smaller the resolution, the higher the computation time and the higher the size of the IRT database, because the visibility relations for more pixels must be computed. This setting does not influence the resolution the building geometry is processed with. The building geometry is always processed at the highest precision.

4.2.2.2 AMan and FEKO

Antenna patterns were required to accurately characterise the mmWave modules in the project, together with the directional 4G LTE transmitters, used as part of creating the multi-source radiating environment that typically exist around urban smart home. All IoT devices in this model were represented using generic omnidirectional (isotropic) antenna patterns.

The selected example of LTE aerial was the LTE-XPOL-002-V2 directional LTE MIMO antenna, which provides future proof solution for 4G/3G and 2G networks. Its pattern is illustrated below – see Figure 33, and the file used in simulations was created in AMAN, using manufacturer data.

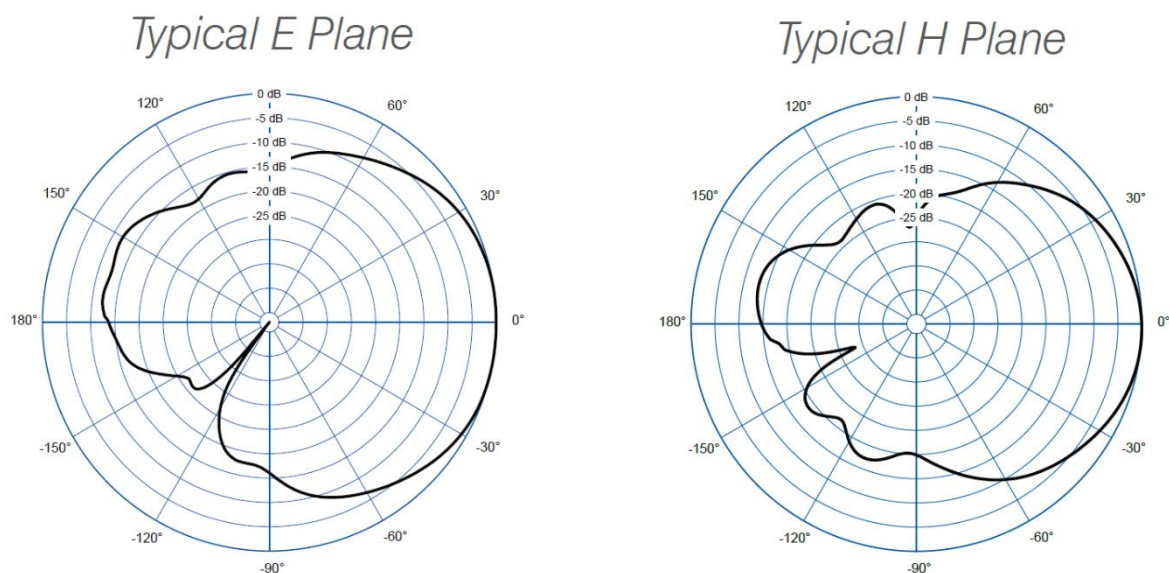


Figure 33: LTE-XPOL-002-V2 directional LTE MIMO antenna pattern

The mmWave antenna pattern data was received in the format of CSV files. It was then converted in FEKO, in order to be applied in ProMan – see Figure 34 and Figure 35.

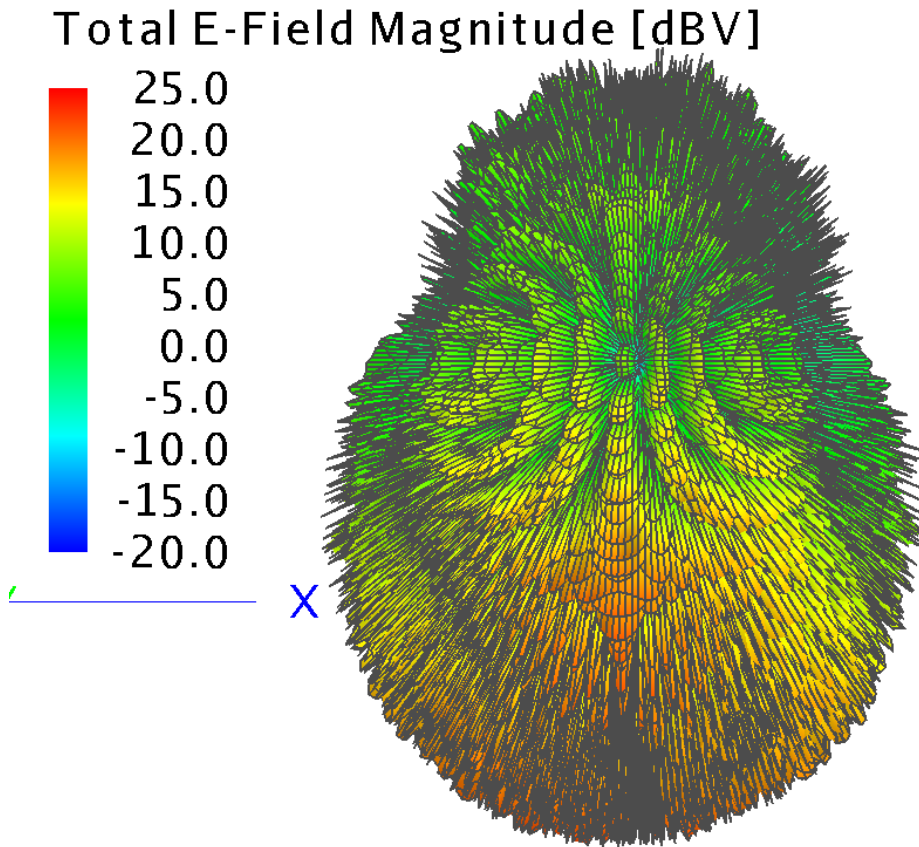


Figure 34: IoRL mmWave antenna pattern in FEKO (dBV)

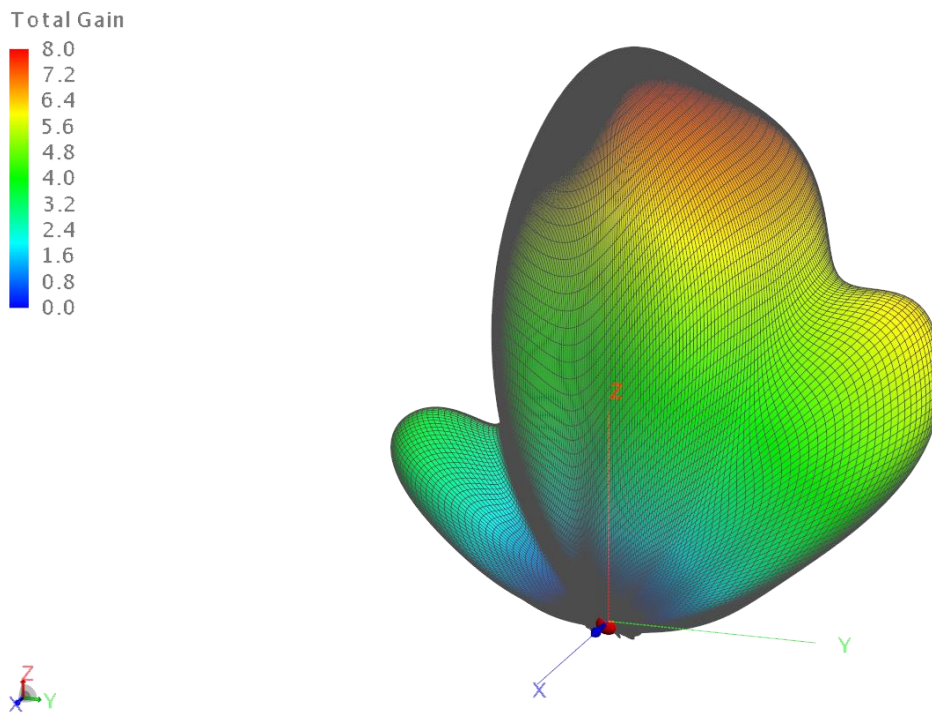


Figure 35: IoRL mmWave antenna pattern in FEKO (Gain)

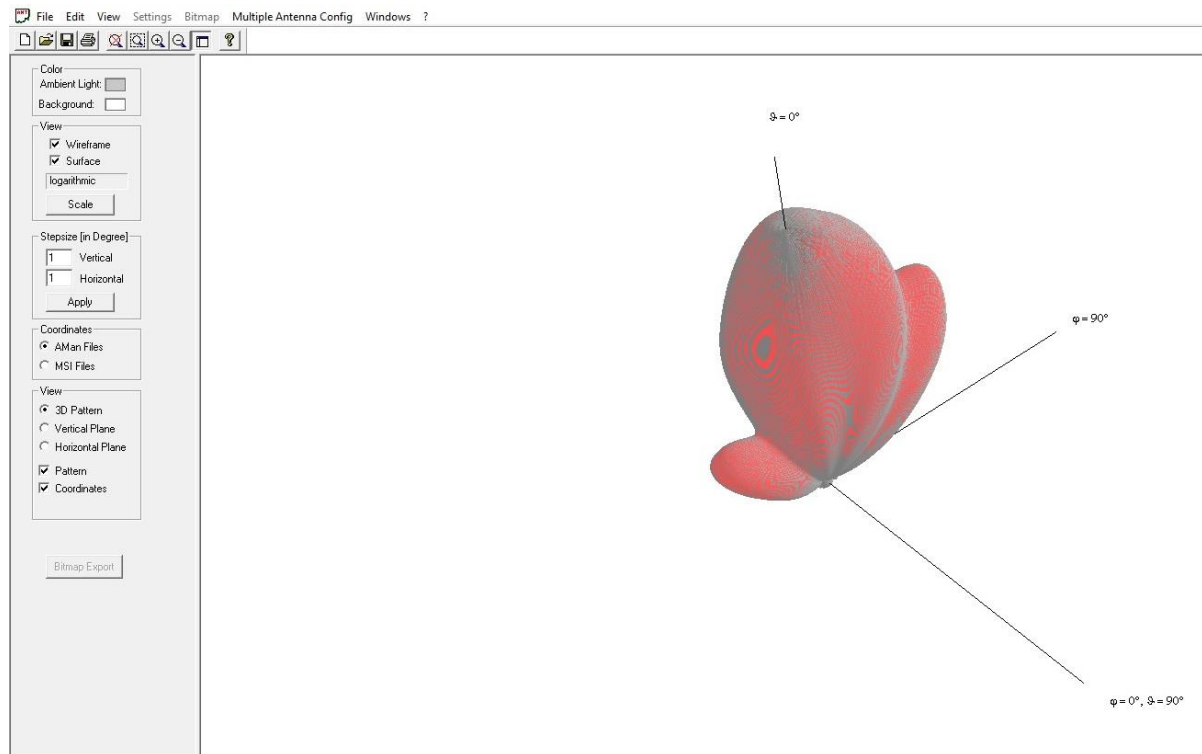


Figure 36: IoRL mmWave antenna pattern in AMan

Technical specifications for the IoRL mmWave module can be found in Del. 4.2.

4.2.2.2.3 ProMan

The prediction model contained 44 transmitters in total, placed at specific locations. That included four IoRL system's directional mmWave antennas, three directional cellular 4G antennas and 37 omnidirectional antennas, representing IoT devices that can be found on site (see **Table 23** in Annex B). Broadcasting power for each smart device was obtained either from the manufacturer or from appropriate communication commissioning regulatory body. As the project focuses on the mmWave devices the gain of each omni-directional transmitter was taken to be equal to the gain of a reference dipole antenna.

IRT parameter setting – “superposition of contributions (rays)”, was chosen to be: “Coherent (with consideration of phase)” for all computations.

For the computation of the rays, not only the free space loss has to be considered but also the loss due to the transmission, reflections and (multiple) diffractions. This is either done using a physical deterministic model or using an empirical model.

Note: This only affects the determination of the transmission, reflection and diffraction coefficients. The prediction itself always remains a deterministic one. Thus, the same rays are taken into account.

The deterministic model uses Fresnel equations for the determination of the reflection and transmission loss and the GTD/UTD for the determination of the diffraction loss. This model has a slightly longer computation time and uses three physical material parameters (permittivity, permeability, and conductivity).

The empirical model uses five empirical material parameters (minimum loss of incident ray, the maximum loss of incident ray, loss of diffracted ray, reflection loss and transmission

loss). For correction purposes or the adaptation to measurements, an offset to those material parameters can be specified.

The empirical model has the advantage that the required material properties are easier to obtain compared to the physical parameters for the deterministic model, and that is why it was chosen in this case. Also, the parameters of the empirical model can more easily be calibrated with measurements. It is, therefore, easier to achieve high accuracy with the empirical model.

ProMan can compute one transmitter per one CPU (central processor unit) core at a time. Number of CPU cores to be used is dependent and limited on type of license and machine hardware capabilities.

4.2.2.3 FEKO

Method of moments is computationally very expensive. Even for a High-performance computing (HPC) device. Due to this reality, it was decided that, an object with very few polygons and low volume should be utilised for the model in CADFEKO. This essentially translates to computing SAR over a spherical segment (see **Figure 37** below for model development journey). This will still allow for high accuracy results provided from MoM.

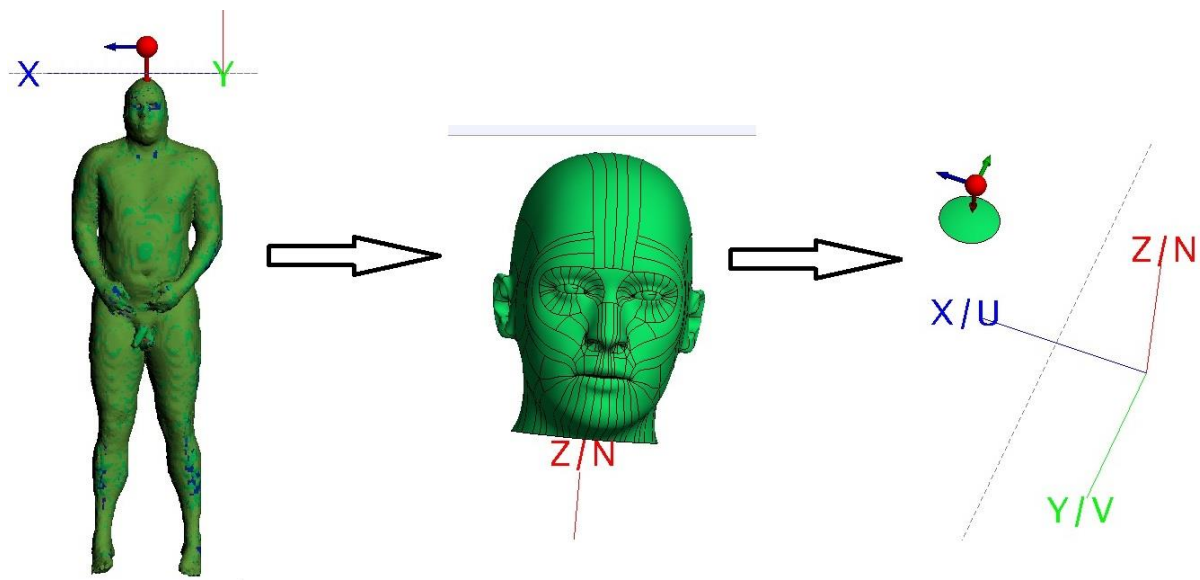


Figure 37: CADFEKO model development

The model was prepared using the provided mmWave antenna pattern, single frequency equal to 40 GHz, with total source power $P = 0.100$ W (20.000 dBm) ERP, per transmitter (see **Figure 38** below). Each antenna was placed at a corner of imaginary square, with side equal to 50 cm (as described in section 3 of this document).

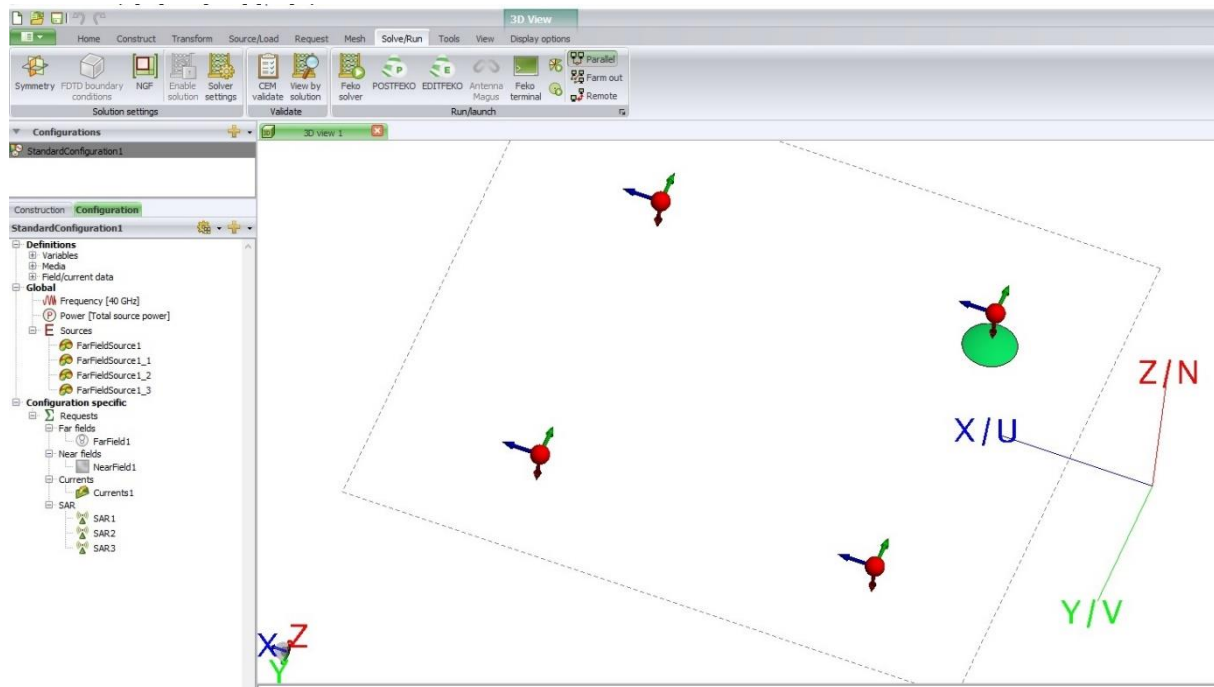


Figure 38: CADFEKO model setup

The dielectric medium applied to the created spherical segment was that of a dry skin with electrical properties displayed in **Table 14**. Distance between the segment and the selected source of radiation was set to be 10 cm (to accommodate for device/system exterior), where strong near field would exist. Such conditions are suitable for SAR measurements too.

Table 14 – Dry skin electrical properties [9]

Relative permittivity ϵ_r	11.69
Dielectric Loss tangent $\tan \sigma$	31.78
Mass Density (S/m)	1109

4.2.3 Results

Due to the size of the simulation model and frequencies involved, WinProp was used for the main simulations and these results are shown below.

4.2.3.1 WinProp

4.2.3.1.1 Dominant electric field

In ProMan, a combination of two result files is possible to get a result file, which contains the maximum, the minimum or the mean value of the two selected result files. To demonstrate direct comparisons between different transmitters and frequencies, combination of maximum value for each individual transmitter is done in this section (as described presently).

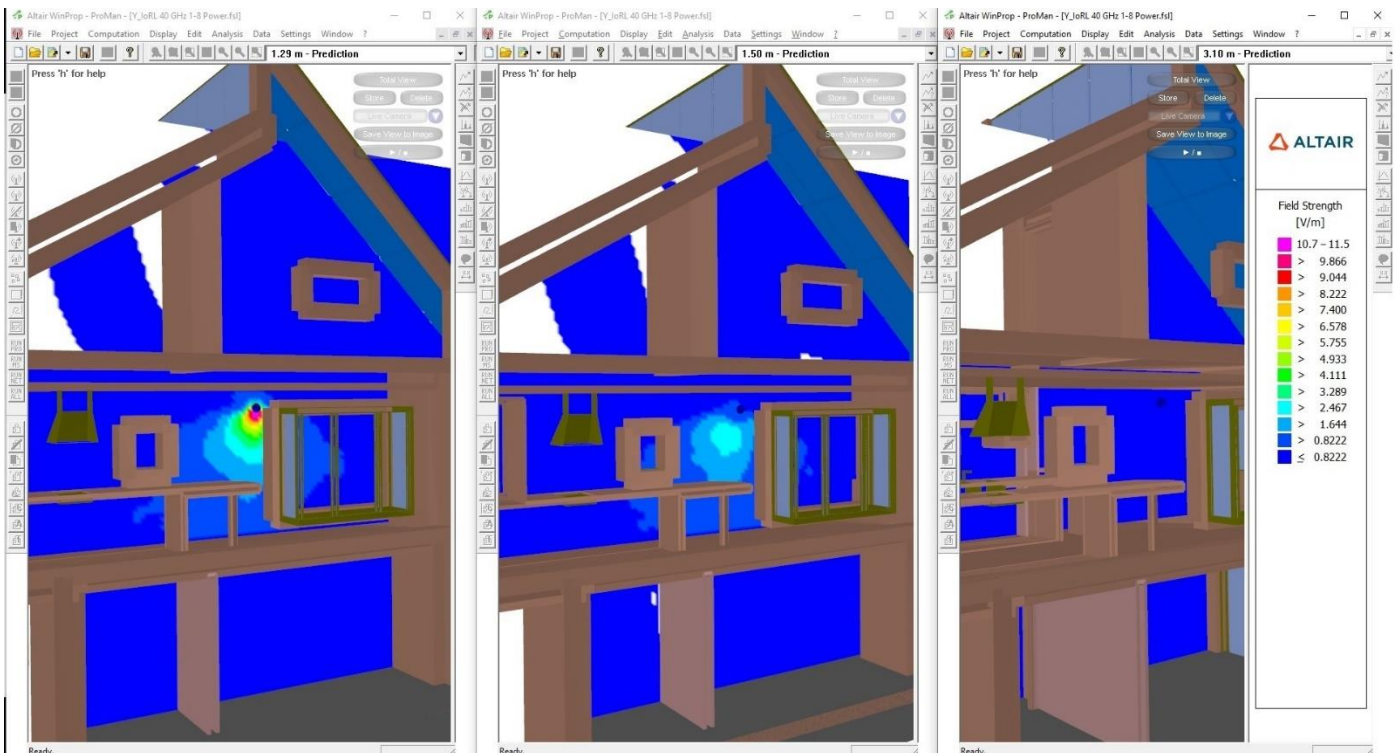


Figure 39: Single mmWave E-Field strength for all vertical prediction planes (most left: 1.29 m; middle: 1.5 m; most right: 3.10 m). V/m linear scale

To set the scene and for better understanding of prediction planes see **Figure 39** above. The left-most image illustrates the vertical top-down distribution of energy of the lone mmWave transmitter modelled in the home. The absolute peak of the electric field strength is below 11 V/m, and this located at the immediate excitation of the antenna, or even at the core of source placement. However, as the distance increases, the intensity of the electric field drops significantly and we can estimate that at the beginning of the far field region, values are in the range of below 2 V/m (see **Figure 40**). These values can be referenced with **Table 8**, where the ICNIRP limit for general public (frequency range 15 GHz to 300 GHz) is 61 V/m.

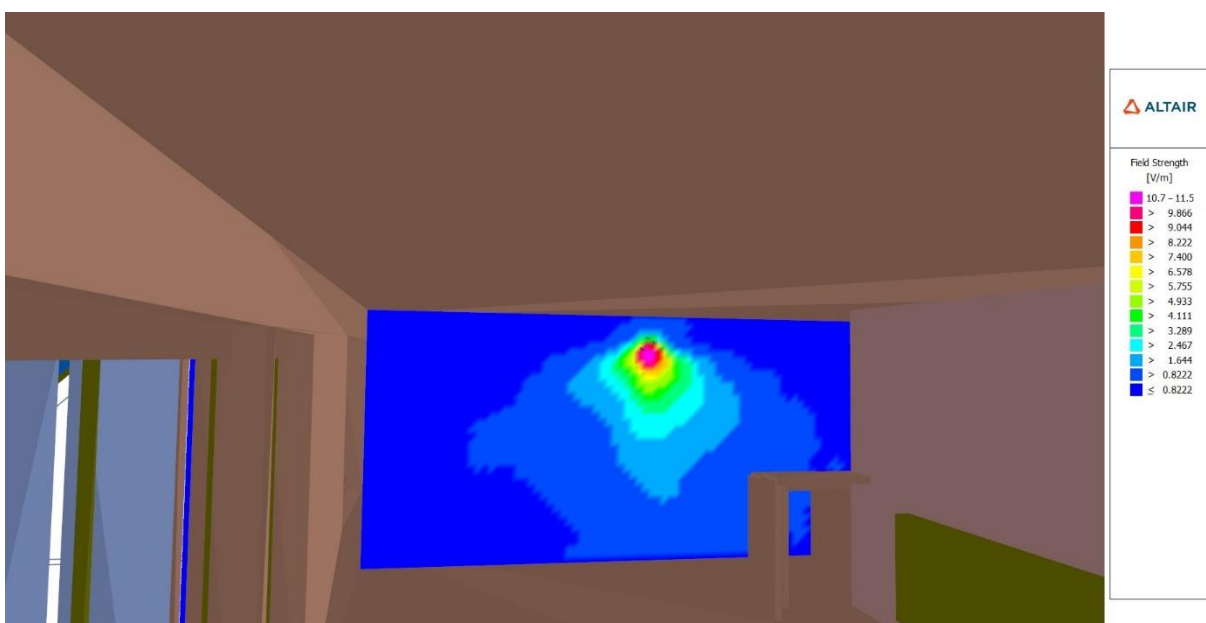


Figure 40: Single mmWave E-Field strength for the first vertical prediction plane. V/m linear scale

Figure 41 demonstrates another view of electric field distribution per transmitter in V/m, whilst **Figure 42** illustrates outcomes of power in logarithmic scale in dBm.

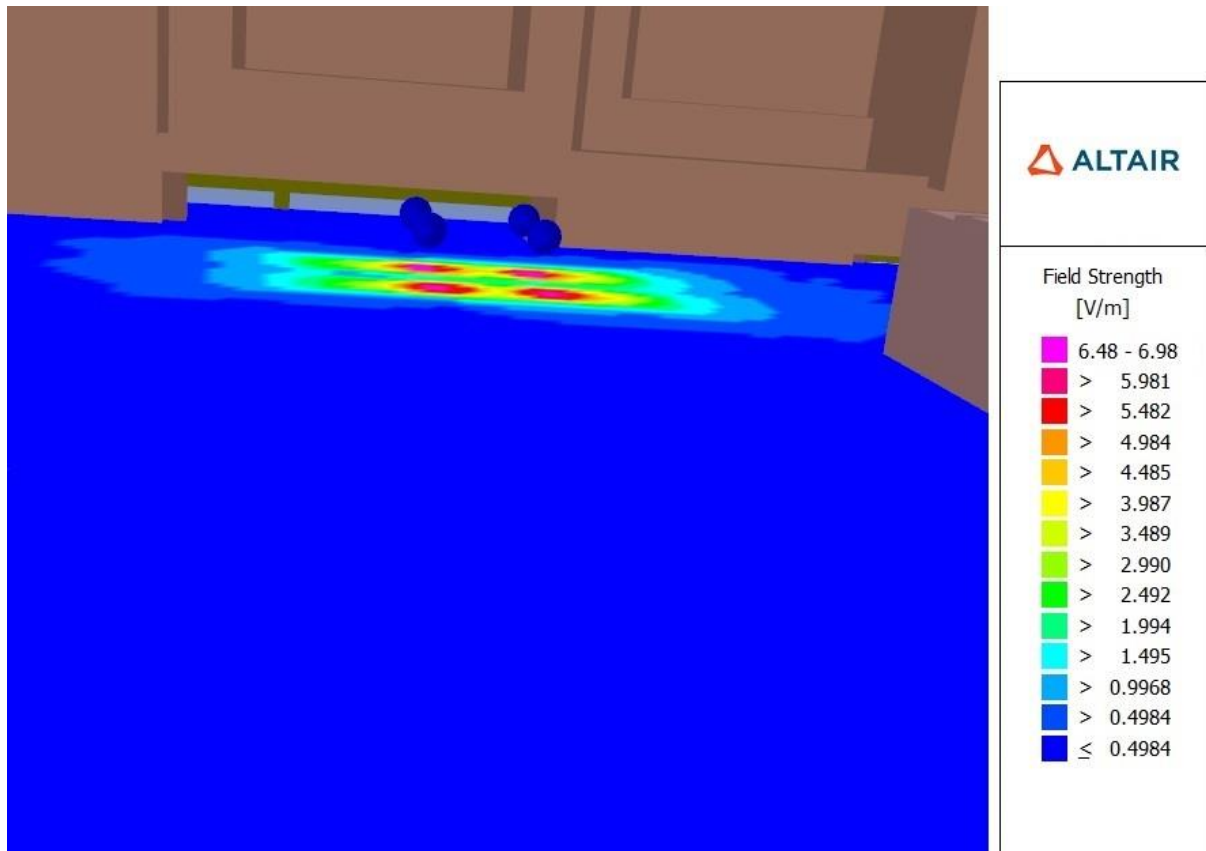


Figure 41 – Indoors 3D view of four mmWave transmitters at height of 1.8 m

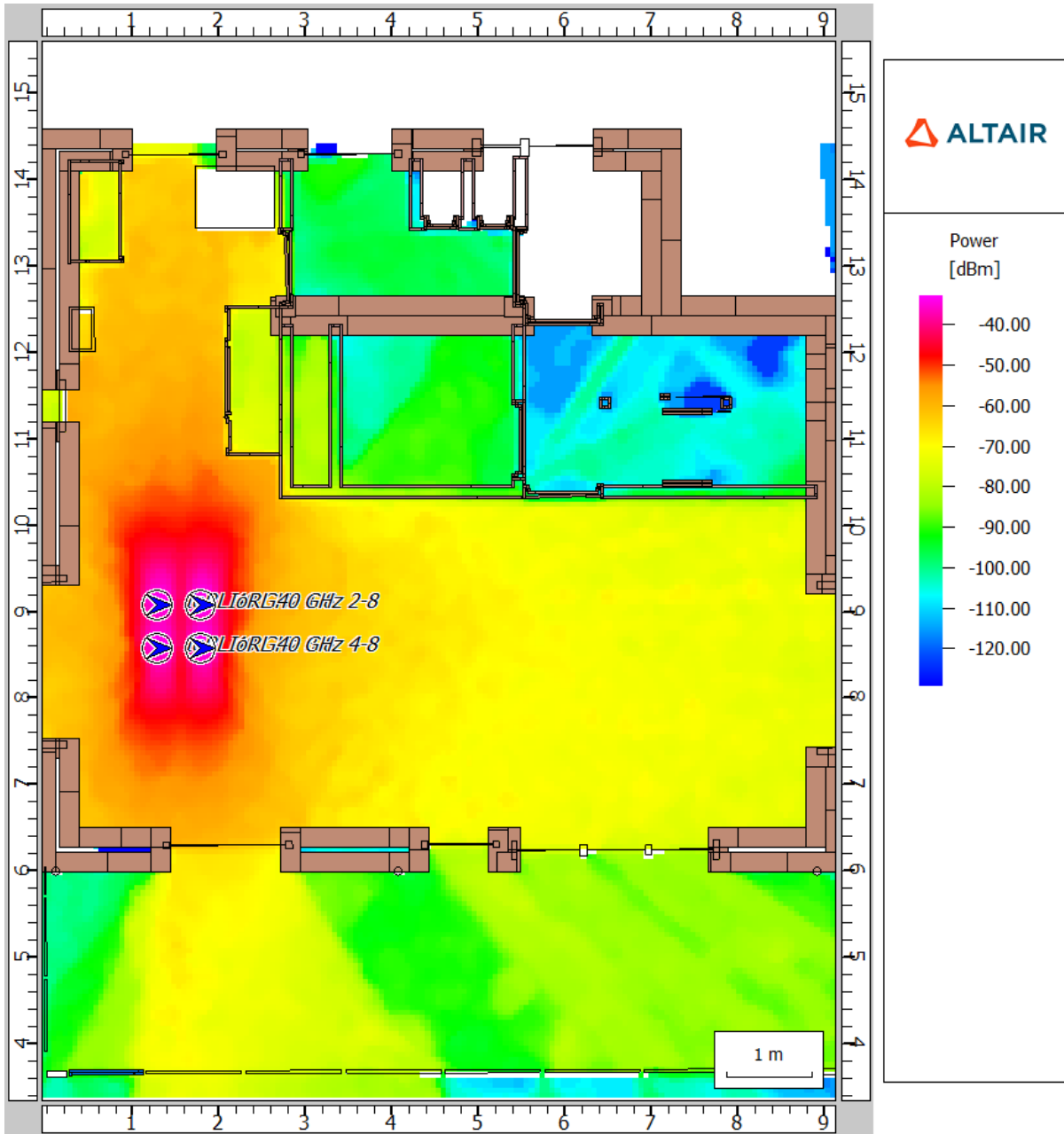


Figure 42 - Four mmWave transmitters power level at height of 1.8 m. Log scale

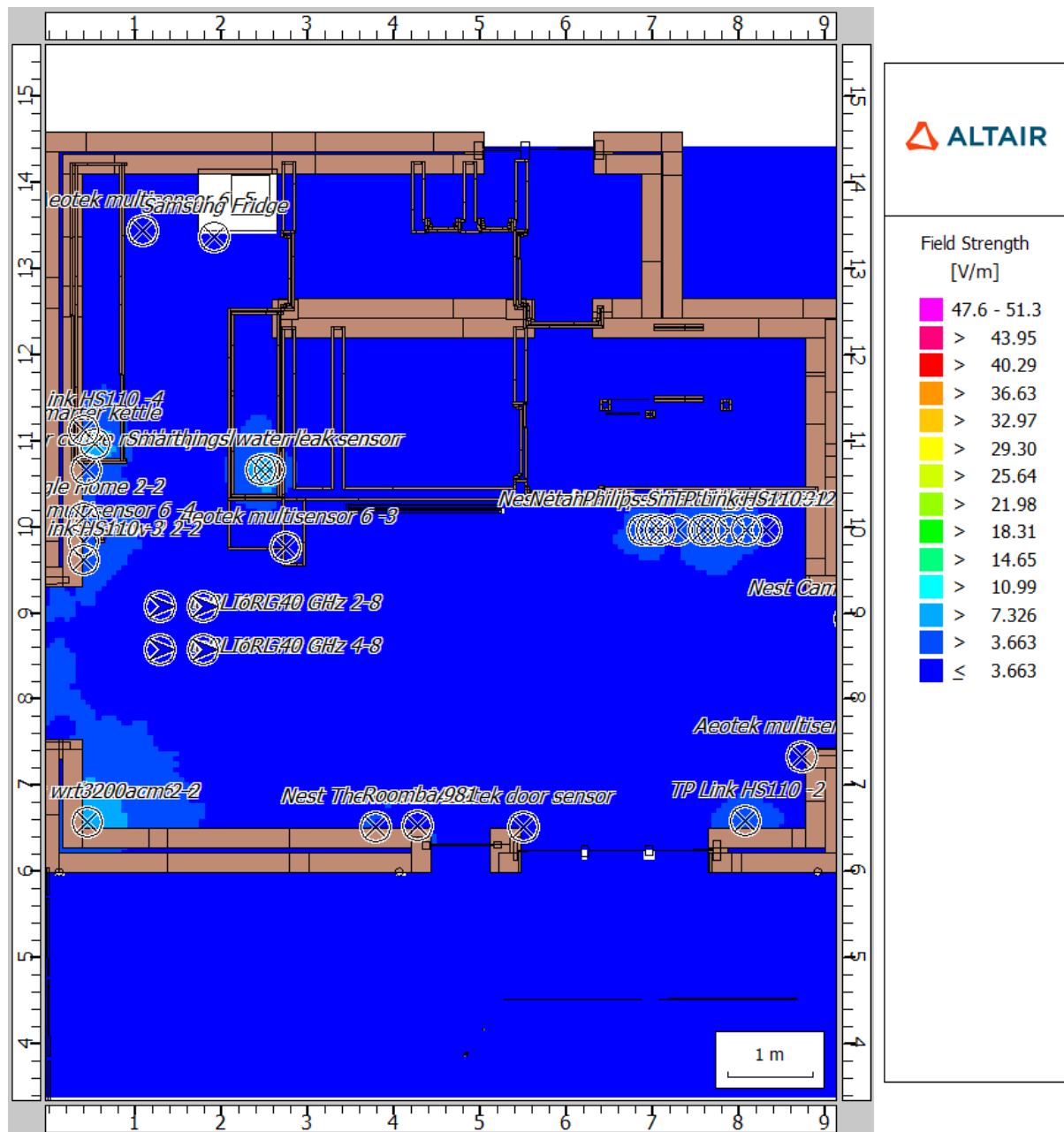


Figure 43 - Simulation of E-Field strength for 4 mmWave Tx and 40 additional Tx at height of 0.70m

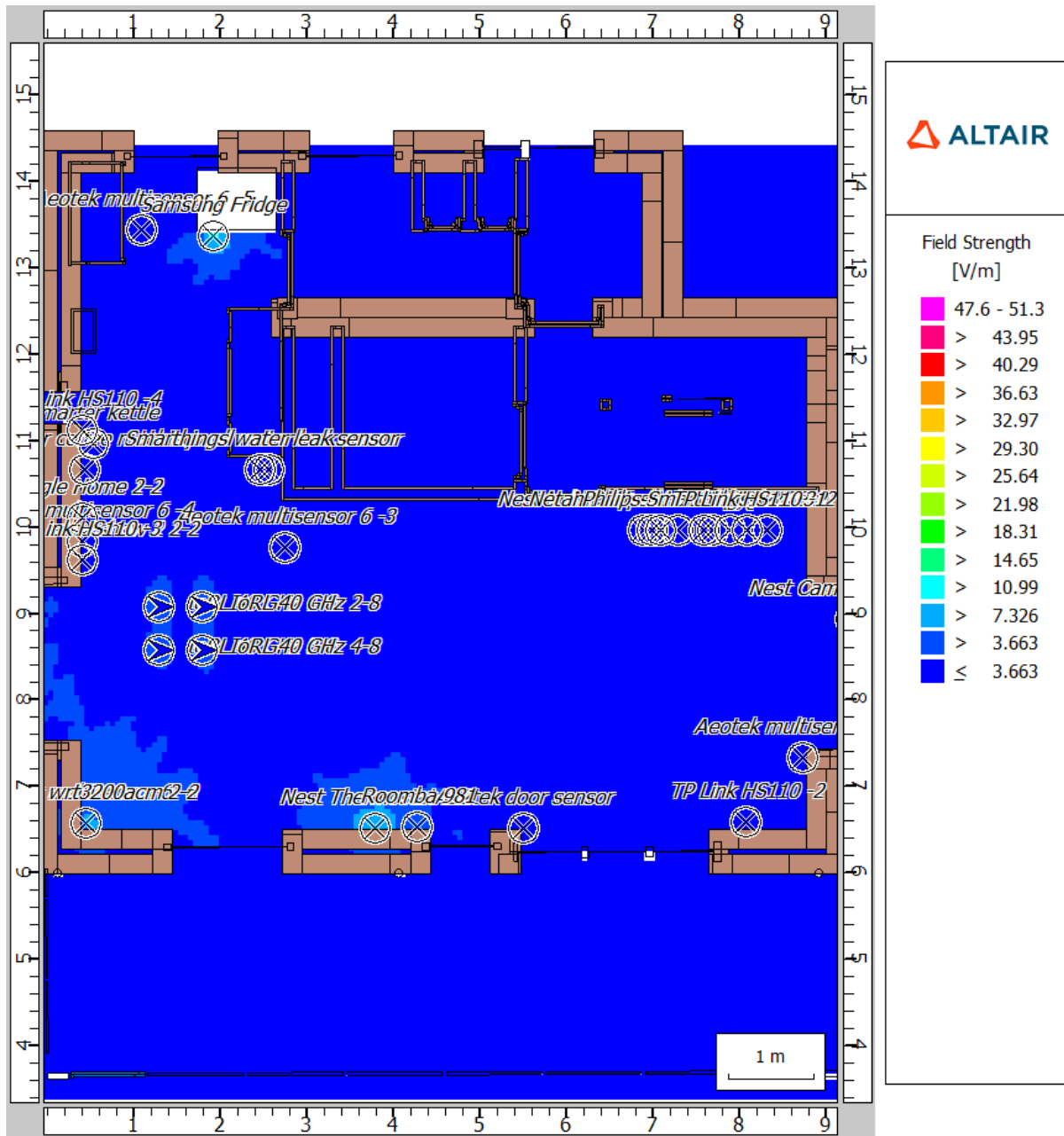


Figure 45 - Simulation of E-Field strength for 4 mmWave Tx and 40 additional Tx at height of 1.80m

Figure 46, Figure 47 and Figure 48 are setting the stage for existing RF environment in the home (see transmitter list in Table 23). The WiFi router has been removed from these three images due to the fact that, at height of 1.2 m, the prediction plane intersected it, and a spike of electric field strength occurred, higher than other transmitters, that reduced the overall visibility of the illustrations. That is especially since the legend refers to all three prediction planes – see Figure 43, Figure 44 and Figure 45. However, all transmitters including the WiFi router were used for the ICNIRP calculations. It should be noted that peak field strengths are shown, and these particular simulations do not take into account the averaging effect for real devices that do not have 100% activation at all times. Therefore, this is somewhat worst-case.

It can be concluded that, the main contributors to E-Field strength are the smart WiFi powered devices such as mains plugs, thermostat, fridge, Hoover, camera, etc. Much less

electromagnetic field intensity is provided by ZigBee and Z-wave devices, which are designed to be low powered.

Additionally, it can be deduced that, electric field strength of 9 V/m and above, hits every prediction plane: 0.7, 1.2 and 1.8 m. This is to do with the number of devices and their placement in the model, which covers more or less the entirety of all elevations.

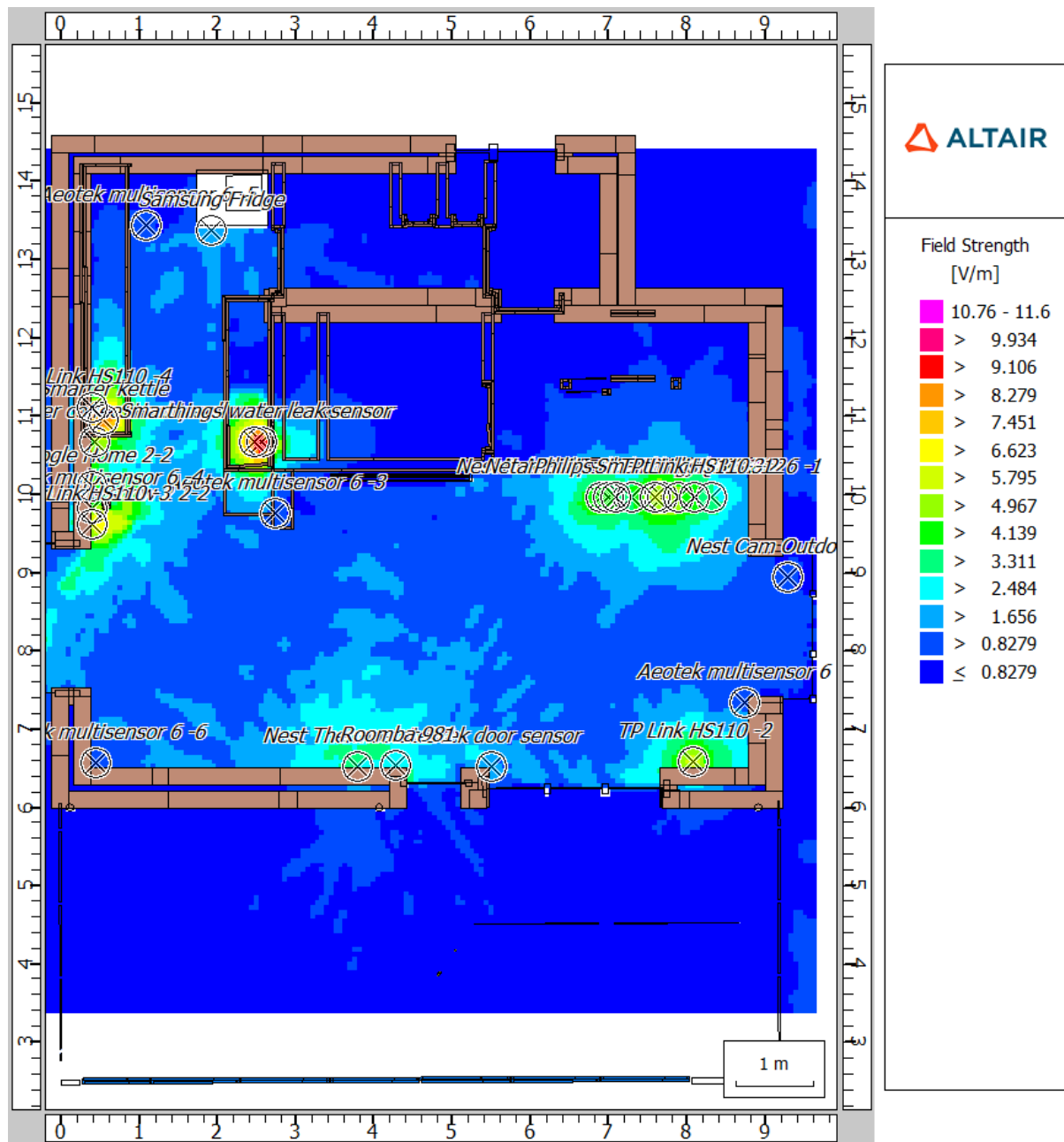


Figure 46 – Horizontal prediction plane at height of 0.70 m, excluding mmWave and including 38 transmitters of lower band communication frequencies (868 MHz to 5 GHz) only. V/m linear scale

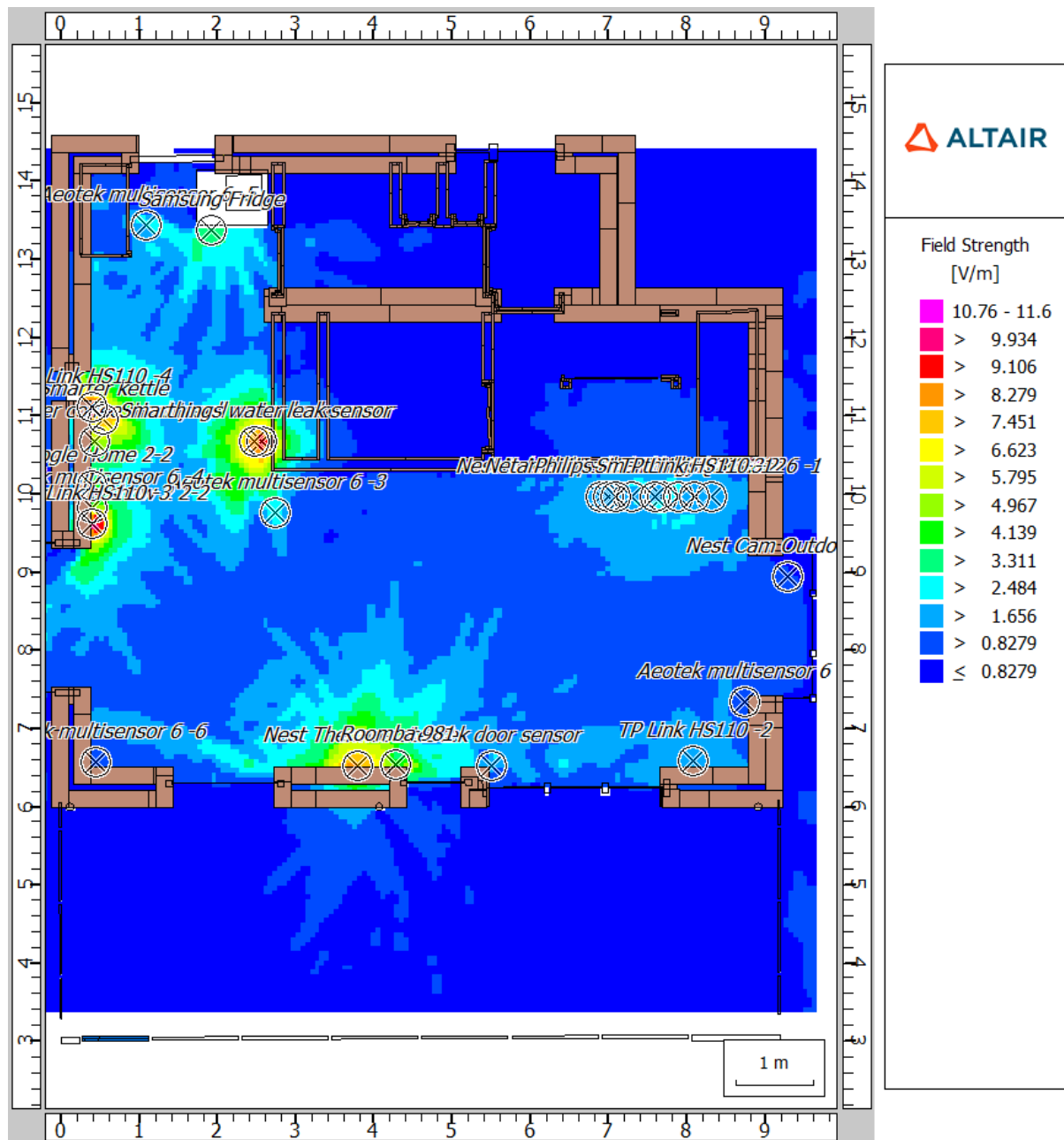


Figure 47 – Horizontal prediction plane at height of 1.20 m, excluding mmWave and including 38 transmitters of lower band communication frequencies (868 MHz to 5 GHz) only. V/m linear scale

Figure 48 below shows that at a height of 1.8 m, major contributors are the smart thermostat and fridge. It was revealed that mmWave antennas have a stronger influence there as well, compared to the lower heights. This is also addressed in Figure 49 and Figure 50.

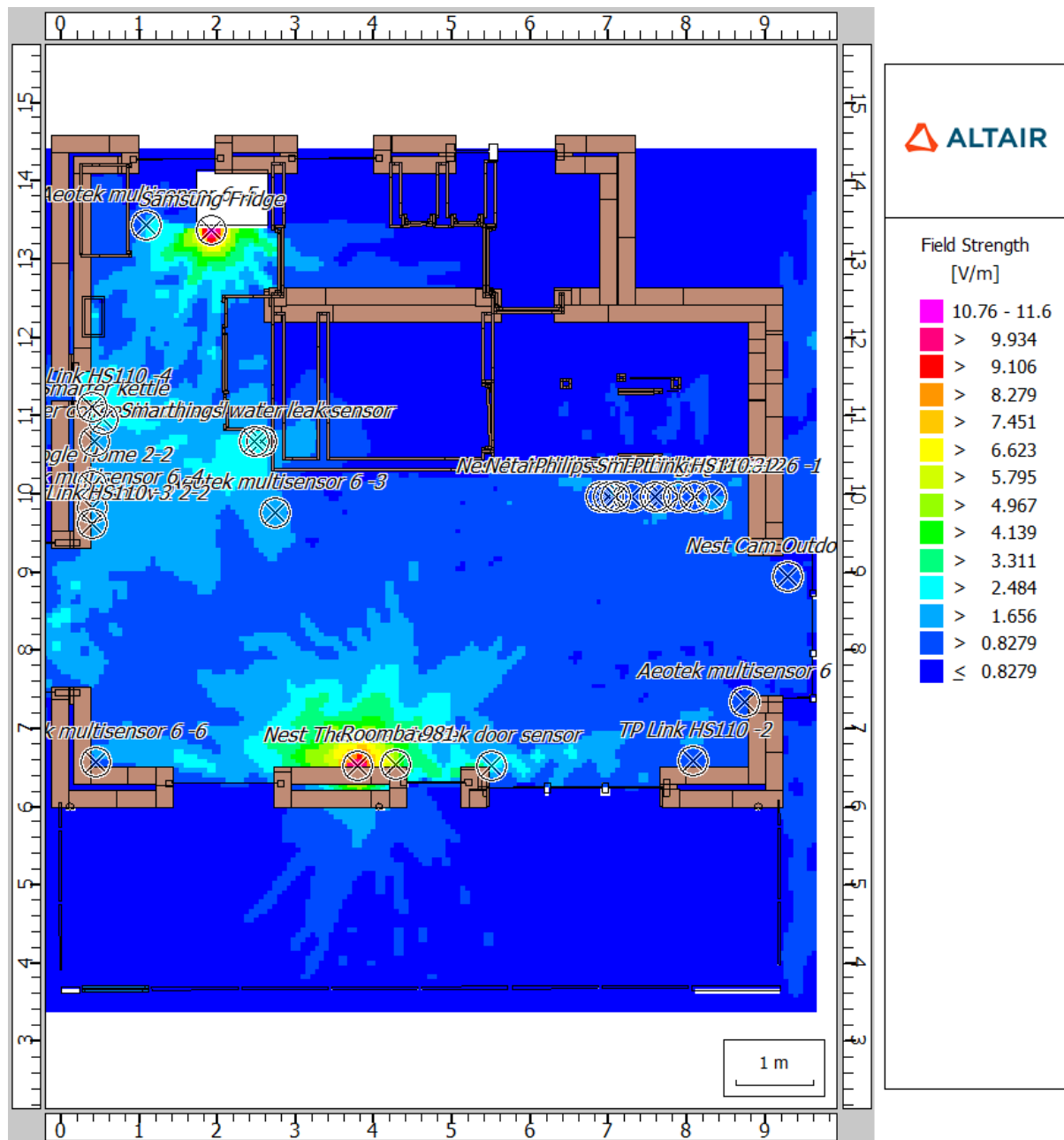


Figure 48 – Horizontal prediction plane at height of 1.80 m, excluding mmWave and including 38 transmitters of lower band communication frequencies (868 MHz to 5 GHz) only. V/m linear scale

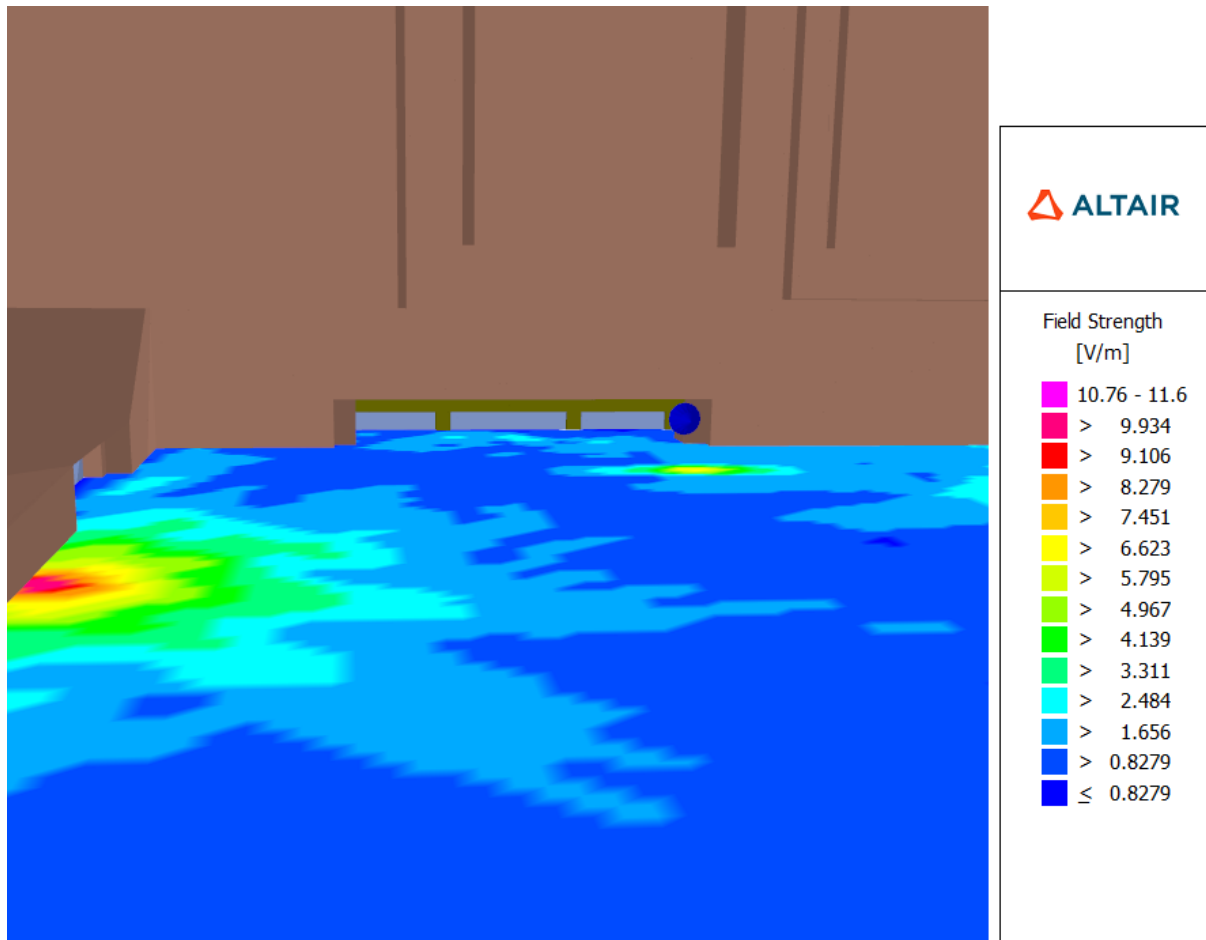


Figure 49 – 3D Horizontal prediction plane at height of 1.80 m, including single mmWave antenna and 38 transmitters of lower band communication frequencies (868 MHz to 5 GHz). V/m linear scale

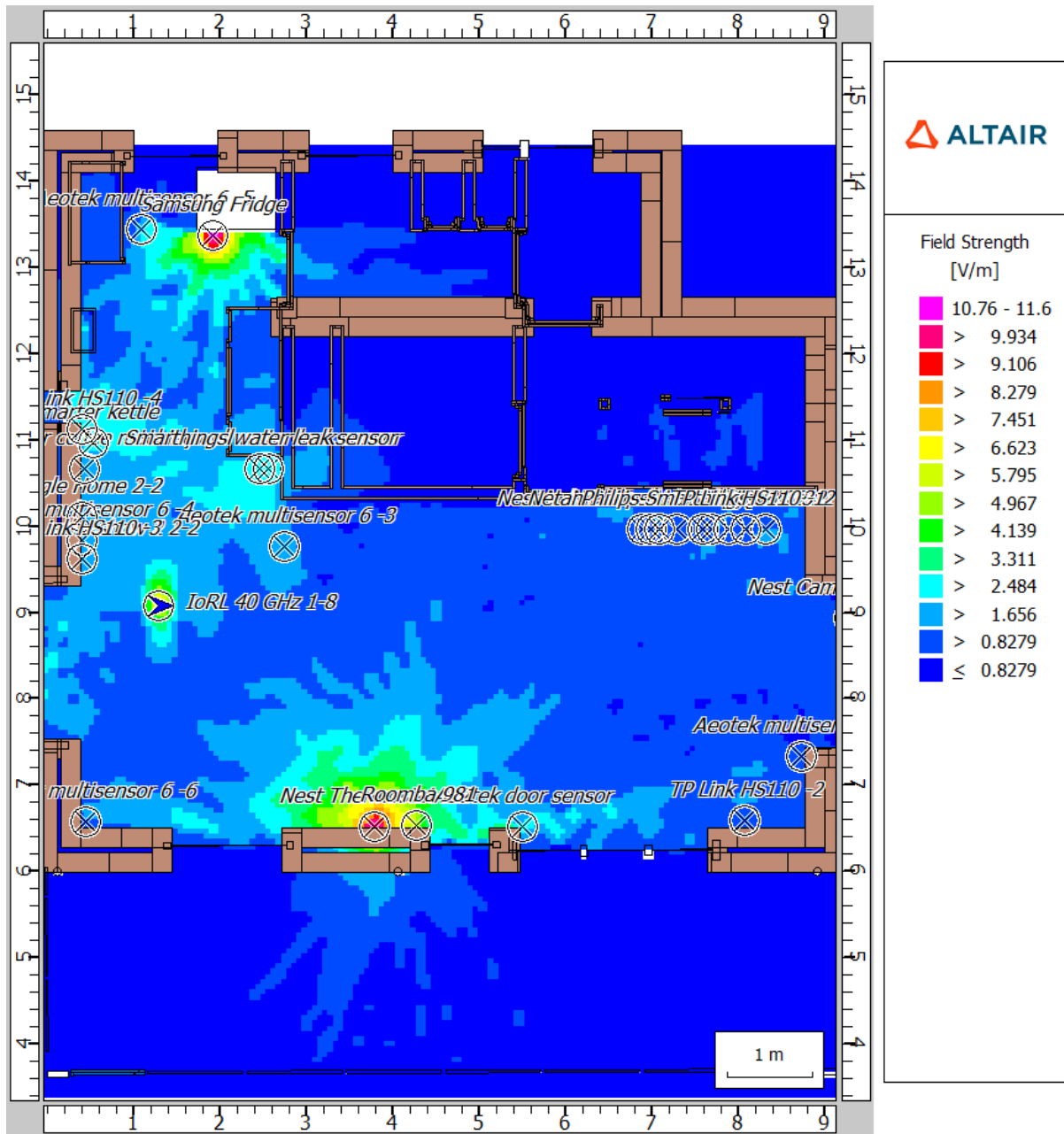


Figure 50 – 2D Horizontal prediction plane at height of 1.80 m, including single mmWave antenna and 38 transmitters of lower band communication frequencies (868 MHz to 5 GHz). V/m linear scale

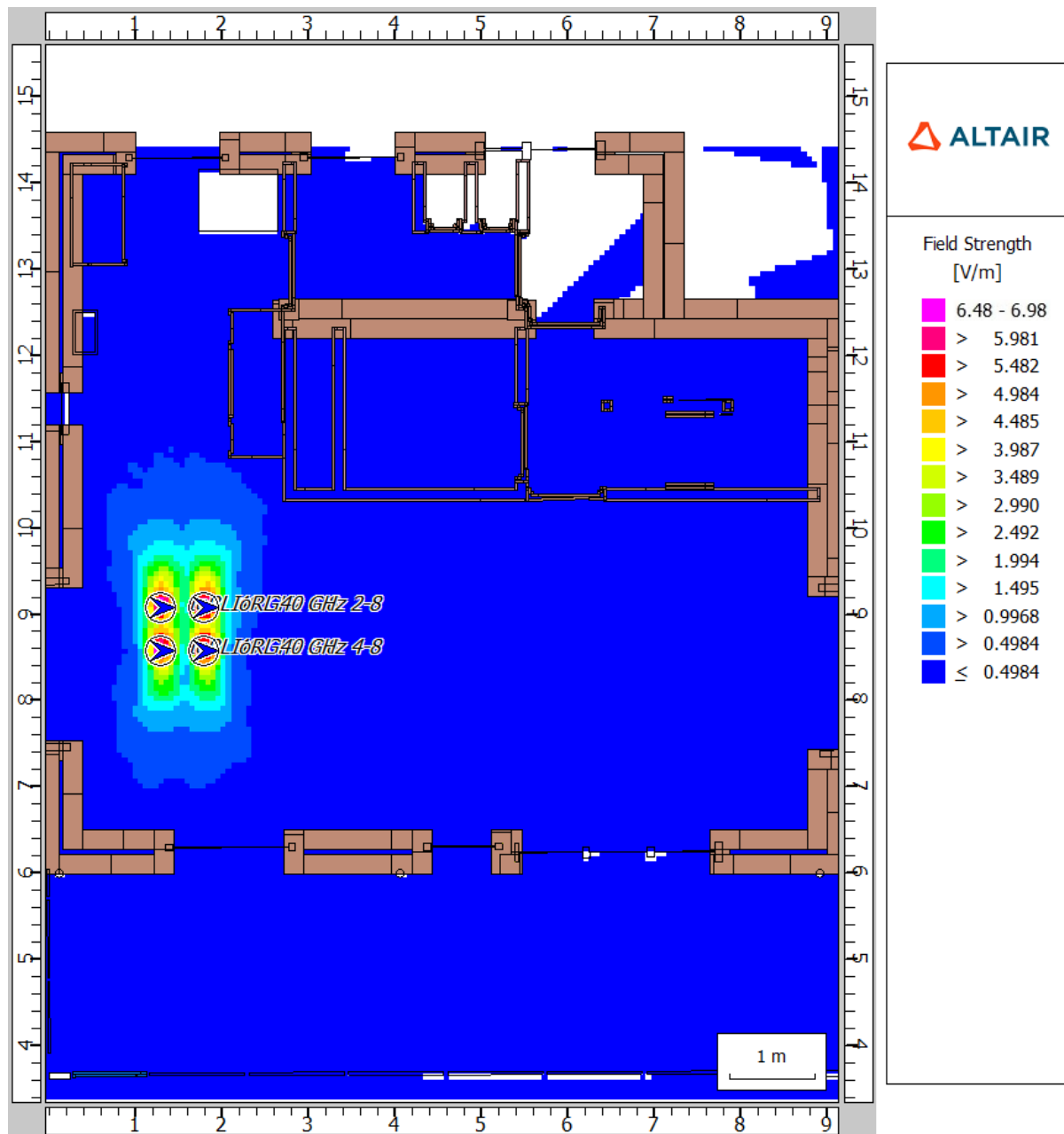


Figure 51: Simulation of E-Field strength for 4 mmWave transmitters at 1.80m height

Figure 52 below demonstrates simulated prediction at 1.80m height, that includes the four mmWave transmitters and 38 other radio transmitting devices, generally found in and around smart homes: Z-Wave devices operating at 868 MHz, Zigbee, WiFi and Bluetooth devices operating at 2.4 GHz and 5 GHz bands and Mobile Base Station operating at 1.8 GHz.

Peak E-field strength of up to 11.7 V/m was produced in that scenario around some of the smart devices, such as the smart thermostat and the smart fridge, as stressed above. In comparison with Figure 51, where only the mmWave antennas are present, E-Field strength surges at 6.48 V/m.

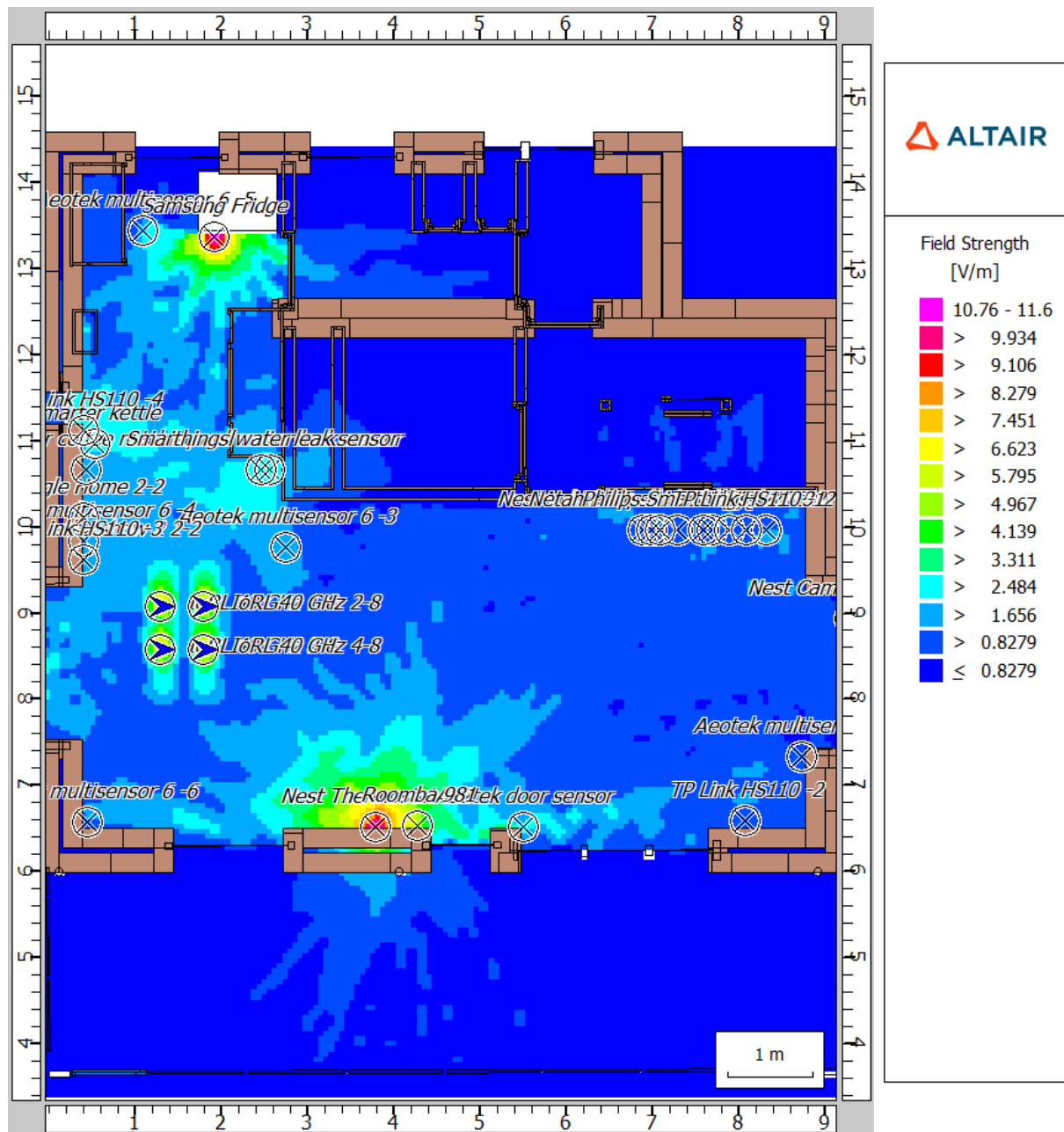


Figure 52: Simulation of E-Field strength for 4 mmWave transmitters and 38 additional Tx (WiFi router not included) at 1.80 m height

Figure 53 shows the vertical distribution of power at the 1.29 m vertical slice, which directly bisects 2 of the mmWave transmitters. This shows the highest electrical field strength from every individual device across the vertical slice. Despite the plane directly intersecting the mmWave radiation sources, the mmWave transmitters peak power sits near the median range for device peak power. Contributing to the upper end of these graphs are WiFi powered devices, whilst the example of 4G antenna given in this scenario (located 90 m away from target), is found at the lower end.

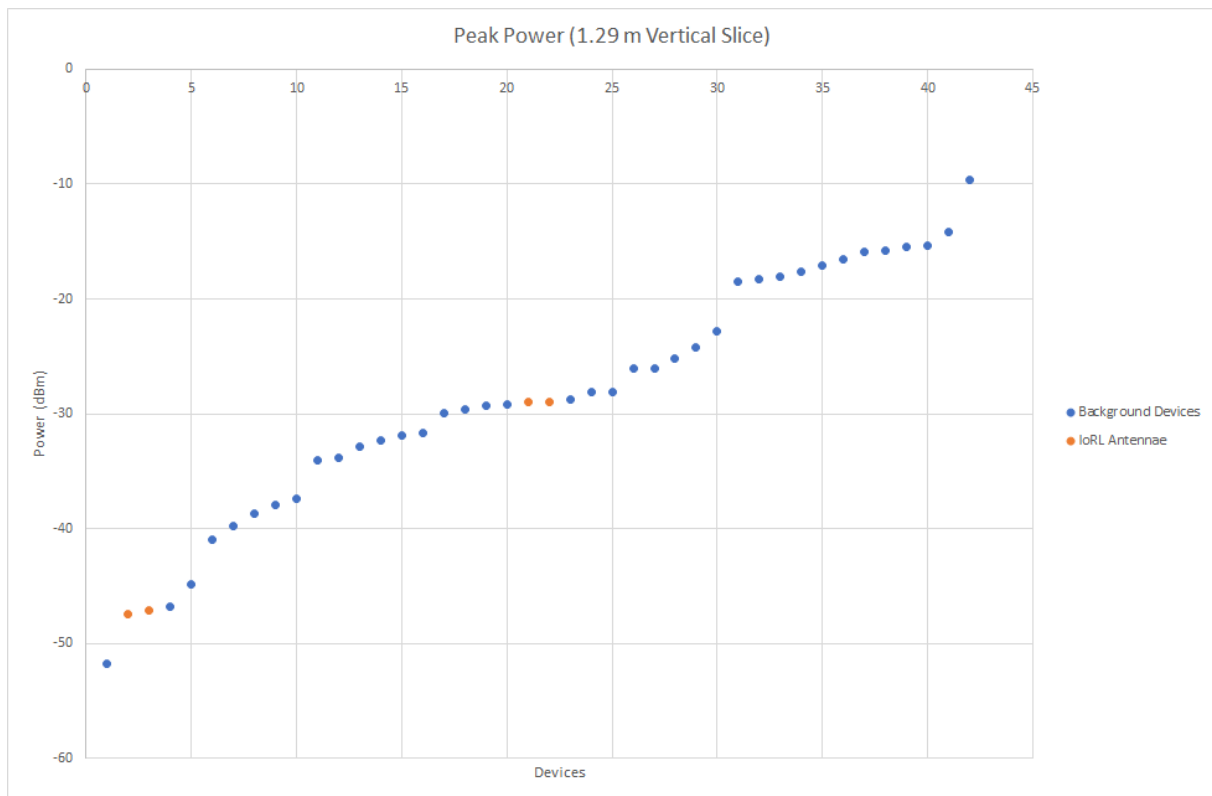


Figure 53 - Individual transmitter power for all devices at vertical prediction plane 1.29 m. Logarithmic scale dBm

From the graph below, it can be assumed that up to a certain height directly beneath the mmWave transmitter, the 40 GHz signal strength will have weaker electric field than other devices. That given height appears to be 1.4 m (see **Figure 54**), which shows the highest field strength from any individual device at a range of heights directly below the IoRL devices, with and without IoRL turned on. Since the background devices are scattered spatially, the peak electric field strength from any individual background device at these points remains at around 2 V/m (represented by the grey line in **Figure 54**). At that vertical prediction plane, above height of 1.4 m, no other transmitter is creating stronger electric field than the mmWave antenna. It must be noted that in this region, the nearest source of radiation is exactly the 40 GHz transmitter.

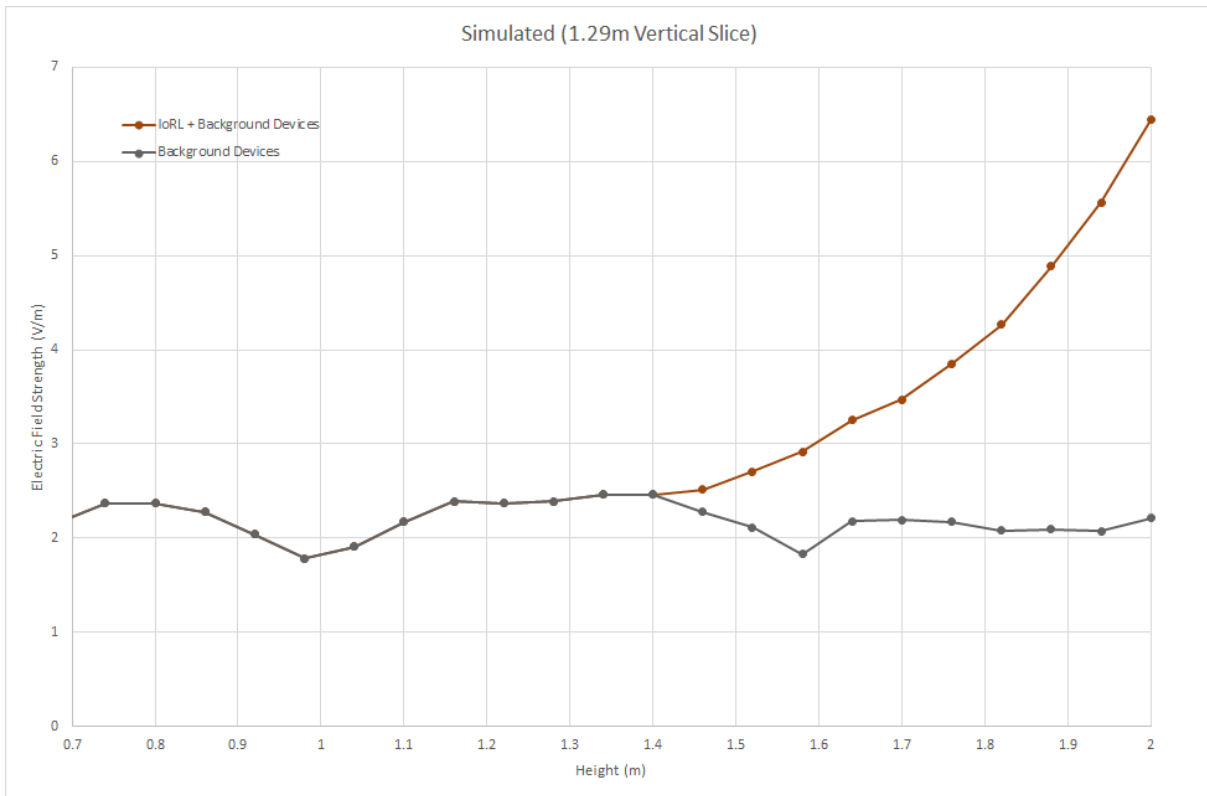


Figure 54 - Dominant E-Field strength for all devices, in a vertical line, directly below mmWave antenna, at vertical prediction plane 1.29 m. Linear scale V/m

4.2.3.1.2 Total electric field

To show the total field in relation to exposure limits, summation of exposure ratios is performed (see section 4.1.1.4). It is important to determine whether, in situations of simultaneous exposure to fields of different frequencies, these exposures are additive in their effects.

For thermal considerations, relevant above 100 kHz [6], the following two requirements should be applied to the field levels:

$$\sum_{i=100\text{ kHz}}^{1\text{ MHz}} \left(\frac{E_i}{c}\right)^2 + \sum_{i>1\text{ MHz}}^{300\text{ GHz}} \left(\frac{E_i}{E_{L,i}}\right)^2 \leq 1$$

and

$$\sum_{i=100\text{ kHz}}^{1\text{ MHz}} \left(\frac{H_i}{d}\right)^2 + \sum_{j>1\text{ MHz}}^{300\text{ GHz}} \left(\frac{H_j}{H_{L,j}}\right)^2 \leq 1$$

where

- E_i = the electric field strength at frequency i ;
- $E_{L,i}$ = the electric field reference level from REF_Ref59022184 \h Table 7;
- H_j = the magnetic field strength at frequency j ;
- $H_{L,j}$ = the magnetic field reference level from REF_Ref536714442 \h Table 8;
- $c = 610/f$ V/m (f in MHz) for occupational exposure and $87/f^{(1/2)}$ V/m for general public exposure; and

$d = 1.6/f \text{ A/m}$ (f in MHz) for occupational exposure and
 $0.73/f$ for general public exposure

The total field strength was calculated for each of the device frequencies at the worst-case location just below the IoRL antennas and compared to the exposure limits and the calculated Exposure Ratios, **Table 15**. The total contribution to Exposure Ratio from all frequencies rounds up to 0.099 ($ER < 1$) so this is considerably below the ICNIRP limits.

Table 15 – Summation of Exposure Ratio contributors (in-phase constructive interference at a point – at the antenna)

Frequency (MHz)	868	1850	2400	5000	40000
Sum E-Field	0.53 V/m	0.12 V/m	15.84 V/m	4.52 V/m	9.791 V/m
E-Field limit	40.51 V/m	59.14 V/m	61 V/m	61 V/m	61 V/m
Individual contribution to Exposure Ratio	0.0001712	0.000004117	0.06743	0.005491	0.02576

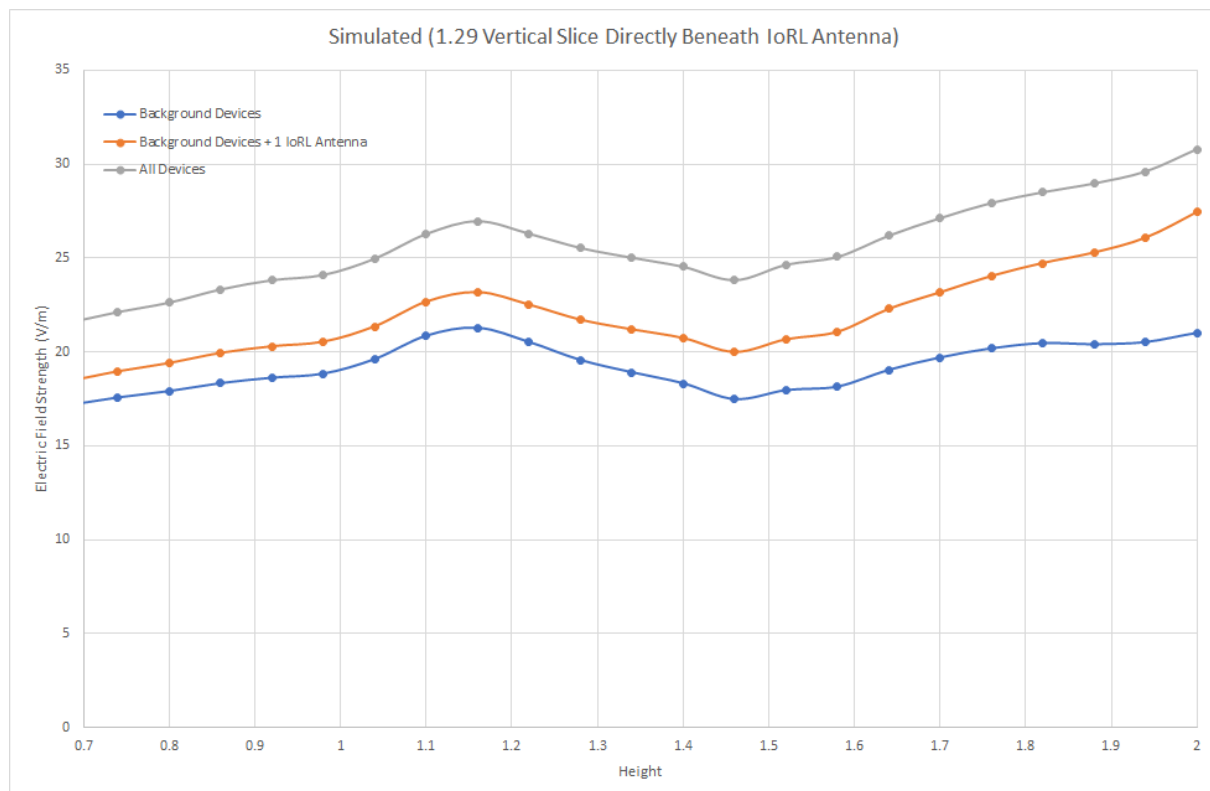


Figure 55 – Summed broadband electric field strength at a point for all heights, in a vertical line, directly below mmWave antenna (summation of electric field strengths, assuming in-phase constructive interference)

Figure 55 shows the total field strength in the region directly below mmWave antenna, when all devices are summed assuming the worst case that they are all in-phase

(constructive interference). It can be observed that there is a spike at 1.15 meters, where majority of IoT devices are vertically located although even higher field strength is observed, as the height approaches the mmWave radiation source height. Comparing the blue and orange lines in that graph, shows that the 40 GHz contribution to the total electric field increases with elevation. It should be noted that this is a somewhat worst-case calculation and that in reality total field strengths are likely to be much lower, which was observed during the measurements detailed below.

4.2.3.2 FEKO

Average-SAR over entire domain for frequency of 40 GHz was computed to be 0.0290921 W/kg (see **Figure 56** below). Both IEEE and ANSI (including ICNIRP) have average SAR limit of 0.08 W/kg for General public / Uncontrolled environments. (refer to Table 7 for SAR limits).

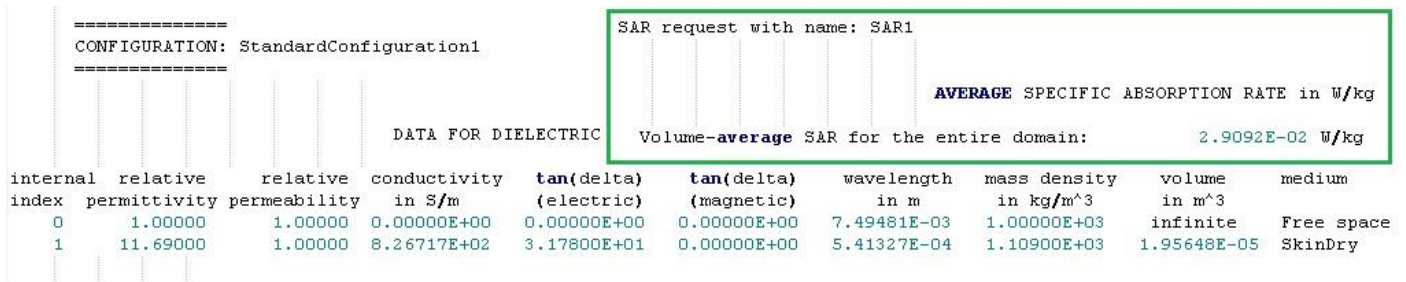


Figure 56 - POSTFEKO Average SAR solution and dielectric data

4.3 Measurements

4.3.1 Measurement Instrument selection

The instrument used to perform the above measurements was a NARDA Broadband Field Meter NBM-520, seen in **Figure 59** and close view in **Figure 62**. Calibration certificate is applied in Annex B (**Figure 66**).

The NARDA Broadband Field Meter NBM-520 is a popular instrument for measuring non-ionizing radiation within the frequency range from 100 kHz to 60 GHz (depending on the probe used). Probes for various measurement applications are connected to the NBM-520 basic unit. Flat frequency response probes are available, as well as so-called shaped probes that evaluate the field according to a specific human safety standard. These probes are calibrated separately from the measuring instrument and include a non-volatile memory containing the probe parameters and calibration data. They can therefore be used with any instrument in the NBM-500 family without any loss in calibration accuracy.

The NBM-520 makes measurements for human safety purposes, particularly in workplace environments where high electric or magnetic field strengths are likely. It can also be used to demonstrate the electromagnetic compatibility (EMC) of devices and equipment. Examples:

- Measuring field strengths as part of general safety regulations
- Measuring the field strengths around transmitting and radar equipment to establish safety zones and for monitoring during operations
- Measuring the field strength emanating from mobile phone repeaters and satellite communications systems to ensure compliance with human safety limit values
- Measuring the field strength in the industrial workplace environment, such as plastics welding equipment, RF heating, tempering, and drying equipment
- Measurements to ensure the safety of persons using diathermy equipment and other medical equipment that generates high frequency radiation
- Field strength measurements in TEM cells and absorber chambers

The measurement probe was selected to be EF4091 (**Figure 57**). The probe contains three orthogonally arranged dipoles with detector diodes. The diode voltages each correspond to the RMS value of the spatial components.

The isotropic measurement result is obtained by addition within the probe. The probe detects electric fields from 40 MHz up to 40 GHz. This frequency range covers almost the entire range of high frequency communications, right up to mobile radio and satellite links. The linearity and sensitivity of the probe ensure its suitability for checking human safety limit values in the occupational and general public environments.



Figure 57 – E-Field probe EF4091

The probe is designed with mechanical and electrical properties ideal for field use. The probe head is made of foam material to provide effective protection for the sensors, while having excellent RF characteristics. The detector elements are also largely protected against overload, since their destruction limit is well above all the human safety limit values.

The probe is calibrated at several frequencies. The correction values are stored in an EPROM in the probe and are automatically taken into account by the NBM instrument. Calibrated accuracy is thus obtained regardless of the combination of probe and instrument.

The measurement probe was selected to be EF4091 (**Figure 57**). The probe contains three orthogonally arranged dipoles with detector diodes. The diode voltages each correspond to the RMS value of the spatial components.



Figure 58 – E-Field probe EF4091

4.3.2 Measurements - procedures and methodologies

There are two type of measurements – broadband and frequency selective. Since the total exposure from all sources in the area is considered, the first of these methods was chosen – see **Figure 27**.

Broadband measurements of the far field consists of electric field strength evaluations in V/m. To evaluate the highest RF field strength or the RF field strength at discrete points in a region, performing a search using the handheld sweep method was used. Spatial averaging of the field was also completed. Investigations of temporal variations in the field were made to ensure a stable indication of the RF field strength.

The appropriate evaluation process for this project is for in-situ RF exposure assessment (See Clause 6 of IEC 62232, EN 62232, Determination of RF field strength, power density and SAR

in the vicinity of radiocommunication base stations for the purpose of evaluating human exposure, 2017.).

Broadband instruments are made with sensors that can be non-isotropic to measure a single spatial component of the field or can be isotropic to measure all three components of the field at the same time. These instruments can measure the total level of the instantaneous electric or magnetic field, or the RMS field value or the average power density value in a time period, typically 6 min in accord with exposure standards.

Measurements.

The aluminium frame on which the RRLH controller and RRLHs are fitted was moved to the kitchen end of the sitting room as shown in **Figure 59** in order for the mmWave antenna location to coincide with the mmWave antenna location used in the EM radio simulations, as shown in **Figure 60**.

The location of the source and RF propagation path during measurements were considered to minimize the influence of the body on the result. A check was made, as per the manufacturer's specifications for the minimum distance between the measurement probe tip and the body of the "operator", as well as to any reflecting object. Non-conductive materials were used, to secure and position measuring device in place. For handheld measurements, the uncertainty due to the scattering of the RF field by the surveyor's body was minimized by:

- holding the probe or antenna away from the surveyor's body (a separation of at least 50 cm should be maintained between the measurement antenna or isotropic probe and the surveyor's body);
- pointing the probe towards the source;
- ensuring that the surveyor's body is not along the direct line of propagation between the source and the measurement probe (either in front of or behind).



(a) Measurements at 0.7 m height

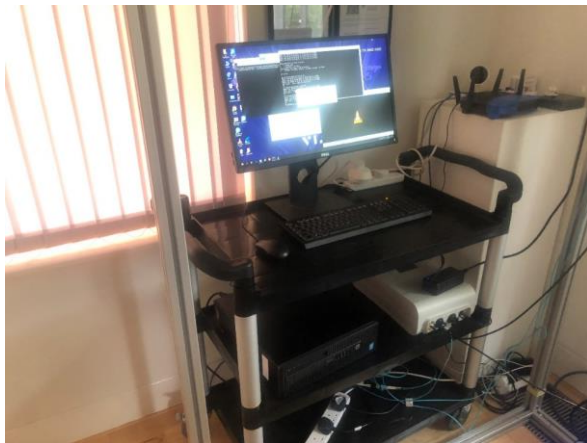
(b) Measurements at 1.2 m height

Figure 59: New Location of RRLH Controller and RRLHs for EM Radiation Measurements



Figure 60: New Location of mmWave Antenna

The Intelligent Home IP Gateway, Layer 2 Processor and DRAN was located on one trolley as shown in **Figure 61a**, whilst the Viavi User Test Terminal was located on a second trolley, as shown in **Figure 61b**. The EM radiation level measurement device, shown in **Figure 62**, can operate independent to the Test End User Terminal.



(a) Intelligent Home IP Gateway, Layer 2 Processor & DRAN

(b) Viavi Test End User Terminal

Figure 61: IoRL Head-end and End User systems

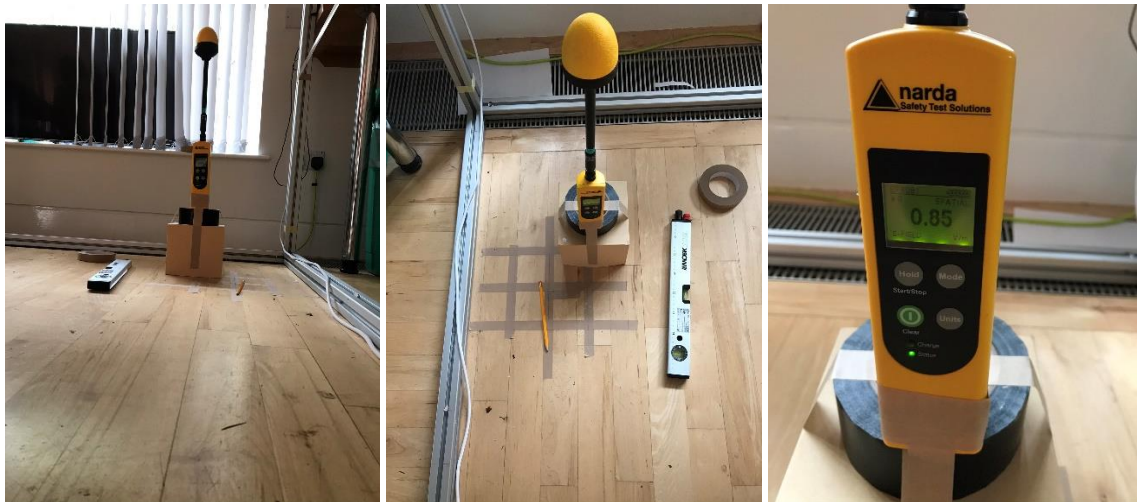


Figure 62: EM Radiation Level Measurement device

The system was set to broadcast at full power. Measurements were performed at three heights: 0.7, 1.2 and 1.8 meters above floor level. Theoretically, at 1.8 m, we are in the Near Field region of the antenna.

Two measurement procedures were performed: with the IoRL system ON and OFF.

Additionally, space averaging, peak and time averaging measurements were done.

Space averaging.

Discreet spatial measurements were performed for each horizontal prediction plane, averaging over a 3x3 grid (9 points, the point in the middle of grid, marked as X5, is located directly below mmWave transmitter – see **Figure 63** below), with 10 cm distance between each measurement point.

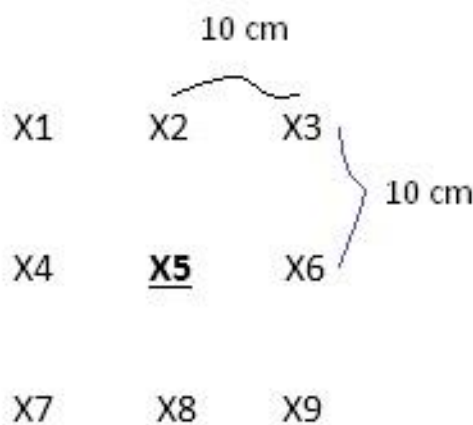


Figure 63 – Diagram of measurement grid

4.3.3 Measurement Results

Measurement results are presented below.

mmWave system turned on.

1. Time averaging peak measurement over 6 minutes, directly below transmitting antenna (probe physically in contact with antenna)
Result is listed below:
 - a. 5.74 V/m
2. Spatial averaging measurement over 9 points consisting of square 3 x 3 grid, with distance of 10 cm between points and middle of grid directly under mmWave antenna, at each height.
Results are listed in Table 16 below:

Table 16 – Measured electric field strength (V/m), spaced averaged, with mmWave transmitter turned on

Meas. Point Height	Height 1 == 0.7 m	Height 2 == 1.2 m	Height 3 == 1.8 m
X1	1.02	1.24	1.61
X2 Averages	0.92	1.15	1.62
X3 Averages	0.85	1.05	1.69
X4 Averages	0.87	1.05	1.75
X5 Averages	0.82	1.06	1.8
X6 Averages	0.82	1.08	1.79
X7 Averages	0.90	1.08	1.70
X8 Averages	0.88	1.05	1.68
X9 Final Average	0.89	1.06	1.65

* Measurements were taken in the following sequence: X1, X2, X3, X6, X5, X4, X7, X8, X9.

3. Absolute peak measurement directly below transmitting antenna (probe physically in contact with antenna)
 - a. 6.44 V/m

mmWave system turned off.

1. Time averaging peak measurement over 6 minutes, directly below transmitting antenna (probe physically in contact with antenna)
Result is listed below:
 - a. 0.69 V/m
2. Spatial averaging measurement over 9 points consisting of square 3 x 3 grid, with distance of 10 cm between points and middle of grid directly under mmWave antenna, at each height.
Results are listed in **Table 17** below:

Table 17 - Measured electric field strength (V/m), spaced averaged, with mmWave transmitter turned off

Meas. Point Height	Height 1 == 0.7 m	Height 2 == 1.2 m	Height 3 == 1.8 m
X1	0.63	0.82	1.22
X2 Averages	0.47	0.74	1.29
X3 Averages	0.54	0.66	1.32
X4 Averages	0.60	0.60	1.25
X5 Averages	0.56	0.60	1.32
X6 Averages	0.54	0.63	1.34
X7 Averages	0.58	0.64	1.19
X8 Averages	0.58	0.67	1.18
X9 Final Average	0.57	0.67	1.21

* Measurements were taken in the following sequence: X1, X2, X3, X6, X5, X4, X7, X8, X9.

4.4 Conclusions

The measurements and simulations are compared in **Figure 64** and **Figure 65**. The orange and blue line in **Figure 64** denote calculations that are based on the simulated data, and were done assuming perfect in-phase constructive interference, as this represent the worst-case scenario possible, although it is recognised that this is not realistic in practice and the measurements confirm this.

In **Figure 65**, the measurements are compared to the simulated dominant field. This shows a much better comparison. At a height of 2 m, where the mmWave transmitter is located, there is a very good match, with both the predicted and measured field strengths being about 6.4 V/m, for the mmWave and background radiation. The main difference is between the measurement and simulation of the background field strengths, with the measurements average about 1 V/m and the simulations 2 V/m over the range of heights.

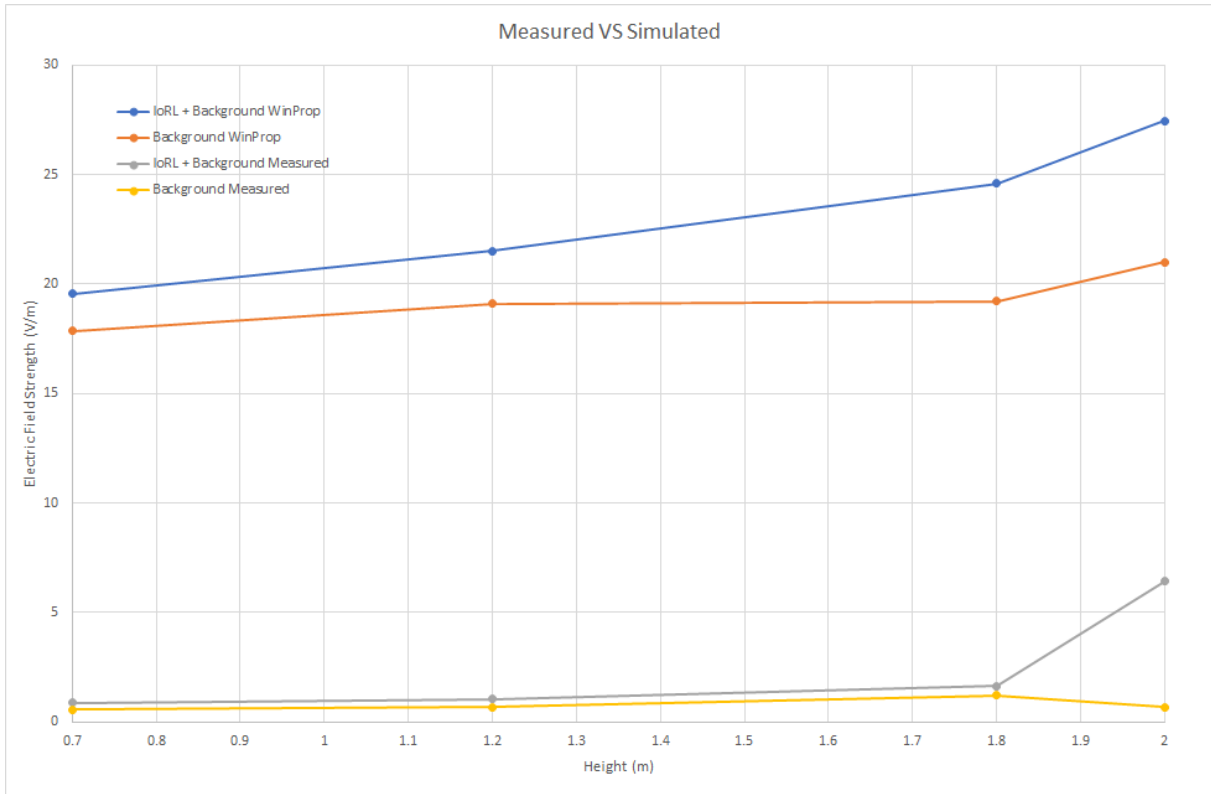


Figure 64 - Comparisons between measured and simulated results (summation of electric field strengths, assuming in-phase constructive interference)

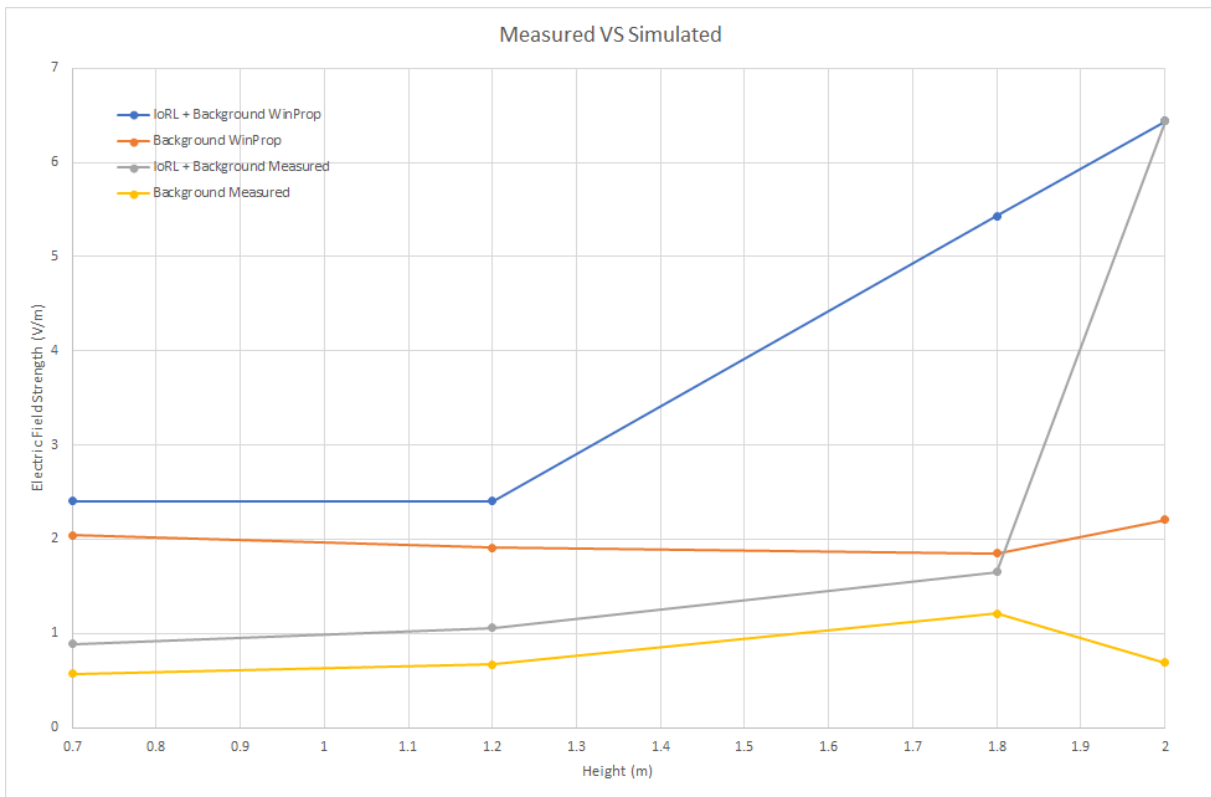


Figure 65 - Comparisons between measured and simulated results (Dominant electric field)

The ICNIRP exposure ratio calculated from the total field strength contributions from the simulated results estimated that the exposure ratio was just less than 0.1, with any value below one being compliant with the ICNIRP limits, and this was therefore considerably below the ICNIRP limits. The measurement field strengths were slightly lower than the simulations and reasonably similar to the simulated results.

This work gives an indication of the estimated levels of risk associated with the scenarios modelled. However, this work should not be taken as any kind of approval for such products to be placed for sale on the market. Any manufacturers placing such products on the market should go through the necessary product approval processes to meet the necessary regulations and standards, including any national standards and guidance, and perform their own assessments of their specific system specifications.

International Committee on Non-Ionizing Radiation Protection (ICNIRP) guidelines are used worldwide, either directly or as the basis for national regulations. These ICNIRP levels have been used in this report as a reference level. It is recognised that there are some variations in some national regulations, and these should be taken into account for any product manufacturers looking to take products to market.

The emissions from other wireless devices in addition to IoRL were included in the calculations to give estimates of other background field strength levels. However, this report is only assessing the potential impact of the IoRL devices with respect to human exposure limits, not any other wireless devices.

Some calculations use a number of worst-case assumptions, such as the contributions from all devices being in-phase and all with 100% activity. These results should not be taken as a representation of actual field strengths that would be experienced in practice. Measurements were made of actual devices which took into account how the devices operate in practice and demonstrated lower levels of field strength as expected.

References

- [1] IEC 62232, EN 62232, *Determination of RF field strength, power density and SAR in the vicinity of radiocommunication base stations for the purpose of evaluating human exposure*, 2017.
- [2] "ICNIRP," [Online]. Available: <https://www.icnirp.org/>. [Accessed 08 01 2019].
- [3] ITU-R BS.1698, *Evaluating fields from terrestrial broadcasting transmitting systems operating in any frequency band for assessing exposure to non-ionizing radiation*.
- [4] ITU-T K.61, *Guidance on measurement and numerical prediction of electromagnetic fields for compliance with human exposure limits for telecommunication installations*, Geneva, Switzerland, 2018.
- [5] ITU-T K.91, *Guidance for assessment, evaluation and monitoring of human exposure to radio frequency electromagnetic fields*, Geneva, Switzerland, 2018.
- [6] ICNIRP, *ICNIRP GUIDELINES FOR LIMITING EXPOSURE TO TIME-VARYING ELECTRIC, MAGNETIC AND ELECTROMAGNETIC FIELDS (UP TO 300 GHZ)*, 1998.
- [7] EN 62311:2008, *Assessment of electronic and electrical equipment related to human exposure restrictions for electromagnetic fields (0 Hz – 300 GHz)*, 2008.
- [8] Dr Richard Rudd (Aegis), Dr Ken Craig (Signal Science), Dr Martin Ganley (BRE), Richard Hartless (BRE), "Building Materials and Propagation," 2014.
- [9] Ting Wu, Theodore S. Rappaport, Christopher M. Collins, "The Human Body and Millimeter Wave Wireless Communication Systems: Interactions and Implications," NYU WIRELESS, New York.
- [10] Kathy L. Ryan, John A D'Andrea, James R. Jauchem, Patrick A Mason, "Radio frequency radiation of millimeter wave length: potential occupational safety issues relating to surface heating," 2000.
- [11] "IoRL 5GPPP," [Online]. Available: <https://iorl.5g-ppp.eu/>. [Accessed 28 01 2019].
- [12] IEEE Std 1720™-2012, *IEEE Recommended Practice for Near-Field Antenna Measurements*.
- [13] ITU-T K.52, *Guidance on complying with limits for human exposure to electromagnetic fields*, 2018.
- [14] IEC 62630, *GUIDANCE FOR EVALUATING EXPOSURE FROM MULTIPLE ELECTROMAGNETIC SOURCES - Technical Report*.

- [15] EBU - European Broadcasting Union, *EBU [November 2001] BPN 023: Radio frequency radiation: Exposure limits and their implication for broadcaster.*, 2001.
- [16] Lina Shi , Dayu Shi, Xun Zhang , Benjamin Meunier, Hequn Zhang , Zhan Wang, Andrei Vladimirescu, Wei Li, Yue Zhang, John Cosmas, Kareem Ali, Nawar Jawad , Rudolf Zetik, Eric Legale, Matteo Satta, Jintao Wang , and Jian Song “5G Internet of Radio Light Positioning System for Indoor Broadcasting Service” IEEE TRANSACTIONS ON BROADCASTING, VOL. 66, NO. 2, JUNE 2020

Annex A Performance Metric Requirements

The performance metrics requirements of the different building blocks and network services follow the specifications defined in Task 2.5 and detailed in deliverables D2.2 and D2.3.

Table 18: Key Performance Metric Requirements for IoRL

Sub-System	Layer	Block	Function Description / Requirement	Comments/Status/Partners
RRLH	L1	VLC MISO driver	4-to-1 multiple-inputs single-output led driver	VLC leds array was updated from 8 to 4
	L1	VLC 1:4 splitter switch	This allows the individual VLC parts of the RRLHs to be successively driven with RSS location estimation reference signals from the RRLH Controller	4-1 Multiplexer operating at 10MHz IF that is controlled from a remote smart phone app using blue tooth wireless to manually switch from one light to another for the purpose of location estimation experiments before committing ourselves to a more complex solution involving the RRLH Controller proving this control automatically.
	L1	VLC array 4 leds	Consumer light system to be used simultaneously for illumination and communication from RRLH light system	The illumination LEDs used a complex parallel-serial circuit whose impedance was too large for the LED modulator driver. Thus, the LED were driven from separate illumination and communication LED circuits using the same illumination LEDs which were found to not be powerful enough. So, the communication LED were upgraded to more power version. The electric cable connecting the LED driver to the LED with IF signal was using electric lighting cable which was found to be inducing interference, so this connection was replaced with a SMA cable and shielded circuit, which reduced the induced noise. It has yet to be tested because of COVID 19 delay.
	L1	VLC MISO module	This consists of 8 RRLHs driven from a splitter	This has been reduced to 4 RRLHs driven from a splitter

			switch providing a manmade multipath environment and more than sufficient RRLHs to estimate location.	switch providing an adequate manmade multipath environment and sufficient RRLHs to estimate location.
	L1	RF 1:8 splitter	This successively receives the mm-Wave part individual RRLHs with TDoA location estimation reference signals under the control of the RRLH Controller	As the mm-Wave uplink has been designed but not yet been implemented this work has been waiting for it to be completed.
	L1	RF/mmW splitter switch for 8N OFDM symbols	This allows the RRLH Controller successively access TDoA location estimation reference signals from UEs via the individual mm-Wave parts of the RRLHs, so that it can measure time of arrival.	As the mm-Wave uplink has been designed but not yet been implemented this work has been waiting for it to be completed. It will replicate the design of the VLC 4-1 Multiplexer but at 3.5 GHz IF that is controlled from a remote smart phone app using blue tooth wireless to manually switch from one light to another for the purpose of mm-Wave location estimation experiments.
	L1	5G lower/upper L1, mmW TDD Tx/Rx	5G transceiver 3GPP Rel.15 sub-6GHz IF with BW up to 100 MHz	This has been designed but not yet been integrated and tested at time of writing 19-04-2020
		5G VLC lower L1	BW up to 20MHz	This has been completed but has the main limitation that it cannot coexist with another component carrier of 100MHz.
	L1	mmW Polarization compensation	Single Tx/Rx antenna in UE requires polarization compensation	Two antennas have been provided one for vertical and one for horizontal polarisation in the RRLH.
	L1	60GHz mmW front-end	Up/down converter (UDC), filtering, amplifier, 2 antennas (Tx, Rx)	The mm-wave antenna system has an antenna operating in TDD downlink and uplink at 60GHz but too big to be designed to be integrated in the RRLH light system. This has been integrated and tested
	L1	40GHz mmW front-end	UDC, filtering, amplifier, 2 antennas (Tx, Rx)	The mm-wave antenna system has two 40 GHz antennas for vertical and horizontal polarisation each operating in TDD downlink and uplink at

				40GHz and designed to be integrated in the RRLH light system. This has not yet been integrated and tested.
	L2/L3	5G FAPI	Functional Access Platform Interface (FAPI) meets 5G-NR requirements	The RRLH Controller is 5G compliant.
	Above L4	eCPRI protocol	Support QoS, security adjusted to IoRL spec between eNB/gNB	DRAN – RRLH Controller L1 eCPRI split has been successfully designed and implemented.
		Coverage indoor planning	S/W to enable optimal distribution of RRLHs to enhance localization and coverage	VLC and mm-Wave coverage tools have been designed. A mm-Wave Geometric dilution of precision (GDOP) has been designed to investigate how errors in the measurement will affect the final location estimation and can potentially use AI to optimise the position of the RRLHs.
		Intra HO Layer 2.	This allows user terminals to move from one RRLH Controller coverage area to another and the L2 controller redirects packets to the appropriate RRLH Controller.	This has been completed but it has not been able to be tested on the downlink. For the uplink we are still in the integration phase that has been delayed due to COVID 19.
		Inter HO Layer 3.	This allows user terminals to move from Indoor coverage area to outdoor coverage area and the L3 controller redirects packets to the appropriate RAN.	This has not been completed because there is no Non-Access Stratum in our user terminals but it has been simulated on Mininet.
	Consumer Product	Ceiling Light	This allows all the mmWave and VLC RRLH components to be integrated into a consumer product which has a ceiling light form factor	The ceiling light was designed in 3D graphics tool and several versions of it were manufactured by SFY. Eight prototypes of the final version were manufactured for the final demonstration
	Consumer Product	Spot Light	This allows all the mmWave and VLC RRLH components to be integrated into a consumer product which has a ceiling light form factor	The spot light was designed in 3D graphics tool but there was not enough time for versions of it to be manufactured.

	Consumer Product	Pendant Light	This allows all the mmWave and VLC RRLH components to be integrated into a consumer product which has a ceiling light form factor	The pendant light was designed in 3D graphics tool but there was not enough time for versions of it to be manufactured.
	Consumer Product	Accessories Light	This allows all the mmWave RRLH components to be integrated into a consumer product which has a ceiling light form factor	The accessories mmWave access point was designed in 3D graphics tool but there was not enough time for versions of it to be manufactured.

Sub-System	Layer	Block	Function Description / Requirement	Comments/Status/Partners
UE	L1	VLC photo detector (PD)	Fc=20MHz, BW=10MHz	This has been successfully designed and implemented
	L1	VLC Amplifier & AGC		Integrated lower power amplifier into their receiver with photo diode
	L1	UE USRP	Universal S/W radio peripheral to implement UE digital front-end	This has been successfully designed and implemented
	L1/L2/L3	5G layers L1-L3 processor	Protocol stack processing Support USB 3.0 up to 640Mbps, TCP/IP	L1 UE processor mainly responsible for cell search (SS/PBCH), blind detection for downlink control channel (PDCCH), decoding data channel (PDSCH), uplink data channel generation (PUSCH) and uplink acknowledge/ Non-acknowledge (ACK/NACK) generation. L1 UE processor by far has completed the development of cell search, PDCCH detection and PDSCH decoding
	L1/L2/L3	5G layers L1-L3 processor	Protocol stack processing Support USB 3.0 up to 640Mbps, TCP/IP	BS L2/SDN interface: employs the UDP protocol to stream live video from SDN to L2 through GRE tunnel. BS L1/L2 interface:

				<p>encapsulates the UDP streaming data to transport block (TB)s. Each TB will be segmented into 3 parts and each part will be patched with some control data. The data and other control information, like DCI and EOSs, will be sent to BS L1 by UDP packets with a specific order.</p> <p>UE UDP Rx (bypass L1): receives and assembles the UDP packets directly from BS L2 and pass the recovered TBs to UE L2. This module is to measure the effectiveness and reliability of BS L1L2 interface processing.</p> <p>UE L1/L2 interface: handles the TBs passed from UE L1 or UDP Rx and send them to TV.</p>
	L1/L2	60GHz mmW transceiver	mmW UDC, filter and antenna. Interface Sparq-2020 over sub-6GHz IF with BW up to 100MHz	Polarization compensation at UE will not be deployed.
	L1/L2	40GHz mmW transceiver	Same as above for 40GHz	Polarization compensation at UE will not be deployed.
	L1/L2	UHDTV	USB 3.0 connection TCP/IP of UE UHDTV panel through SoC containing USB driver, DRAM controller, low-voltage diff. signalling (LVDS) driver	4k TV has been streamed using Internet browser access and with direct mode access. 4k picture in picture Android TV has been streamed.
	L1/L2/L3		Integration of VLC and mmW modules to UE	This has been completed but only VLC or mmWave can be accessed at any one time. To access both at the same time a second instance of the UE receiver is required.

Sub-System	Layer Network	Block	Function Description / Requirement	Comments/Status/Partners
SDN	L3	LTE eNB emulator	Emulates eNB-UEs access	This was not achieved because we did not have the UE non-access stratum working for it to be tested with.
	L3	Open EPC emulator	Support evolved packet core (EPC) through mobility mng. entity (MME), serving gateway (SGW) and packet-data gateway (PGW)	Protocol sequencing example for 4G/5G is given in deliverable D2.2 and model of it is provided in D3.3
	L3	Open source LTE control plane protocol	Process the LTE control plane externally	The 5G control plane (CP) and 5G, data plane (DP) cannot be implemented as the complete protocol stack on the UE has not been implemented and the UE has not been interface to a 5G core. However, of the Virtual Gateway: Mobility management for 5G Internet of Radio Light gNB has been simulated and performance results obtained.
	L3	Open source LTE data plane protocol	Process the LTE data plane protocols	

Sub-System	Layer SDN/NFV	Block	Function Description / Requirement	Comments/Status/Partners
IHIPG Dell 730-2	L3	NFVO	NFV-Orchestration entity for managing network service (NS) life cycle	This has been implemented and is working under manual management (as opposed to autonomous).
	L3	VNF repository	Repository to store virtual network functions (VNFs) and deployed / instantiated upon request.	This includes VNFs as: video Stream Server, Transcoder, MSS, location app., load balancing, slicing, multipath TCP, security monitoring. Intra HO is being taken care of by Layer 2. The 5G control plane (CP) and 5G, data plane (DP) can not be implemented as the complete protocol stack on the UE has not been implemented and the UE has not been interface to a 5G core. However, of the Virtual Gateway: Mobility management for 5G Internet of Radio Light gNB has been simulated and performance

				results obtained.
		SDN FD	SDN -compatible virtual network device as virtual switch to enable FD	This has been implemented using OvS and is working.
		SDN Controller	To support location based scenarios (as museum, supermarket)	A location database and a location server has been implemented. The location database holds location data whilst the location server processes RSS and TDoA data to obtain locations and uses a Kalman filter to perform the location data fusion.
		4G/5G control plane VNF	To enable outdoor HO for 4G/5G in home	Has not been implemented because the lack of Non-access stratum in the UE but has been simulated in mininet.
	L3/L4	MNO EPC	Integration of MNO EPC with SDN VNFs: 4G/5G control and user planes	The 5G control plane (CP) and 5G, data plane (DP) cannot be implemented as the complete protocol stack on the UE has not been implemented and the UE has not been interface to a 5G core. However, of the Virtual Gateway: Mobility management for 5G Internet of Radio Light gNB has been simulated and performance results obtained.
	L3/L4		Integration of e/gNB with SDN VNFs: 4G/5G control and user planes	

Sub-System	Layer Service	Block (responsible)	Function Description / Requirement	Comments/Status/Partners
CHDCS	App	CHDCS	Interaction server to store and process data and images	Location database has been implemented from which an Android app on the UE can access location information for location-based applications
UE	App	UE	Interaction app on the UE to access and retrieve images and data on physical/virtual server	An Android app on the UE can access location information for location-based applications from the Location database on the IHIPG.
CHDCS	App	CHDCS	Streaming audio/video of different formats as UHDTV, 360° video to/from multiple users	ffMPEG and VLC server VNFs can stream 4k AV onto TVs and Laptops with Internet access and stand alone versions.
UE	App	UE	Streaming audio/video app of different formats as UHDTV, 360° video	Theta-V camera can stream video through the SDN/NFV to a VR headset.
CHDCS	App	CHDCS	Server providing indoor	Location based data in the

			location-based data to multiple users. It provides, routes, maps and recording of UE movements.	location database is available for UE apps to access for location-based data access, monitoring and guiding applications have been developed
UE	App	UE	indoor location-based data. It provides, routes, maps and recording of UE movements.	Location based data access, monitoring and guiding android apps have been developed for the UE.
CHDCS	App	CHDCS		
UE	App	UE		

Annex B EMF Exposure Analysis

Table 19 – Electrical properties wood and concrete

Frequency GHz	Wood permittivity	Wood conductivity	Concrete permittivity	Concrete conductivity
0.169	1.99	0.000699	5.31	0.007730221
0.458	1.99	0.002035	5.31	0.017325597
0.726	1.99	0.003335	5.31	0.025156244
0.9	1.99	0.004198	5.31	0.029934838
1.5	1.99	0.007258	5.31	0.045265099
1.8	1.99	0.008825	5.31	0.052463915
2	1.99	0.00988	5.31	0.057134888
2.37	1.99	0.011851	5.31	0.065550557
3.55	1.99	0.018274	5.31	0.090913306
5	1.99	0.026379	5.31	0.119959271
15	1.99	0.085631	5.31	0.291919747
27	1.99	0.160781	5.31	0.469793028
30	1.99	0.180002	5.31	0.511619697
38	1.99	0.231905	5.31	0.619515849
40	1.99	0.245011	5.31	0.645780851
60	1.99	0.378373	5.31	0.896666691
75	1.99	0.480605	5.31	1.074186507

Table 20 - Electrical properties plasterboard and glass

Frequency GHz	Plasterboard permittivity	Plasterboard conductivity	Glass permittivity	Glass conductivity
0.169	2.94	0.003297	6.27	0.000516088
0.458	2.94	0.006676	6.27	0.001694535
0.726	2.94	0.009248	6.27	0.002935184
0.9	2.94	0.010767	6.27	0.0037923
1.5	2.94	0.015455	6.27	0.006973604
1.8	2.94	0.017583	6.27	0.008667242
2	2.94	0.018944	6.27	0.009827583
2.37	2.94	0.021361	6.27	0.0120325
3.55	2.94	0.028431	6.27	0.019481203
5	2.94	0.036228	6.27	0.02930827
15	2.94	0.078824	6.27	0.108631877
27	2.94	0.119479	6.27	0.218962501
30	2.94	0.128727	6.27	0.248276464
38	2.94	0.152164	6.27	0.329124638
40	2.94	0.157789	6.27	0.349884735
60	2.94	0.210222	6.27	0.567431997
75	2.94	0.246179	6.27	0.740421485

Table 21 - Electrical properties chipboard and ceiling board

Frequency GHz	Chipboard permittivity	Chipboard conductivity	Ceiling board permittivity	Ceiling board conductivity
0.169	2.58	0.005423	1.5	6.31966E-05
0.458	2.58	0.011801	1.5	0.000201568
0.726	2.58	0.016904	1.5	0.000344496
0.9	2.58	0.019988	1.5	0.000442319
1.5	2.58	0.029772	1.5	0.000801373
1.8	2.58	0.034322	1.5	0.000990727
2	2.58	0.037262	1.5	0.001119923
2.37	2.58	0.042537	1.5	0.001364433
3.55	2.58	0.058296	1.5	0.002183261
5	2.58	0.076148	1.5	0.003252009
15	2.58	0.179395	1.5	0.0116744
27	2.58	0.283742	1.5	0.023132289
30	2.58	0.308045	1.5	0.026148867
38	2.58	0.370417	1.5	0.034426291
40	2.58	0.385537	1.5	0.036543202
60	2.58	0.528954	1.5	0.058569453
75	2.58	0.629517	1.5	0.075930503

Table 22 - Electrical properties floorboard

Frequency GHz	Floorboard permittivity	Floorboard conductivity
0.169	3.66	0.000398
0.458	3.66	0.001531
0.726	3.66	0.002854
0.9	3.66	0.003816
1.5	3.66	0.007611
1.8	3.66	0.009738
2	3.66	0.011228
2.37	3.66	0.014123
3.55	3.66	0.024383
5	3.66	0.038736
15	3.66	0.170978
27	3.66	0.378391
30	3.66	0.436297
38	3.66	0.600524
40	3.66	0.643631
60	3.66	1.11333
75	3.66	1.505213

Table 23 – Transmitters list and parameters

Prediction area	
Lower left corner	(-0.5406, 3.3791, 4.9800)
Upper right corner	(9.6594, 14.4191, 4.9800)
Resolution	0.060 m
Transmitters List	
Transmitter 1 (Aeotec door sensor)	
Coordinates	(5.5100, 6.5000, 5.1500 m)
Frequency (used in propagation models)	868.000 MHz
Maximum transmitter power	P = -1.249 dBm EIRP
Antenna Gain	dBi = -2.148 dBd (dBi = relative to isotropical radiator)
Transmitter 2 (Aeotec multisensor 6 -1)	
Coordinates	(8.3200, 9.9500, 3.5200 m)
Frequency (used in propagation models)	868.000 MHz
Maximum transmitter power	P = -1.249 dBm EIRP
Antenna Gain	dBi = -2.148 dBd (dBi = relative to isotropical radiator)
Transmitter 3 (Aeotec multisensor 6 -2)	
Coordinates	(8.7400, 7.3200, 3.6400 m)
Frequency (used in propagation models)	868.000 MHz
Maximum transmitter power	P = -1.249 dBm EIRP
Antenna Gain	dBi = -2.148 dBd (dBi = relative to isotropical radiator)
Transmitter 4 (Aeotec multisensor 6 -3)	
Coordinates	(2.7500, 9.7400, 4.2300 m)
Frequency (used in propagation models)	868.000 MHz
Maximum transmitter power	P = -1.249 dBm EIRP
Antenna Gain	dBi = -2.148 dBd (dBi = relative to isotropical radiator)
Transmitter 5 (Aeotec multisensor 6 -4)	
Coordinates	(0.4000, 9.8100, 4.1200 m)
Frequency (used in propagation models)	868.000 MHz
Maximum transmitter power	P = -1.249 dBm EIRP
Antenna Gain	dBi = -2.148 dBd (dBi = relative to isotropical radiator)
Transmitter 6 (Aeotec multisensor 6 -5)	
Coordinates	(1.0900, 13.4200, 4.3600 m)
Frequency (used in propagation models)	868.000 MHz
Maximum transmitter power	P = -1.249 dBm EIRP
Antenna Gain	dBi = -2.148 dBd (dBi = relative to isotropical radiator)
Transmitter 7 (Aeotec multisensor 6 -6)	
Coordinates	(0.4500, 6.5500, 4.3400 m)
Frequency (used in propagation models)	868.000 MHz
Maximum transmitter power	P = -1.249 dBm EIRP
Antenna Gain	dBi = -2.148 dBd (dBi = relative to isotropical radiator)
Transmitter 8 (Amazon echo show 2 1-2)	
Coordinates	(0.4000, 9.6000, 4.1200 m)
Frequency (used in propagation models)	2400.000 MHz

Maximum transmitter power Antenna Gain	P = 0.135 W (21.303 dBm) EIRP dBi = -2.148 dBd (dBi = relative to isotropical radiator)
Transmitter 9 (Amazon echo show 2 2-2) Coordinates Frequency (used in propagation models) Maximum transmitter power Antenna Gain	(0.4000, 9.6000, 4.1200 m) 5000.000 MHz P = 0.097 W (19.868 dBm) EIRP dBi = -2.148 dBd (dBi = relative to isotropical radiator)
Transmitter 10 (Google Home 1-2) Coordinates Frequency (used in propagation models) Maximum transmitter power Antenna Gain	(0.4000, 10.0900, 4.1200 m) 2400.000 MHz P = 0.064 W (18.062 dBm) EIRP dBi = -2.148 dBd (dBi = relative to isotropical radiator)
Transmitter 11 (Google Home 2-2) Coordinates Frequency (used in propagation models) Maximum transmitter power Antenna Gain	(0.4000, 10.0900, 4.1200 m) 5000.000 MHz P = 0.062 W (17.924 dBm) EIRP dBi = -2.148 dBd (dBi = relative to isotropical radiator)
Transmitter 12 (GSM 4G 2nd) Coordinates Frequency (used in propagation models) Maximum transmitter power Azimuth (Horizontal Orientation) Downtilt (Vertical Orientation) Pattern file Antenna Gain	(101.0500, 1.9500, 15.0000 m) 1850.000 MHz P = 10.000 W (40.000 dBm) EIRP 150.000° 0.000° 4G -0.122 dBi = -2.270 dBd (dBi = relative to isotropical radiator)
Transmitter 13 (GSM 4G 3rd) Coordinates Frequency (used in propagation models) Maximum transmitter power Azimuth (Horizontal Orientation) Downtilt (Vertical Orientation) Pattern file Antenna Gain	(101.0500, 2.0500, 15.0000 m) 1850.000 MHz P = 10.000 W (40.000 dBm) EIRP 30.000° 0.000° 4G -0.122 dBi = -2.270 dBd (dBi = relative to isotropical radiator)
Transmitter 14 (GSM 4G) Coordinates Frequency (used in propagation models) Maximum transmitter power Azimuth (Horizontal Orientation) Downtilt (Vertical Orientation) Pattern file Antenna Gain	(101.0000, 2.0000, 15.0000 m) 1850.000 MHz P = 10.000 W (40.000 dBm) EIRP 270.000° 0.000° 4G -0.122 dBi = -2.270 dBd (dBi = relative to isotropical radiator)
Transmitter 15 (Honeywell water leak sensor) Coordinates	(2.5700, 10.6500, 4.1200 m)

Frequency (used in propagation models)	2400.000 MHz
Maximum transmitter power	P = 0.270 W (24.314 dBm) EIRP
Antenna Gain	dBi = -2.148 dBd (dBi = relative to isotropical radiator)
Transmitter 16 (Linksys wrt3200acm 1-2)	
Coordinates	(0.4500, 6.5500, 4.3400 m)
Frequency (used in propagation models)	2400.000 MHz
Maximum transmitter power	P = 0.700 W (28.451 dBm) EIRP
Antenna Gain	dBi = -2.148 dBd (dBi = relative to isotropical radiator)
Transmitter 17 (Linksys wrt3200acm 2-2)	
Coordinates	(0.4500, 6.5500, 4.3400 m)
Frequency (used in propagation models)	5000.000 MHz
Maximum transmitter power	P = 0.760 W (28.808 dBm) EIRP
Antenna Gain	dBi = -2.148 dBd (dBi = relative to isotropical radiator)
Transmitter 18 (Nest Cam Outdoor 1-2)	
Coordinates	(9.2900, 8.9200, 6.6400 m)
Frequency (used in propagation models)	2400.000 MHz
Maximum transmitter power	P = 0.196 W (22.923 dBm) EIRP
Antenna Gain	dBi = -2.148 dBd (dBi = relative to isotropical radiator)
Transmitter 19 (Nest Cam Outdoor 2-2)	
Coordinates	(9.2900, 8.9200, 6.6400 m)
Frequency (used in propagation models)	5000.000 MHz
Maximum transmitter power	P = 0.064 W (18.062 dBm) EIRP
Antenna Gain	dBi = -2.148 dBd (dBi = relative to isotropical radiator)
Transmitter 20 (Nest indoor camera - not IQ 1-2)	
Coordinates	(6.9000, 9.9500, 3.5200 m)
Frequency (used in propagation models)	2400.000 MHz
Maximum transmitter power	P = 0.100 W (20.000 dBm) EIRP
Antenna Gain	dBi = -2.148 dBd (dBi = relative to isotropical radiator)
Transmitter 21 (Nest indoor camera - not IQ 2-2)	
Coordinates	(6.9000, 9.9500, 3.5200 m)
Frequency (used in propagation models)	5000.000 MHz
Maximum transmitter power	P = 0.057 W (17.559 dBm) EIRP
Antenna Gain	dBi = -2.148 dBd (dBi = relative to isotropical radiator)
Transmitter 22 (Nest Thermostat 1-2)	
Coordinates	(3.7900, 6.5000, 4.7200 m)
Frequency (used in propagation models)	2400.000 MHz
Maximum transmitter power	P = 0.277 W (24.425 dBm) EIRP
Antenna Gain	dBi = -2.148 dBd (dBi = relative to isotropical radiator)
Transmitter 23 (Nest Thermostat 2-2)	
Coordinates	(3.7900, 6.5000, 4.7200 m)
Frequency (used in propagation models)	5000.000 MHz
Maximum transmitter power	P = 0.036 W (15.563 dBm) EIRP
Antenna Gain	dBi = -2.148 dBd (dBi = relative to isotropical radiator)
Transmitter 24 (Netamo Indoor Unit 1-2)	

Coordinates	(7.0000, 9.9500, 3.5200 m)
Frequency (used in propagation models)	2400.000 MHz
Maximum transmitter power	P = 0.038 W (15.775 dBm) EIRP
Antenna Gain	dBi = -2.148 dBd (dBi = relative to isotropical radiator)
Transmitter 25 (Netamo Indoor Unit 2-2)	
Coordinates	(7.3000, 9.9500, 3.5200 m)
Frequency (used in propagation models)	868.000 MHz
Maximum transmitter power	P = -8.239 dBm EIRP
Antenna Gain	dBi = -2.148 dBd (dBi = relative to isotropical radiator)
Transmitter 26 (Netamo Weather Station Out)	
Coordinates	(7.1000, 9.9500, 3.5200 m)
Frequency (used in propagation models)	868.000 MHz
Maximum transmitter power	P = -8.239 dBm EIRP
Antenna Gain	dBi = -2.148 dBd (dBi = relative to isotropical radiator)
Transmitter 27 (Philips Hue Bridge v2.1 1-2)	
Coordinates	(7.7000, 9.9500, 3.5200 m)
Frequency (used in propagation models)	2400.000 MHz
Maximum transmitter power	P = 0.160 W (22.041 dBm) EIRP
Antenna Gain	dBi = -2.148 dBd (dBi = relative to isotropical radiator)
Transmitter 28 (Philips Hue Bridge v2.1 2-2)	
Coordinates	(7.6000, 9.9500, 3.5200 m)
Frequency (used in propagation models)	2400.000 MHz
Maximum transmitter power	P = 0.035 W (15.441 dBm) EIRP
Antenna Gain	dBi = -2.148 dBd (dBi = relative to isotropical radiator)
Transmitter 29 (Roomba 981)	
Coordinates	(4.2850, 6.5200, 3.2700 m)
Frequency (used in propagation models)	2400.000 MHz
Maximum transmitter power	P = 0.100 W (20.000 dBm) EIRP
Antenna Gain	dBi = -2.148 dBd (dBi = relative to isotropical radiator)
Transmitter 30 (Samsung Fridge)	
Coordinates	(1.9200, 13.3500, 4.8500 m)
Frequency (used in propagation models)	2400.000 MHz
Maximum transmitter power	P = 0.100 W (20.000 dBm) EIRP
Antenna Gain	dBi = -2.148 dBd (dBi = relative to isotropical radiator)
Transmitter 31 (Smarter coffee machine)	
Coordinates	(0.4400, 10.6500, 4.1200 m)
Frequency (used in propagation models)	2400.000 MHz
Maximum transmitter power	P = 0.071 W (18.500 dBm) EIRP
Antenna Gain	dBi = -2.148 dBd (dBi = relative to isotropical radiator)
Transmitter 32 (Smarter kettle)	
Coordinates	(0.5400, 10.9400, 4.1200 m)
Frequency (used in propagation models)	2400.000 MHz
Maximum transmitter power	P = 0.199 W (22.980 dBm) EIRP
Antenna Gain	dBi = -2.148 dBd (dBi = relative to isotropical radiator)
Transmitter 33 (Smarthings V3 1-3)	

Coordinates	(7.9000, 9.9500, 3.5200 m)
Frequency (used in propagation models)	2400.000 MHz
Maximum transmitter power	P = 0.020 W (13.010 dBm) EIRP
Antenna Gain	dBi = -2.148 dBd (dBi = relative to isotropical radiator)
Transmitter 34 (Smarthings V3 2-3)	
Coordinates	(7.9000, 9.9500, 3.5200 m)
Frequency (used in propagation models)	868.000 MHz
Maximum transmitter power	P = -3.979 dBm EIRP
Antenna Gain	dBi = -2.148 dBd (dBi = relative to isotropical radiator)
Transmitter 35 (Smarthings V3 3-3)	
Coordinates	(7.9000, 9.9500, 3.5200 m)
Frequency (used in propagation models)	5000.000 MHz
Maximum transmitter power	P = 0.026 W (14.150 dBm) EIRP
Antenna Gain	dBi = -2.148 dBd (dBi = relative to isotropical radiator)
Transmitter 36 (Smarthings water leak sensor)	
Coordinates	(2.4700, 10.6500, 4.1200 m)
Frequency (used in propagation models)	2400.000 MHz
Maximum transmitter power	P = 0.040 W (15.980 dBm) EIRP
Antenna Gain	dBi = -2.148 dBd (dBi = relative to isotropical radiator)
Transmitter 37 (TP Link HS110 -1)	
Coordinates	(8.1000, 9.9500, 3.5200 m)
Frequency (used in propagation models)	2400.000 MHz
Maximum transmitter power	P = 0.082 W (19.117 dBm) EIRP
Antenna Gain	dBi = -2.148 dBd (dBi = relative to isotropical radiator)
Transmitter 38 (TP Link HS110 -2)	
Coordinates	(8.0800, 6.5700, 3.6400 m)
Frequency (used in propagation models)	2400.000 MHz
Maximum transmitter power	P = 0.082 W (19.117 dBm) EIRP
Antenna Gain	dBi = -2.148 dBd (dBi = relative to isotropical radiator)
Transmitter 39 (TP Link HS110 -3)	
Coordinates	(0.4000, 9.6000, 4.2600 m)
Frequency (used in propagation models)	2400.000 MHz
Maximum transmitter power	P = 0.082 W (19.117 dBm) EIRP
Antenna Gain	dBi = -2.148 dBd (dBi = relative to isotropical radiator)
Transmitter 40 (TP Link HS110 -4)	
Coordinates	(0.4000, 11.1000, 4.2600 m)
Frequency (used in propagation models)	2400.000 MHz
Maximum transmitter power	P = 0.082 W (19.117 dBm) EIRP
Antenna Gain	dBi = -2.148 dBd (dBi = relative to isotropical radiator)
Transmitter 41 (IoRL 40 GHz 1-8)	
Coordinates	(1.2900, 9.0600, 5.2200 m)
Frequency (used in propagation models)	40000.000 MHz
Maximum transmitter power	P = 0.100 W (20.000 dBm) ERP
Azimuth (Horizontal Orientation)	90.000°
Downtilt (Vertical Orientation)	0.000°

Pattern file	mm_wave
Antenna Gain	8.813 dBi = 6.665 dBd (dBi = relative to isotropical radiator)
Transmitter 42 (IoRL 40 GHz 2-8)	
Coordinates	(1.7900, 9.0600, 5.2200 m)
Frequency (used in propagation models)	40000.000 MHz
Maximum transmitter power	P = 0.100 W (20.000 dBm) ERP
Azimuth (Horizontal Orientation)	90.000°
Downtilt (Vertical Orientation)	0.000°
Pattern file	mm_wave
Antenna Gain	8.813 dBi = 6.665 dBd (dBi = relative to isotropical radiator)
Transmitter 43 (IoRL 40 GHz 3-8)	
Coordinates	(1.2900, 8.5600, 5.2200 m)
Frequency (used in propagation models)	40000.000 MHz
Maximum transmitter power	P = 0.100 W (20.000 dBm) ERP
Azimuth (Horizontal Orientation)	90.000°
Downtilt (Vertical Orientation)	0.000°
Pattern file	mm_wave
Antenna Gain	8.813 dBi = 6.665 dBd (dBi = relative to isotropical radiator)
Transmitter 44 (IoRL 40 GHz 4-8)	
Coordinates	(1.7900, 8.5600, 5.2200 m)
Frequency (used in propagation models)	40000.000 MHz
Maximum transmitter power	P = 0.100 W (20.000 dBm) ERP
Azimuth (Horizontal Orientation)	90.000°
Downtilt (Vertical Orientation)	0.000°
Pattern file	mm_wave
Antenna Gain	8.813 dBi = 6.665 dBd (dBi = relative to isotropical radiator)

Narda Safety Test Solutions GmbH
 Sandwiesenstrasse 7 - 72793 Pfullingen - Germany
 Phone: +49 7121 9732 0 - Fax: +49 7121 9732 790



Calibration Certificate

Narda Safety Test Solutions hereby certifies that the object referenced to this certificate has been calibrated by qualified personnel using Narda's approved procedures. The calibration was carried out in accordance with a certified quality management system which conformed to ISO 9001.

OBJECT	Broadband Field Meter NBM-520
MANUFACTURER	Narda Safety Test Solutions GmbH
PART NUMBER (P/N)	2403/01B
SERIAL NUMBER (S/N)	D-0662
CUSTOMER	
CALIBRATION DATE (YYYY-MM-DD)	2020-07-09
RESULT ASSESSMENT	within specifications
AMBIENT CONDITIONS	Temperature: (23 ± 3) °C Relative humidity: (20 to 60) %
CALIBRATION PROCEDURE	2401-8700-00A

ISSUE DATE: 2020-07-09
(YYYY-MM-DD)


 CALIBRATED BY
 M. Wittig


 AUTHORIZED SIGNATORY



This calibration certificate may not be reproduced other than in full except with the permission of the issuing laboratory. Calibration certificates without signature are not valid.

Figure 66 - NARDA NBM-520 Calibration certificate

Narda Safety Test Solutions GmbH
 Sandwiesenstrasse 7 - 72793 Pfullingen - Germany
 Phone: +49 7121 9732 0 - Fax: +49 7121 9732 790



Calibration Certificate

Narda Safety Test Solutions GmbH hereby certifies that the referenced equipment has been calibrated by qualified personnel to Narda's approved procedures. The calibration was carried out within a certified quality management system conforming to ISO 9001.

OBJECT	Probe EF 4091, E-Field
MANUFACTURER	Narda Safety Test Solutions
PART NUMBER (P/N)	2402/19B
SERIAL NUMBER (S/N)	A-0057
CUSTOMER	
CALIBRATION DATE (YYYY-MM-DD)	2020-07-10
AMBIENT CONDITIONS	Temperature: (23 ± 3) °C Relative humidity: (20 to 60) %
CALIBRATION PROCEDURE	2402-8704-00A

ISSUE DATE: 2020-07-10
(YYYY-MM-DD)



 CALIBRATED BY
 Chr. Milinkovic



 AUTHORIZED SIGNATORY



This calibration certificate may not be reproduced other than in full except with the permission of the issuing laboratory. Calibration certificates without signature are not valid.

240219B-A0057-20200710-18733

PAGE 1 OF 6

Figure 67 – EF4091 Probe certificate

[end of document]